

**Picosecond Fluorescence Studies of Physical Processes in
Green-Plant Chloroplasts and Green Algae**

by
Su Lin

Submitted in Partial Fulfillment
of the
Requirement for the Degree
Doctor of Philosophy

Supervised by Professor Robert S. Knox
Department of Physics and Astronomy

The University of Rochester
Rochester, New York USA

1990

VITA

Su Lin, born July 23, 1956 in Beijing, China, received her Bachelor of Arts degree from the Beijing Normal University in 1982. Being a physics major, she was appointed teaching assistant in the Department of Physics in the same university. After one and a half years, she began her graduate study in the Department of Physics and Astronomy at the University of Rochester. She got her Master of Arts degree in physics in 1985. Most of her research was done at Laboratory for Laser Energetics under the guidance of Professor Robert S. Knox.

She is a member of the American Physical Society and the American Society for Photobiology.

ACKNOWLEDGEMENT

In the past six years of study I received a lot of advice, support and help from people. Without them I could not have finished my Ph. D program successfully. Here I would like to express my appreciation.

My warmest thanks go to my thesis adviser, Prof. Robert S. Knox. He gave me excellent guidance during my thesis work and helped me start my scientific career. His advice on both professional and personal subjects was invaluable. Without his patient teaching, constant support and encouragement I could not have finished this project successfully.

I thank Prof. Thomas M. Nordlund for his kind and honest advice on scientific and technical topics, and very patient discussions on experimental details.

I appreciated Dr. Bruce P. Wittmershaus's friendly help and teaching, which helped a lot to start my project. I enjoyed very much learning from him and collaborating with him later.

I cannot forget the time working with: Demet Gülen, Cheryl Hanzlik, Xiaoyuan Liu, Robert H. Hwang-Schweitzer, Thomas H. Foster and Pengguang Wu. Their helpful suggestions and discussions and their cooperation were very important supports for my thesis work.

My thanks also go to Prof. Thomas T. Bannister for letting me use his laboratory to culture the green algae and teaching me many aspects of biology.

I thank Prof. Laurens Mets and Prof. Thomas G. Owens for providing Chlamydomonas reinhardtii mutant samples and for giving me detailed information about working with those mutants. Prof. Owens also taught me how to culture the mutants from the beginning.

I thank Betty J. Cook for all the administrative help she gave me during my stay in Rochester.

Finally, I thank my husband Jian Fei for his understanding, encouragement, and support.

This research was supported by the United States Department of Agriculture Grant 82-CRCR-1-1128 and 87-CRCR-1-2424.

ABSTRACT

Fluorescence from green plant chloroplasts and green algae was studied in the picosecond time region using streak camera and interference filter techniques. The measurements were done at low temperatures (10K--110K). The goal was to observe and measure the lifetime of the fluorescence associated with light-harvesting complex-protein (LHC) in the intact cell membrane in order to understand the pathways of excitation energy transfer from LHC to the photosystems.

Low temperature time-resolved fluorescence studies at 660 nm, 670 nm and 680 nm showed that there were at least two emission bands in green plant chloroplasts. The one with a shorter decay lifetime was seen clearly at very low temperature on the shorter wavelength side. Three coupled kinetic equations were used in fitting the data. Further analysis indicated that the short-lived emission band centered at 677 nm with a 9 ± 1 ps lifetime. This strong early emission was attributed to system antennae, i.e., LHC. Its temperature dependence was explained by energy transfer and back transfer kinetics. These processes involved excitation transfer from LHC to photosystem II (PSII) core antennae with very high efficiency.

Our kinetic model was substantiated by studies on the green alga Chlamydomonas reinhardtii and its mutants. The fast fluorescence decay was also resolved from fluorescence decay curves of wild type and from cells lacking photosystem I in the same wavelength region. The mutant called LM15-4D1C which lacks LHC did not show the emission band at 680 nm in the steady-state fluorescence spectrum and no fast decay was observed in time-resolved fluorescence measurements. A strong emission band around 681 nm appeared in the steady-state fluorescence spectrum of the mutant B1 which does not contain PSII and corresponding time dependent data only showed a

slow decay. The study of Chlamydomonas reinhardtii in 700 nm to 720 nm region shows that LHC also provides excitation energy to photosystem I through LHCI, the light-harvesting complex proteins closely associated with photosystem I.

TABLE OF CONTENTS

Vita	ii
Acknowledgements	iii
Abstract	iv
Table of Contents	vi
List of Tables	ix
List of Figures	x
I. Introduction	1
II. Background	
2.1 Overview of Photosynthesis Studies	4
2.2 Structure and Function of the Photosynthetic Apparatus in Green Plants and Green Algae	
A. Chloroplasts	4
B. Light-Harvesting Complex Proteins and the Photosystems	6
C. Chlorophyll Molecules and Protein Complexes	8
2.3 Primary Processes of Photosynthesis	
A. Physical Processes: Excitation Energy Transfer	10
B. Chemical Processes: Energy Conversion	12
2.4 Mechanism and Models of Energy Transfer	
A. Three Levels of Studies	15
B. Spectral Studies and Kinetic Models for Energy Transfer in Chloroplasts at Low Temperatures	20
2.5 Questions to be Answered	25
III. Materials and Methods	
3.1 Sample Preparation	
A. Spinach Chloroplasts	26

B. <u>Chlamydomonas Reinhardtii</u>	26
C. Sample Cooling	27
3.2 Steady-State Spectral Measurements	
A. Absorption Spectra	28
B. Emission and Excitation Spectra	28
3.3 Time-Dependent Fluorescence Measurements	
A. General Description	28
B. Laser System	31
C. Detecting System	32
D. Data Acquisition	34
E. System Calibration	34
3.4 Data Analysis	
A. Fourth Derivative Analysis of Spectra	38
B. Data Correction	38
C. Least Squares Fitting	43
D. Kinetic Modeling	44
IV. Low Temperature Time-Resolved Fluorescence Studies of F680 in Green Plant Chloroplasts	
4.1 Overview	
A. Spectral Characteristics of F680	48
B. Kinetics in the 680-685 nm Region	49
C. About This Study	50
4.2 Experimental Results	
A. Spectral Properties of Spinach Chloroplasts at 77 K	51
B. Time-Resolved Fluorescence Measurements	53
C. Least-Squares Fitting Results	55
4.3 Kinetic Analysis	
A. Fluorescence Decay Kinetics at 20 K	59
B. Kinetics at Higher Temperatures	63
4.4 Summary and Discussion	70

V. Studies of the Green Alga <u>Chlamydomonas reinhardtii</u> and its Mutants at 77 K	
5.1 Overview	
A. <u>Chlamydomonas reinhardtii</u>	73
B. Spectral Studies of <u>Chlamydomonas reinhardtii</u> and its mutants at Low Temperatures	74
C. Time-Resolved Fluorescence Studies at 77 K	76
D. About This Study	77
5.2 Characteristics and Spectral Properties of Mutant Strains of <u>Chlamydomonas reinhardtii</u>	78
5.3 Time-Resolved Fluorescence at 77 K	
A. The F680 Region	91
B. The F715 Region	95
5.4 Kinetic Analysis	
A. The F680 Region	95
B. The F715 Region	101
5.5 Summary and Discussion	108
References	112
List of Abbreviations	122
Index	124

LIST OF TABLES

#	Caption Title	Page
3.1	Fluorescence lifetimes of dyes.	35
4.1	Comparison of fitting parameters from photon counting data and streak camera data.	57
4.2	Results from two-exponential least-squares fitting of fluorescence from spinach chloroplasts measured at 660 nm, 670 nm and 680 nm at low temperatures.	58
5.1	List of the components, functions, and emission peaks of chlorophyll-protein complexes of <u>Chlamydomonas reinhardtii</u> .	75
5.2	Complexes content of wild type and mutant strains of <u>Chlamydomonas reinhardtii</u> .	83
5.3	Parameters used in kinetic model simulations of fluorescence in the F680 region.	97
5.4	Parameters used in kinetic model simulations of fluorescence in the PSI emission region.	103
5.5	Comparison of energy back transfer rates from different kinetic models.	104

LIST OF FIGURES

#	Caption Title	Page
2.1	Photosynthetic structures of higher plants.	5
2.2	Organization of thylakoid membranes.	7
2.3	Structures of chlorophyll molecule and pigment protein.	9
2.4	Absorption spectra of chlorophyll a , chlorophyll b and intact chloroplast.	11
2.5	The series scheme for describing the primary processes of photosynthesis.	13
2.6	Fluorescence emission spectra of spinach chloroplasts at room temperature and at 77 K.	22
3.1	Geometry of the optics used in the measurement of steady-state fluorescence at 77 K.	29
3.2	Experimental layout for time-resolved fluorescence measurements.	30
3.3	Schematic drawing of the laser, Pockels cell and amplifier system.	30
3.4	Streak camera image converter tube with GaAs:Cr switching circuit.	33
3.5	Time-dependent intensity of an excitation pulse sent through an etalon.	36
3.6	Single-exponential fit of time-resolved fluorescence of dyes.	37
3.7	Determination of the linearity response factor.	40
3.8	A time-resolved fluorescence curve and its residual background.	41
3.9	Fluorescence decay curve of rhodamine 6G.	42
3.10	A typical least-squares fitting result.	45
3.11	Three-population kinetic model.	46
4.1	77 K emission spectrum of spinach chloroplasts and the fourth derivative spectrum.	52
4.2	Time-resolved fluorescence of spinach chloroplasts measured at various wavelengths and temperatures.	54

#	Caption Title	Page
4.3	Time-resolved fluorescence and theoretical fitting (spinach, 77 K).	56
4.4	Two-population kinetic model for simulating fluorescence decay curves.	60
4.5	Theoretical curves calculated from a proposed kinetic model.	62
4.6	Reconstructed emission bands from the model simulation of time-resolved fluorescence.	64
4.7	Simulated time-resolved fluorescence curves at various temperatures.	66
4.8	Time-resolved fluorescence with theoretical fittings.	67
4.9	Fluorescence intensity of F680 as a function of temperature.	69
5.1	Emission spectrum of DES15 at 77 K and its fourth derivative.	79
5.2	Emission spectrum of B4 at 77 K.	80
5.3	Emission spectrum of B1 at 77 K.	81
5.4	Emission spectrum of LM15-4D1C at 77 K.	82
5.5	Emission spectrum of 10-3C at 77 K.	84
5.6	Comparison of 77 K emission spectra of DES15 and 10-3C.	86
5.7	Comparison of 77 K emission spectra of DES15 and B4.	87
5.8	Comparison of 77 K emission spectra of DES15 and B1.	88
5.9	Comparison of 77 K emission spectra of 10-3C and LM15-4D1C.	89
5.10	Comparison of 77 K emission spectra of DES15 and LM15-4D1C.	90
5.11	Fluorescence rise and decay profiles of DES15, 10-3C and LM15-4D1C at 77 K.	93
5.12	Fluorescence decay curve of B1 measured at 670 nm and at 77 K.	94
5.13	Fluorescence decay curve of DES15 and 10-3C measured at 710 nm and at 77 K.	96

#	Caption Title	Page
5.14	Curve fitting of fluorescence decay of DES15 at 660 nm, 670 nm and 680 nm measured at 77 K.	98
5.15	Curve fitting of fluorescence decay of 10-3C at 660 nm, 670 nm and 680 nm measured at 77 K.	99
5.16	Fluorescence intensities from two decay components.	100
5.17	Kinetic model for the data simulation in PSI emission region.	102
5.18	Fluorescence decay curves of DES15 and the theoretical fitting by using model \mathfrak{h} .	105
5.19	Fluorescence decay curves of 10-3C and the theoretical fitting by using model \mathfrak{h} .	106
5.20	Fluorescence decay curves of B1 and the theoretical fitting by using model \mathfrak{h} .	107

INTRODUCTION

Photosynthesis is the process in which green plants, algae and some types of bacteria capture solar energy and convert it into chemically useful energy that is used to synthesize organic compounds from inorganic materials. The major outcome of photosynthesis is the conversion of carbon dioxide and water to carbohydrates and oxygen [1,2]. The overall reaction can be described with the following equation:



Here (CH₂O) represents a carbohydrate. The fundamental and applied aspects of photosynthesis interest a wide range of scientists. Detailed and comprehensive knowledge of this process enables us to understand how nature handles energy capture and conversion and may allow us to apply the knowledge to harvest and use solar energy in the future.

The primary process of photosynthesis can be divided into two parts: a physical part and a chemical part. The function of the physical part is of light capture and transfer and that of the chemical part is to convert light energy into chemical energy through a series of oxidation-reduction reactions. One of the things which interests physicists is to find energy transfer pathways in the photosynthetic systems by using physical methods. Investigating the physical part of photosynthesis provides information about the organization and function of pigments involved and the dependence of the photosynthetic system on its environment.

In green plants and green algae, photosynthesis occurs in a special organelle called the chloroplast, the detailed structure of which is discussed in chapter 2.

Chlorophylls are the principal molecules in the chloroplast that absorb and transfer the excitation energy. They associate with optical transparent polypeptides to form complexes. A very small number of chlorophyll molecules are located in special sites called reaction centers (RC) where photochemical reactions occur. Others serve as “antennae”, part of them in contact with RCs and part of them distant. Those functionally and spectrally defined pigment protein complexes form a large network to channel the excitation energy to the RC [3,4]. Information of energy capture and transfer can be obtained from spectroscopic studies. Fluorescence, for example, is the “waste” of the photosynthesis. Under normal physiological conditions only up to 2% of the excitation is released through this channel [5], but it has proved to be a valuable probe in elucidating many processes (see review [6,7]) because it provides a direct measure of the excited electronic state population that results from the absorption of light and excitation transfer. The quantities usually measured are the wavelengths of the fluorescence emission bands, their shapes, and their fluorescence rise and decay times. Excitation transfer within photosynthetic systems is a highly efficient process; the transfer time between molecules can be as short as picoseconds (10^{-12} s) or even femtoseconds (10^{-15} s) [8]. Therefore studies in the short time region play a very important role in the kinetics of photosynthesis.

The complexity of some photosynthetic systems and the spectral overlapping of its components make the spectral study difficult. One way to enhance the resolution of individual pigment-protein complexes in a complex spectrum is to vary the temperature. At low temperatures, with the energy transfer and photochemical processes are still active inside photosynthetic membranes [9], the spectra show more and clearer structures and temperature-dependent changes of the spectra provide additional information for elucidating the data at physiological temperatures.

In order to understand the working principles of the primary events of photosynthesis, the following questions have usually been posed: what are the energy transfer processes from the antenna part to the RCs and what are the pigment complexes involved in each of the processes? In this study, the rates of excitation energy transfer between some of the pigment complexes of spinach chloroplasts and of the green alga Chlamydomonas reinhardtii (C. reinhardtii) were measured by using picosecond time-resolved fluorescence techniques at low temperatures and different detection wavelengths. A short-lived fluorescence emission which corresponds to a rapid energy transfer was resolved from spinach chloroplasts at low temperatures. Further studies on the green alga C. reinhardtii and its mutants provided information for the origin of this fast transfer and substantiated our model for energy transfer pathways. Chapter 2 gives an overview of the structure and organization of the photosynthetic apparatus, a description of primary processes of photosynthesis, and a brief review of the physical approaches to the study of photosynthesis. Chapter 3 contains the specific experimental procedures and the techniques used in this study. Chapter 4 describes our study for resolving a short-lived fluorescence component from green-plant chloroplasts at low temperatures. A kinetic model of energy transfer is proposed to explain the results. Further study on the green alga C. reinhardtii and its various mutants, described in chapter 5, provides additional support to the assignment of the origins of the fast energy transfer.

Chapter 2 Background

2.1 Overview of Photosynthesis Studies

Photosynthesis is a complex process. A knowledge of biology, chemistry, engineering and physics is required to understand all of its working principles. From a physical point of view, the photosynthetic apparatus is a very well organized system with high heterogeneity. Since its mass densities, binding energies, optical properties and other physical characteristics are similar to those of liquids and solids, many principles of the liquid and solid state can be applied to study the physical properties of the system [10]. However, care must be taken when applying these principles to biological systems, since very specific details must be considered.

2.2 Structure and Function of the Photosynthetic Apparatus in Green Plants and Green Algae

The interactions between pigment molecules that carry out photosynthesis require a large complex network which leads to a multilevel-organized system. In this overview, the organizational schemes of the photosynthetic apparatus will be described in order from large scale to small scale.

A. Chloroplasts

In green plants and green algae, chloroplasts contain the basic photosynthetic apparatus within the plant cells. A cell of a higher plant, shown in Fig. 2.1a, contains typically 20 to 40 chloroplasts. Fig. 2.1b is a thin-section electron micrograph of a

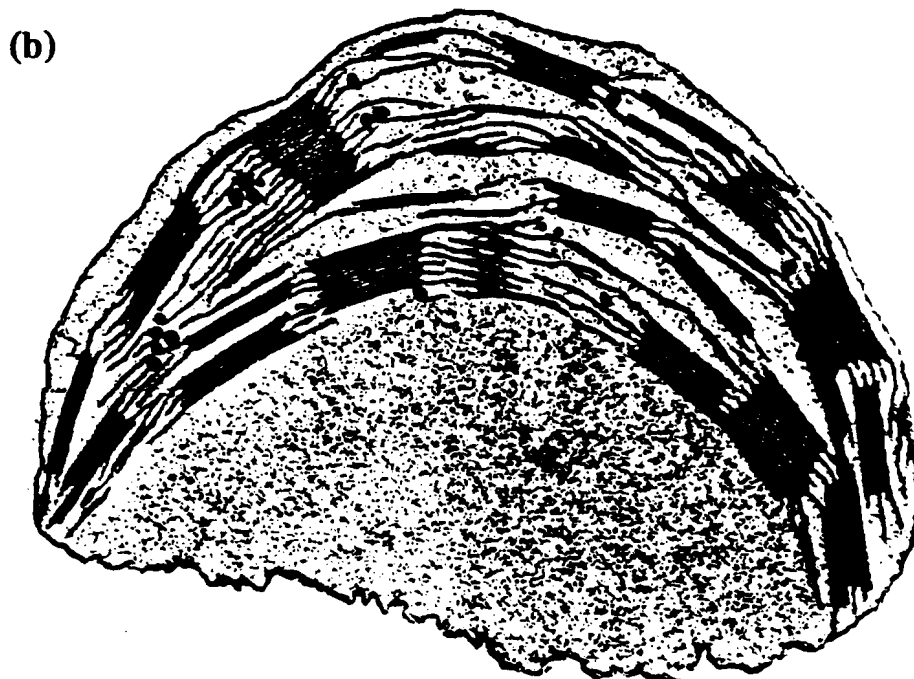
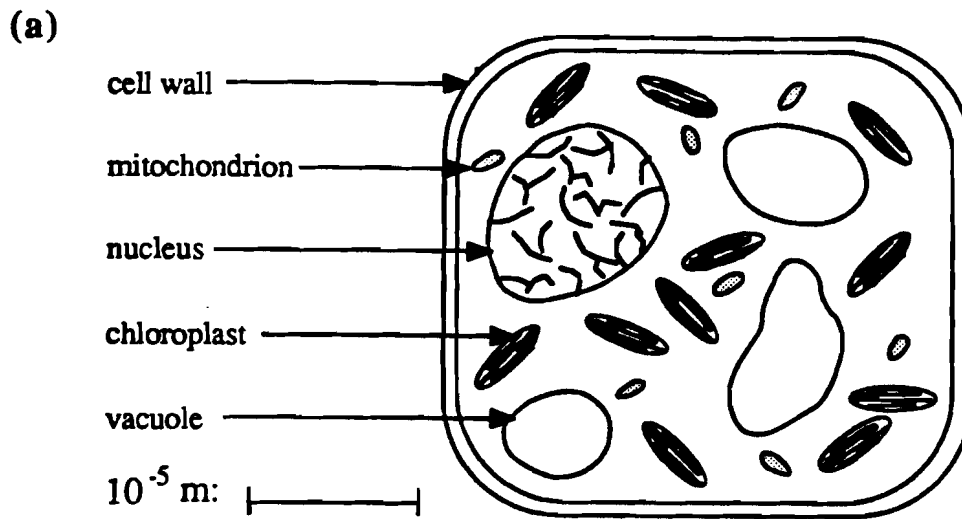


Fig. 2.1 Photosynthetic structures of higher plants: (a) a plant cell and its organelles; (b) a thin-section electron micrograph of a spinach chloroplast. Thylakoids are distinctly differentiated into stacked regions (grana) and unstacked regions (stroma) (Micrograph courtesy of K.R. Miller).

chloroplast isolated from a spinach leaf. Its length is 5-7 μm on the long axis and it is 1-3 μm in thickness [11]. The chloroplast envelope membrane surrounds a stroma containing soluble enzymes and thylakoid membranes. The sheet-like parts are the thylakoid membranes which actually exist as flattened vesicles. The stacked parts of the thylakoids are called grana and the unstacked parts are the stromal thylakoids. Processes of light harvesting, energy transduction and conversion are confined in thylakoid membranes. The energy-storing products synthesized by the thylakoids are utilized by enzymes to convert CO_2 to sugar in the stroma. A single chloroplast of the green alga C. reinhardtii has many features in common with those of green plant chloroplasts although its shape is different. It contains a single cup-shaped chloroplast which is filled with long thylakoid membranes without clear differentiation into grana and stroma [11].

B. Light-Harvesting Complex Proteins and the Photosystems

The thylakoid membranes of the green plant and green algae chloroplasts contain lipids and proteins in a weight ratio of about one to one. There are five major functional assemblies within the membranes. Three of them are involved in the excitation energy transfer processes. They are the light-harvesting complexes (LHC), photosystem I (PSI), and photosystem II (PSII). The other two assemblies are the carriers, the cytochrome b_6 -f complex, for electron and proton transport across the membrane and the coupling factor complex for ATP (adenosine triphosphate) synthesis to store chemical energy. Fig. 2.2 is an illustration of part of thylakoid membranes which gives a topological view of the photosynthetic apparatus and processes. Those assemblies composed of pigments and proteins are embedded within the lipid bilayer of the membrane in a specific organization determined by their physical and chemical

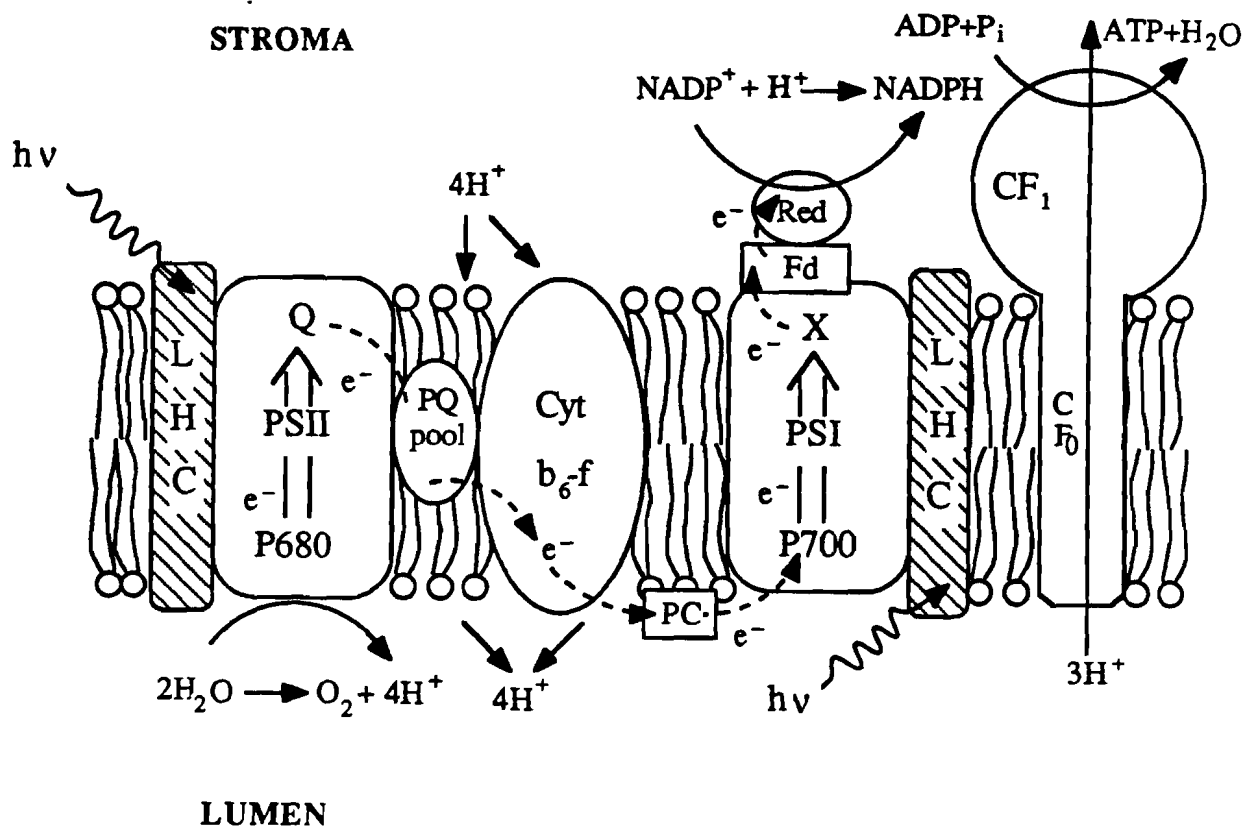


Fig. 2.2 Organization of thylakoid membranes. Five functional assemblies embedding in lipid bilayer membranes are: LHC (light-harvesting complex), PSI (photosystem I), PSII (photosystem II), Cyt b_6 -f (the cytochrome b_6 -f complex) and CF_0 - CF_1 ATP synthetase complex. The sequence of photochemical reactions, electron transport, ATP synthesis and oxidation of $NADP^+$ are also shown. Other elements are: Q, the electron acceptor of PSII; PQ, plastoquinone; PC, plastocyanin; X, the electron acceptor of PSI; Fd, ferredoxin; Red, $NADP^+$ reductase; CF_0 and CF_1 , the ATPase.

properties [12-14].

LHC, composed of chlorophyll a/b proteins and other pigments, serves as the primary system antenna. Its role is to absorb and transfer light to the photosystems. Recent studies show that the LHC a/b-protein complex has various forms which associate with different part of the photosystems [3,15,16].

PSI and PSII contain mainly chlorophyll a molecules. Each of these photosystems has its own RC. About 1 out of 200 chlorophyll molecules in PSI and PSII are associated with RCs. In the RC of PSII there is a dimer of chlorophyll a-molecule (P680) with its absorption maximum around 680 nm. It becomes the primary electron donor after excitation [17]. In the RC of PSI, a dimer of chlorophyll a-molecule with its absorption maximum at 700 nm (P700), plays a similar role [18].

C. Chlorophyll Molecules and Protein Complexes

Chlorophyll molecules are the major pigments of photosynthesis. They are associated with the polypeptides in the form of chlorophyll-protein complexes [19]. The chemical structures of chlorophyll a, chlorophyll b and an X-ray structure of a bacteriochlorophyll a-protein from the green photosynthetic bacterium Prosthecochloris aestuarii [20] are shown in Fig. 2.3. (As of this writing, structures of chlorophyll a/b proteins have not yet been determined in atomic detail. However, the structures are expected to be similar to that of the bacteriochlorophyll a-protein.) Probably a primary function of the protein in these complexes is to maintain an optimal geometry for energy transfer between molecules. About 50% of chlorophyll a molecules and almost all chlorophyll b in higher plants and green algae belong to the chlorophyll a/b protein complexes. Recent studies show that LHC is a trimer consisting of three monomers with 8 chlorophyll a and 7 chlorophyll b per monomer [21-24]. Two other major

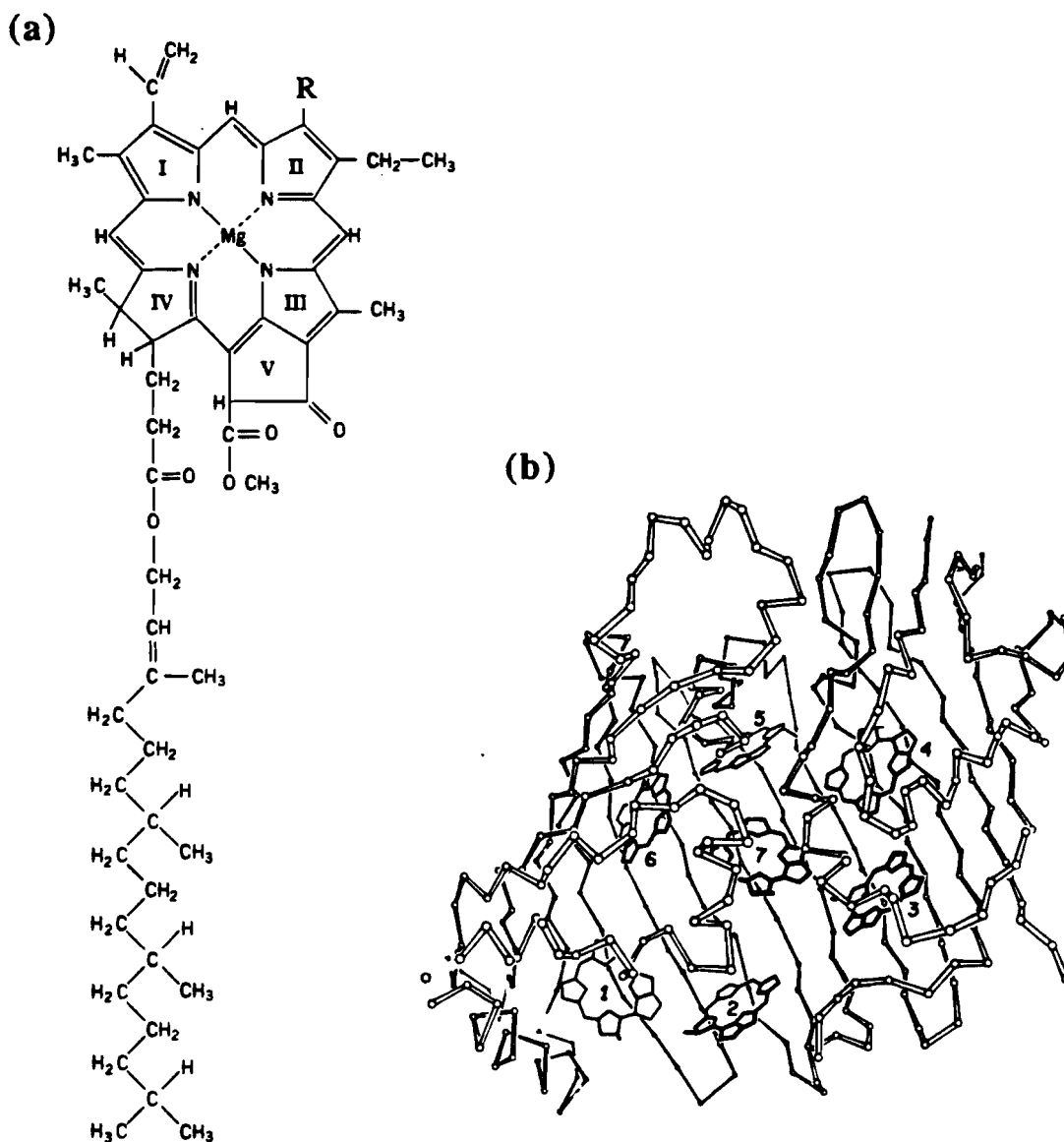


Fig. 2.3 Structures of chlorophyll molecule and pigment protein. (a) Structure of chlorophyll **a** ($R = \text{CH}_3$) and chlorophyll **b** ($R = \text{CHO}$). (b) X-ray structure of a bacteriochlorophyll **a**-protein from the green photosynthetic bacterium *Prosthecochloris aestuarii*. Bacteriochlorophylls (Bchl) (the numbered structures) attach to the backbone which is formed by polypeptides. (reproduced with permission from [20]).

functional chlorophyll a-protein complexes are associated with PSI and PSII respectively. Their structures and compositions vary from pigment to pigment and are still under investigation.

Absorption spectra of chlorophyll a and b in methanol are shown in Fig. 2.4a. The spectral properties of the complex are different from those of individual chlorophyll molecules in solution. For example, the absorption spectrum of intact chloroplast (Fig. 2.4b) is quite different from that of chlorophyll a or b in solution. The environment within the chlorophyll-protein complex is responsible for the changes.

Because of their similar structure and thylakoid membrane organization of the photosynthetic unit, the green plant chloroplasts and green algae can be described by similar energy transfer kinetics.

2.3 Primary Processes of Photosynthesis

A. Physical Process: Excitation Energy Transfer

An electronic excited state of a molecule is created when it absorbs a photon. There are a number of ways for this excited molecule to revert to the ground state: by transferring the excitation energy to another molecule, by forming a triplet excited state and phosphorescing, by fluorescing or undergoing other nonradiative processes such as dissipating heat to the bath. Within the photosynthetic units most of the excitation energy is transferred step by step quickly enough that it is trapped by the RC before other processes destroy it. At the RC photochemical conversion can take place or, instead, the exciton can hop back into the antenna pigment. An excitation may visit the RC many times before it is used in the process of photochemical conversion. The characteristic times for energy transfer from pigment to pigment vary from

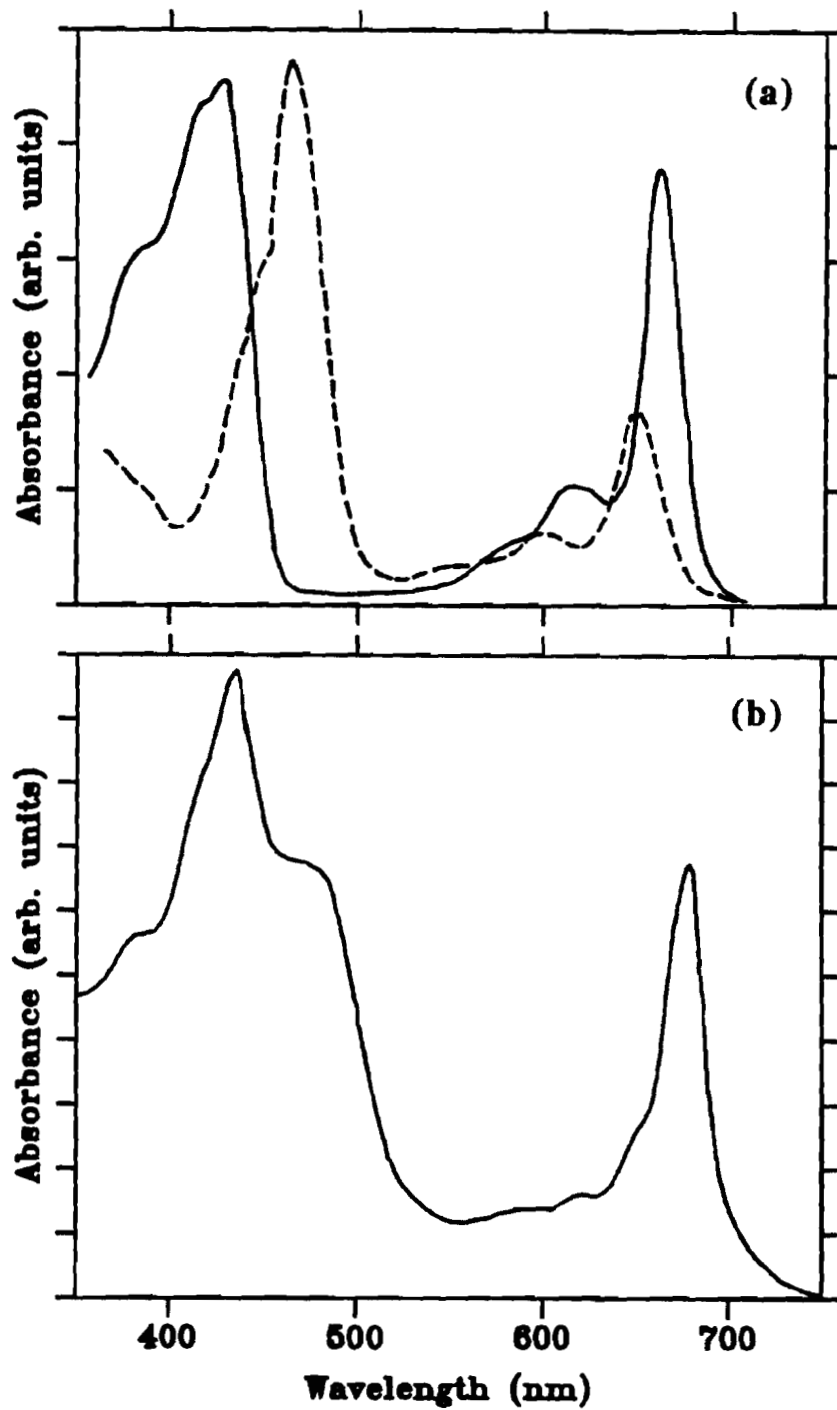


Fig. 2.4 Room temperature absorption spectra of (a) chlorophyll a (solid line) and chlorophyll b (dashed line) in methanol and (b) spinach chloroplasts.

femtoseconds to picoseconds, depending on the geometry and the environment of the pigments [25-27].

B. Chemical Process: Energy Conversion

A chemical process starts after the excitation energy is trapped by the RC. In contrast to the antenna chlorophylls, the chlorophyll molecules located in the RC are photochemically active. A "series scheme" has been found to be very successful to describe the initial chemical process of photosynthesis (Fig. 2.5). When the primary electron donor of PSII (P680) traps a exciton, it forms an excited state. Then P680 provides an electron which goes through a series of electron transfer components to P700, P700 being previously photo-oxidized. H_2O supplies the electrons needed to fill the holes produced by P680 electron transfer, liberating oxygen molecules and creating H^+ ions. During the electron transport from P680 to P700, ADP (adenosine diphosphate) is converted to ATP and free energy is stored. When P700 is excited, it donates an electron through an electron transport chain to convert $NADP^+$ (nicotinamide adenine dinucleotide phosphate) to NADPH (a reduced form of $NADP^+$), thus storing energy. A cyclic electron transport process occurs when there is insufficient $NADP^+$ to accept electrons. In this case, an electron generated from P700 flows back to the oxidized form of P700 through an electron transport chain and ATP is generated without NADPH formation. Eventually the energy-rich molecules ATP and NADPH are used to convert CO_2 to glucose. The two photosystems work cooperatively to complete the processes of photosynthesis. At least eight photons (with energy equal to or greater than 1.8 eV for each) are required to drive the chemical reaction to produce one O_2 and one carbohydrate (CH_2O) unit and store approximately 4.8 eV of energy for the use of biosynthesis [28,29].

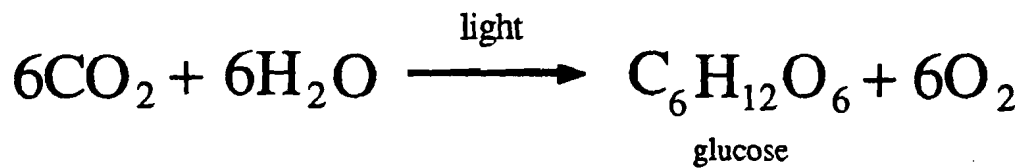
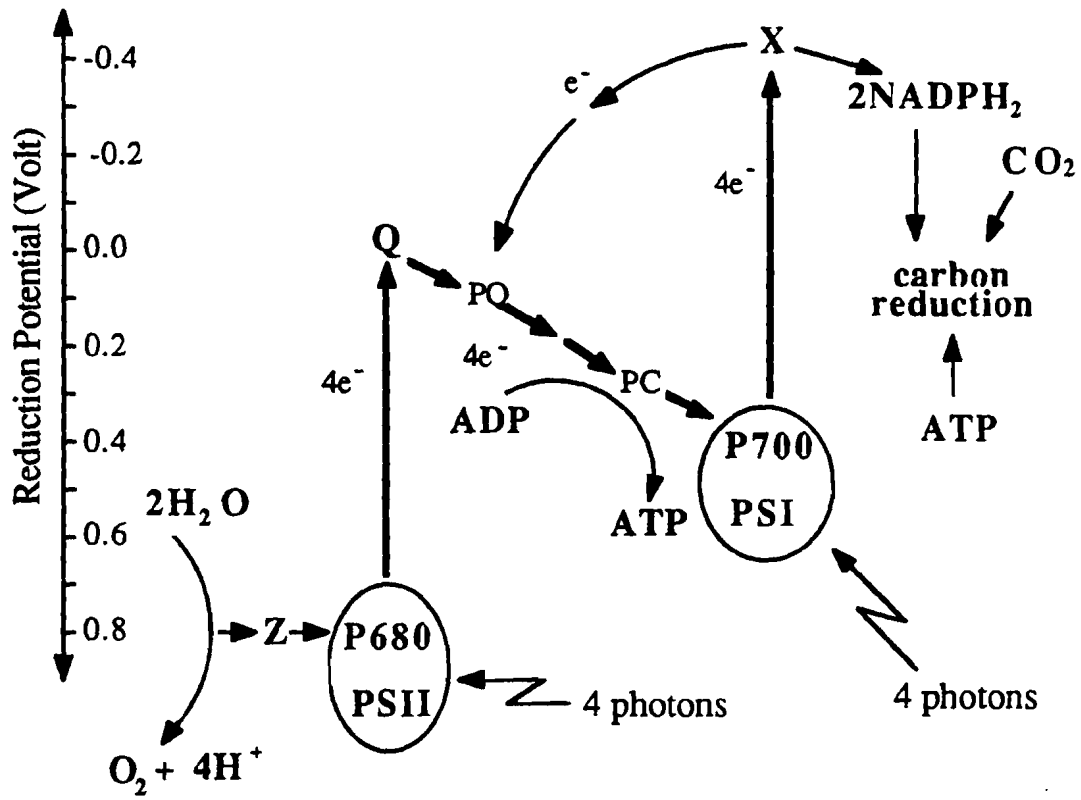


Fig. 2.5 The series scheme for describing the initial chemical processes of photosynthesis. The processes of light absorption, electron transport, H_2O splitting, ATP and NADPH generation are illustrated. For details, see text, section 2.3. The numbers in the reactions are not necessarily stoichiometric.

At the RC of PSII, the first three members in the electron transfer chain are those of the electron donor P680, the primary electron acceptor pheophytin I and the electron acceptor, a quinone Q. After the charge separation occurs between the P680 and I, the latter is reduced and it then delivers the electron to the quinone Q. In the case that Q is reduced chemically or optically, it can not accept the electron from I anymore, thus the electron transfer is blocked. A RC of PSII is closed if Q is reduced, otherwise it is open.

2.4 Mechanism and Models of Energy Transfer

Understanding the mechanism of energy transfer in photosynthesis has been a goal for decades. Both theoretical and experimental approaches have been made. A noncoherent random-walk process is believed to be the mechanism of excitation migration among molecules in the majority of cases (for discussion of the role of coherence, see references [30]). The interaction between molecules which causes energy transfer is a long range transition dipole-dipole interaction. The theory of this process was developed by Förster [31]. The exciton transfer rate may be calculated from

$$k_{DA} = (1/\tau_D)(R_0/R)^6 \quad (2.1).$$

Here k_{DA} is the energy transfer rate from the donor to the acceptor molecule; τ_D is the lifetime of the donor; R is the distance between the donor and acceptor molecules and R_0 is called the critical transfer distance which is defined in eq. 2.2.

$$R_0^6 = (3/4\pi)(c/2\pi n)^4 \int_0^{\infty} [I(\nu)\sigma(\nu)/\nu^4] d\nu \quad (2.2)$$

In equation 2.2, c is the speed of the light; n is the refractive index of the solvent; ν is optical frequency; $I(\nu)$ is the spectral distribution of fluorescence of the donor (measured in quanta per unit frequency) and $\sigma(\nu)$ is the optical cross-section of the acceptor. This equation is an average of the R_0^6 factor over all mutual orientations of the donor and acceptor transition dipoles [31]. We see therefore that the transfer rate depends on the distance between the two molecules and the overlap of the fluorescence spectrum of the donor with the absorption spectrum of the acceptor. The formula thus provides a way to estimate the probabilities of energy transfer between molecules in a given system.

A. Three Levels of Studies

Photosynthetic systems such as green-plant and green-alga chloroplasts are the most complicated, with highly overlapping spectra. Therefore, to understand the energy transfer processes in such systems one must approach the problem in many ways. The methods used in time-dependent spectroscopic studies of excited state kinetics have been classified according to three levels: the physical level, the compartmental level and the decay level [32].

(i) Physical Level

Study at this level is based on the knowledge of the mechanisms described above and a proposed or known structure of the system in which an individual molecule or

pigment-protein complex is considered as the basic unit. The goal is to relate measured observables with the physical quantities which describe the details of the mechanism of the excitation migration in the system. Theoretical approaches have been made including the work of Knox [33,34], Pearlstein [35] and Paillotin [36,37]. A summary of the work has been recently provided by Van Grondelle [27]. Generally it is assumed that the antenna molecules or protein complexes occupy the sites of a regular lattice to form an array and an exciton undergoes a random walk process from one molecule to another until it is trapped by an RC. Physical quantities, such as the random walk lifetime, first passage time and single-step hopping time are calculated from various proposed models, which are in turn related to the experimentally measurable quantities.

As an example of a calculation at the “physical level”, Pearlstein proposed a method to determine the first passage time experimentally [38]. In his simplest model calculation, N antenna molecules and one RC are assumed to form a regular lattice ($N \gg 1$). An exciton can be generated anywhere with an equal probability and executes a random walk until it reaches the trap (RC). At the trap, it can be either returned to the antenna or used to initialize the photochemical process. The random walk lifetime of an exciton can be expressed as a function of the number of antenna molecules N , a factor which depends on the geometry of the lattice, the Förster transfer rate between adjacent antenna molecules, and the rates for an exciton to transfer into and out of the trap. This lifetime is further related to the probability of exciting an RC and the first passage time. From this relationship, the first passage time and other transfer rates can be determined by measuring the fluorescence decay time at selected wavelengths which excite different portions of the RC. The prediction gives a rather straightforward relationship between the physical parameters and experimental observables which needs to be studied further by experiment.

Most of the studies at the physical level are based on the assumed or known structures of the system on a molecular level. Since very little is known on details about the arrangement of individual pigment molecules in most antenna complexes, the problem of relating experimental observations to specific structural features is difficult. In addition, there are too many parameters to take into account in the model while only a few of them are measurable, therefore the uncertainty of the solution is large. Indeed, models at the physical level often involve assumptions or implications which are readily dashed by experiment; for example, Freiberg's report on the fluorescence measurement of R. rubrum showed independence of the decay profile with excitation wavelength [39], so the Pearlstein calculation would be difficult to use in this case.

(ii) Compartmental Level

A compartmental or species-associated level of study is based on the collective properties of the various components, classified either by pigment type or by actual units (PSI, PSII LHC, for example). Thus all microscopic details of the energy transfer, trapping and detrapping processes are neglected. Model parameters are commonly used to simulate the experimental curves. It is a useful approach for simulation of excitation migration and for attempting to correlate the resulting fluorescence properties from a model system. At this level, kinetic models are proposed to associate with energy distribution, transfer rates and fluorescence spectral characteristics of the system. Details such as the structure related to the RC and antenna size, the statistical considerations of energy transfer and arrival times are replaced by phenomenological kinetic rate constants referring to processes within and between components.

For example, in a three-population kinetic model the time-dependence of the excited state populations are expressed in terms of intrinsic fluorescence lifetimes, excitation transfer rates between compartmental elements, absorption cross-sections, annihilation rates and so on [see chapter 3 for the equations]. The excited state population is proportional to the fluorescence intensity at a particular wavelength; therefore the solution of the equations can be used to simulate the profile of the fluorescence decay curve. Wittmershaus *et al.* studied the time-dependent fluorescence decay of spinach chloroplasts at 77 K [40]. The decay profiles at 685 nm changed upon exciting the sample at different intensities. Rise phase changes were mainly observed in the 735 nm region, where a biphasic rise appeared at low excitation intensity and a monophasic rise at high intensity. A three-population kinetic model was used to fit the decay curves. For the data taken at 685 nm, the result suggests that energy is transferred from a large pool of antenna chlorophyll to a small pool closely connected to the RC of PSII and all exciton annihilation occurs in the small pool. For the fluorescence at 735 nm, the biphasic rise and its sensitivity to the excitation intensity are explained by a three-pools model. The three pools are “nearby” and “distant” pools related to a third pool which is the only one contributing to fluorescence. The “nearby” pool of excitation first flows into the fluorescing species at a high rate and after the “nearby” pool’s initial population is transferred, the “distant” pool supplies its excitation at a limited rate.

There are still more kinetic parameters in the models than experimental observables, so it is still not sufficient to accurately determine all the parameters in the model. However, study at the compartmental level is a lot better in this aspect than that at the physical level. Two major efforts can be made to improve the solutions. One is to vary the experimentally controllable parameters, such as the excitation intensity as in

Wittmershaus's work. The other is to get parameters from other independent experiments or from the literature.

(iii) Decay Level

Studies at this level involve extracting parameters directly from the experiments. In the case of fluorescence decay measurements, it is generally assumed that each curve can be described by a sum-of-exponentials convoluted with the system response of the excitation pulse. Each decay lifetime might correspond to an eigenvalue of the matrix of kinetic coefficients in the equations mentioned above (compartmental level). The amplitude of a component is often assumed associated with the absorption cross-section of the antenna pigments. By solving the kinetic equations at the compartmental level, expressions for the decay lifetimes and amplitudes in terms of kinetic model parameters can be obtained in principle [41]. While the decay-level fitting parameters are well defined and related with the experimental data directly, their relationship with kinetic parameters is not necessarily simple. As at the compartmental level, additional information is needed from other sources to relate the picture to a deeper level.

Schatz *et al.* measured time-dependent fluorescence of PSII particles isolated from a blue-green alga *Synechococcus* by using photon counting techniques [42a]. The two-exponential fit indicates decay lifetimes of 80 and 520 ps with open RC and 220 and 1300 ps with closed RC. The fluorescence yield increased 3-4 fold in the latter case. A kinetic model of the primary reactions in the RCs of PSII was proposed which included the rate constants for describing the processes of radiative decay, charge separation, charge recombination and charge stabilization [42b]. The absorbance change measured by pump-probe apparatus was used as the additional information in solving the kinetic parameters. One of the interesting results from the model calculation was that the long-

lived fluorescence component is the emission from equilibrated excited states of antenna chlorophyll rather than the charge-recombination luminescence as suggested by Klimov [43].

Generally speaking, study at the physical level deals with more detailed physical properties of the system; on the other hand, studies at the compartmental level and at the decay level are more directly related to the experimental observables. There are connections among the three levels of study. The compartmental parameters can be, in some cases, related to the quantities at the physical level and a component at the decay level can be expressed in terms of the compartmental parameters. In this study, the methods of the compartmental level are used.

B. Spectral Studies and Kinetic Models For Energy Transfer in Chloroplasts at Low Temperatures

For a quantitative description of the energy transfer process in a given case, two kinds of information are required: the spectra associated with individual components and their time behavior, which can be obtained from steady-state and time-resolved fluorescence measurements, respectively. A very large number of papers have dealt with the process of sorting out the compartments of the spectra of green plants and green algae. The brief review here will concentrate only on two aspects of special relevance to us: characterization of the emission bands in terms of pigment complexes at low temperatures and picosecond fluorescence kinetics related to the energy transfer between the pigment complexes.

(i) Steady-State Fluorescence Studies

The fluorescence of *in vivo* photosynthetic systems is not homogeneous in origin.

Steady-state emission spectra of spinach chloroplasts measured at room temperature (dashed line) and 77 K (solid line) are shown in Fig. 2.6. At 295 K, the spectrum of green plant chloroplasts contains a major band at 685 nm, mostly from PSII, and a broad shoulder in the region of 710-740 nm attributed to PSI [27,44,45]. The spectrum at 77 K is markedly different from that at 295 K. Five emission bands, F680, F685, F695, F720 and F735, are generally resolved [46-49]*. The spectrum of green algae at 77 K is similar to that of green plant chloroplasts on the short wavelength side, containing F680, F685 and F695, while at longer wavelengths the emission bands are F707 and F717 which originate from PSI [50,51].

Characterization of the emission bands has been made in terms of the pigment-protein complexes involved in the energy transfer processes or emission (see a review [45]). Assigning the origin of the emission bands has also been approached by investigating isolated particles or photosynthetic mutants to reduce the complexity of the photosynthetic system. Based on the facts that F680 disappears in mutant chloroplasts missing LHC [48,49] and that the purified LHC has its emission maximum at 680 nm [52-54], the emission band at 680 nm is assigned to LHC emission. The fluorescence yields of F685 and F695 change with the redox state of the RC of PSII and the similarity is observed in the study of isolated PSII particles and LHC-less mutants [55-57]. The F685 band is attributed mostly to PSII emission and probably a small part contributed by LHC [58]. Most F695 is thought to originate from PSII. However, there exists disagreement about the precise origin of the F695 [42,43,59-61]; a clear consensus awaits further work. The emission band F720 of chloroplasts is attributed

* We use abbreviation "F_{nnn}" to denote fluorescent emission centered at nnn nm and "C_{nnn}" for absorption band centered at nnn nm.

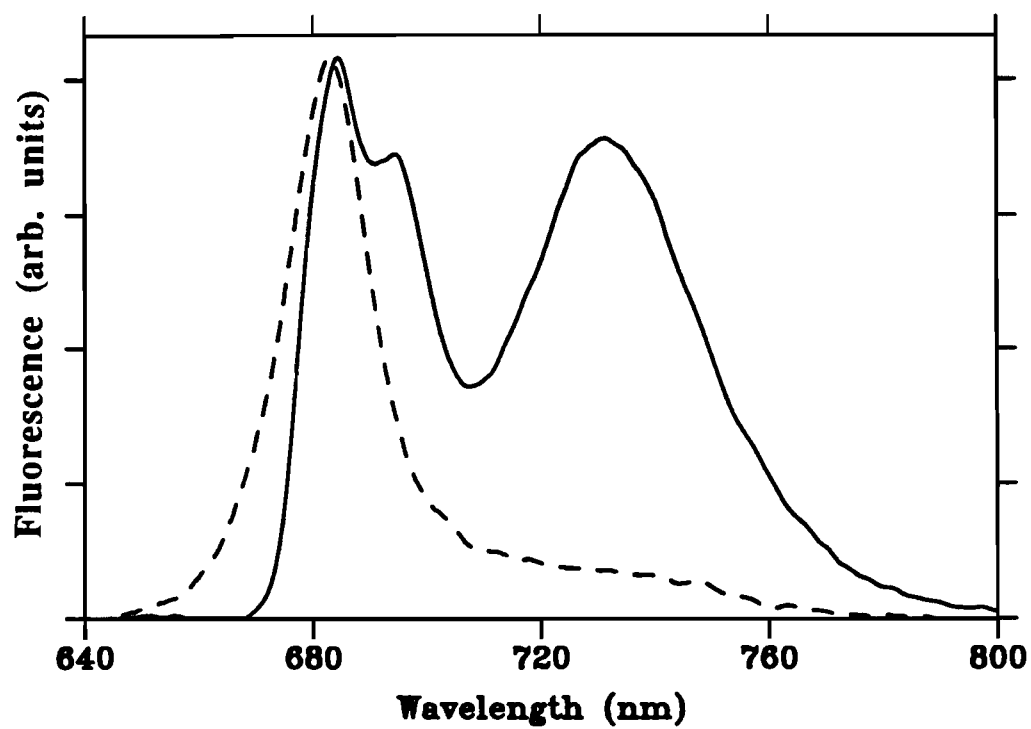


Fig. 2.6 Fluorescence emission spectra of spinach chloroplasts at room temperature (dashed line) and at 77 K (solid line).

to the internal antenna (a pigment called C697) of PSI while F735 is attributed to a pigment C705 which is part of the PSI complex [3,62]. The PSI fluorescence has been studied extensively in isolated PSI particles (for details see [57,63,64]). Similar studies on the green alga C. reinhardtii and its various mutants were done by Garnier et al. [51]. Each emission band at 77 K was associated with a specific pigment. The details are discussed in chapter 5.

In spectral studies, it is generally assumed that the different fluorescence components arise from different portions of the antenna pigment complex or from the RCs themselves, but definite evidence to support this assumption is lacking. The complexity of the network of deexcitation paths available in vivo has complicated the analysis and interpretation of fluorescence in photosynthetic systems. The assignment of an emission band to a particular photosynthetic pigment is tentative in most cases.

(ii) Time-Resolved Fluorescence Studies

Various kinetic models for excitation energy distribution and transfer have been proposed based on the spectral properties and the time dependent behaviors of the fluorescence (see recent reviews [7,65,66]). Fluorescence characteristics in the time domain provide information about the path of excitation flow and excitation transfer, trapping and even the repopulation of excited electronic states. In picosecond studies, several groups have reported the detection of three to four decay components in the 50-3000 ps time range [67-71] at room temperature. At low temperatures, time-dependent fluorescence is investigated in two wavelength regions: wavelengths below 700 nm, mainly associated with PSII kinetics, and those above 700 nm, associated with PSI kinetics.

In the PSII emission region, measurements with intact thylakoids or isolated PSII particles show that at least three exponentials are required to fit the decay curves [72-75]. In Reisberg's experiment, the three decay components were similar to those at room temperatures and were thus assigned to have the same origin independent of temperature, mainly from PSII [75]. However, one has to be careful in interpreting the meaning of these decay lifetimes. In the previous studies, those decay components were either related directly to the transfer rates in the kinetic model or converted to the kinetic parameters such as excitation transfer rates and charge separation rates. Clear and definite relationships between the transfer rates and emission bands are lacking. There are some studies which investigated the time-dependent fluorescence at various wavelengths and related transfer rates with specific emission bands. Avarmaa *et al.* measured the time-dependent fluorescence of PSII particles at wavelengths 681, 685 and 695 nm at low temperatures [76]. A tentative scheme of excitation transfer was proposed in which energy is transferred from light-harvesting system of PSII (F681 and F685) to the RC (F695). A time-resolved fluorescence spectra study done by Mimuro *et al.* provided a more complete picture of the time-dependent behavior of each emission band [77]. An emission band at 680 nm appeared right after the excitation, shifted to 685 nm within 160 ps and further shifted to 695 nm within 350 ps. The entire process was explained as energy flow from LHCI to the 685 nm component and further to the 695 nm component, the latter two being assigned to PSII chlorophyll *a*. However, no quantitative compartmental model was proposed.

Upon cooling, a remarkable change has been observed in the long wavelength region where PSI emits (F735). A risetime of 50-150 ps and a decay time around 3 ns are observed [75,78,79]. This is not seen at room temperature. Utilizing the streak camera detecting system with the capability of measuring the fluorescence risetime in a

picosecond order, Wittmershaus *et al.* measured time-resolved fluorescence from spinach chloroplasts at 77 K and revealed a biphasic rise [40]. A three-pool kinetic model was proposed to explain the data, as already mentioned in section 2.4.A. The fluorescence kinetics in this region were extensively investigated on the various isolated PSI particles which gave a detailed model [64,80,81].

The heterogeneous origin of the fluorescence from photosynthetic membranes is clearly shown in these kinetic studies. Our knowledge of the whole process of the energy transfer is limited by incomplete experimental data. Two useful approaches have been made in this study to provide more information for better describing the energy transfer process in photosynthesis. They are: (1) to relate the room temperature data with low temperature data and (2) to relate the fluorescence origin of the fluorescence assigned from steady-state spectra with time-dependent data.

2.5 Questions to be Answered

The goal of the study reported here is to identify and characterize a kinetic component which gives information about energy transfer from LHC to PSII. The spectral properties of this component have been studied at low temperatures [47,48]. The questions to be answered in the study are: what is the energy transfer rate and pathway between LHC and PSII? How does this transfer process change with different conditions and associate with other parts of the system? Time-dependent fluorescence from spinach chloroplasts and the green alga *C. reinhardtii* were measured at low temperatures to investigate the questions posed.

Chapter 3. Materials and Methods

3.1 Sample Preparation

A. Spinach Chloroplasts

Fresh spinach leaves were obtained from a local supermarket (Chummy Bunny brand). The sample preparation procedures for obtaining chloroplasts are those of Breton, Roux and Whitmarsh [82]. The leaves were washed and ground in a buffer solution of 20 mM Tris at pH 8.0, 0.4 mM sucrose and 20 mM KCl. After centrifugation at about 2000g for 1 minute the top and middle part of the pellet were taken and resuspended in the same buffer. The sample was kept in the dark on ice until use. Before low temperature measurements, the suspension of chloroplasts was diluted with the same buffer solution and mixed with about $75 \pm 10\%$ (v/v ratio) of glycerol to a final concentration of 0.1 to 0.4 optical density (OD) at 532 nm in order to prevent crystallization upon cooling.

B. C. reinhardtii and its Mutants

C. reinhardtii and its mutants were kindly provided by Prof. L. Mets of the University of Chicago. Wild-type C. reinhardtii (DES15) and five different mutant strains (called B4, LM15-4D1C, B1, 10-3C and 12-7) were studied. All of them were grown under the same conditions. The cells were kept on agar plates for long-term storage and inoculated in 100 ml of Tris-acetate phosphate (TAP) medium [83] in 200-ml Erlenmeyer flasks with a stirrer bar in each. The cells were placed on a magnetic stirrer and grown in the dark at 25°C. They were extracted for use during the

the growth curve (usually 4-6 days after inoculation), at a concentration of about 10^5 -- 10^6 cells/ml.

C. Sample Cooling

For steady-state measurements, a 4-mm diameter EPR tube (the name originates from its use in electron paramagnetic resonance measurements) was used to contain the sample. This was put into a liquid nitrogen dewar which had a clear finger for optical measurements. To cool the sample to 77 K, it was necessary first to let the EPR tube rest directly above the liquid nitrogen so that the sample froze from bottom to top to prevent the tube from cracking. Then it was put quickly into the dewar.

For time-dependent fluorescence measurements, the sample was kept in a home-made cuvette with 10 by 10 mm frontal area and 0.5 to 1 mm depth. Its back wall was made of 4 mm thick glass to prevent reflected-beam excitation. When cooling the chloroplasts, five-minute epoxy was used to seal the cuvette with the sample inside. The cuvette was then attached to the cold finger of a closed-cycle helium refrigerator system (CTI Cryogenics Model 21). The chamber was evaporated to 50 μ Torr by a roughing pump and then cooled to the desired temperature. When cooling whole cells, the same type of cuvette was used. In order to keep the cell structure unchanged during the cooling, the sample was frozen by dipping it into liquid nitrogen first, then quickly attaching it to the cold finger of the cooling system to attain temperatures equal to or lower than 77 K.

3.2 Steady-State Spectra Measurements

A. Absorption Spectra

Absorption spectra were taken on a Perkin-Elmer UV/VIS spectrophotometer model λ -3 and plotted by a Perkin-Elmer 561 recorder. The cuvette was the same as that used in the corresponding fluorescence measurement.

B. Emission and Excitation Spectra

Fluorescence emission and excitation spectra were taken on a Perkin-Elmer spectrophotometer model MPF-66 controlled by a series 7000 professional computer. The experimental configuration for measurements at 77 K is shown in Fig. 3.1. The intensity of the excitation beam was controlled by the width of the slit S1 and filters F1. Fluorescence was collected at a 90-degree angle. In order to collect more signal, a 50-mm focus lens L was added after the dewar to correct for the defocusing effect caused by the shape of the dewar and the cuvette. Short-wavelength cutoff filters F2 were used in front of the emission slit S2. Sample concentrations were kept low (OD < 0.1 at 680 nm) to avoid reabsorption. The data were later transferred and analyzed on a VAX computer (Digital Equipment Corporation).

3.3 Time-Resolved Fluorescence Measurements

A. General Description

The experimental layout is shown in Fig. 3.2. A single 1064-nm 30-ps pulse was generated from an active-passive modelocked Nd³⁺:YAG (neodymium³⁺:yttrium aluminum garnet) laser [84,85] and a Pockels cell switchout system. The pulse was

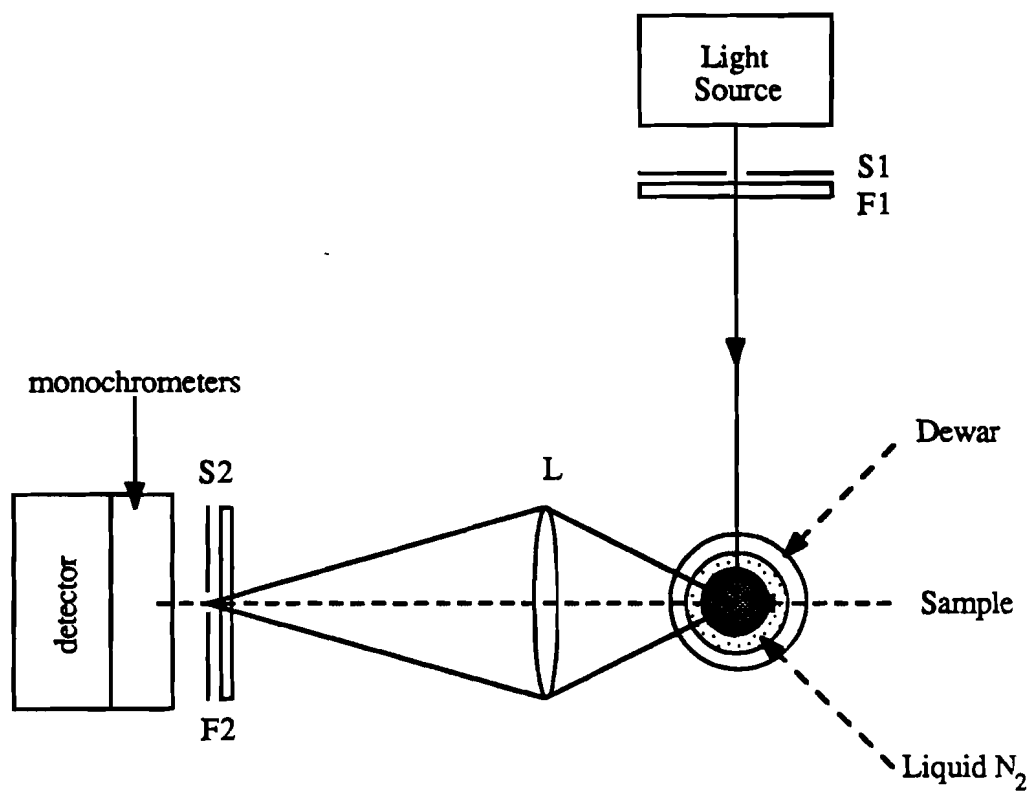


Fig. 3.1 The set up inside the sample housing of the Perkin-Elmer MPF-66 spectrophotometer for fluorescence measurements at liquid nitrogen temperature. S1 and S2 are excitation and emission slits respectively. F1 and F2 are filters. L is a focus lens.

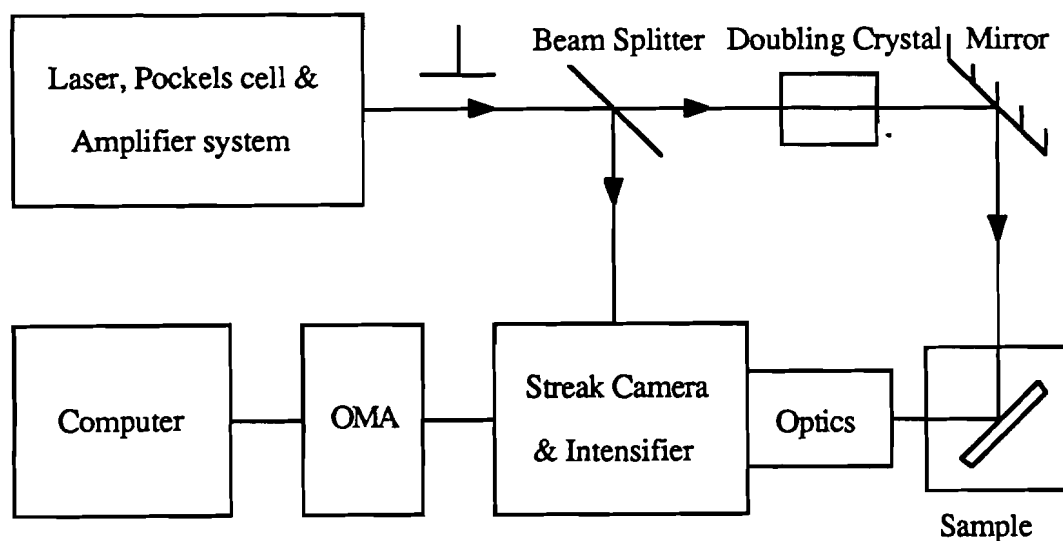


Fig. 3.2 Experimental layout for time-resolved fluorescence measurements.

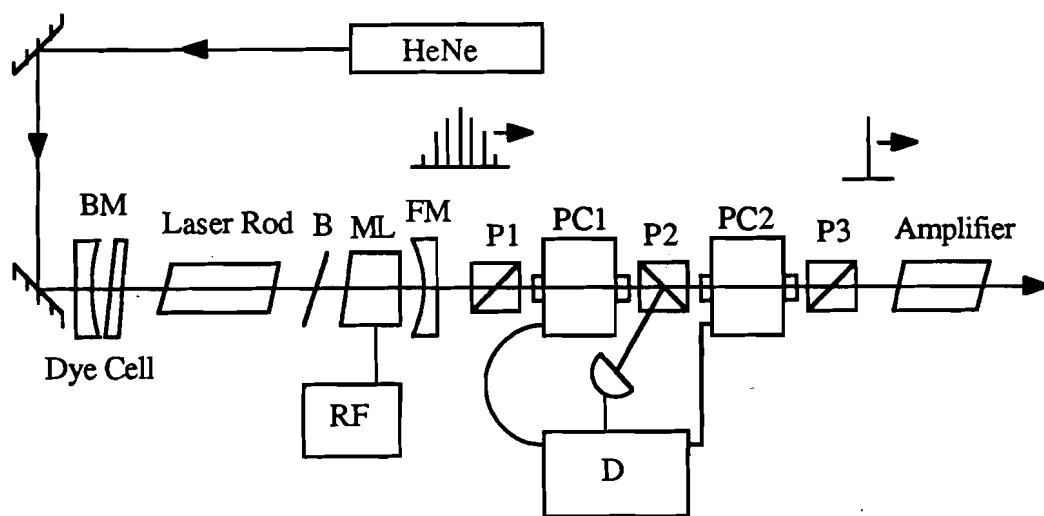


Fig. 3.3 Schematic drawing of the laser, Pockels cell and amplifier system. HeNe laser is used to align the system. FM and BM are front and back mirrors. B is a Brewster window polarizer. ML is a crystal of the acousto-optic modelocked, RF is its radio-frequency generator. P1, P2 and P3 are polarizers. PC1 and PC2 are Pockels cells controlled by a discriminator and time-delay system D.

amplified by a second laser head to 400-600 μJ . A beam splitter was used to divide the pulse into two parts. One was frequency doubled to excite the sample and the other was used to trigger a GaAs:Cr semiconductor switch in order to trigger the streak camera [86]. In most of the experiments, the excitation intensity was kept below 5×10^{13} photons/cm² per pulse in order to avoid nonlinear processes during the excitation transfer [40,87]. The sample was mounted on the cold finger of a closed-cycle helium refrigerator inside a vacuum chamber to attain low temperatures. Fluorescence was collected at a 90-degree angle by a set of collecting lenses. Various cutoff filters and interference filters were placed between the sample and lenses, the configuration depending on the measurement. A streak camera-intensifier-optical multichannel analyzer (OMA) system was used to detect, amplify and digitize the signal. An EG&G Princeton Applied Research computer (Model 1215) was used to control the experiment and record the data.

B. Laser System

A Nd³⁺:YAG laser, shown in Fig. 3.3, was used as an excitation source for the time-dependent fluorescence measurements. Inside the laser cavity were a temperature controlled acousto-optic modelocker and a flowing dye cell acting as an active and a passive modelocker respectively. Kodak Q-switch dye dissolved in chlorobenzene was used at a concentration which gave 9-12 pulses at full width half maximum (FWHM) of the pulse train envelope. These pulses were 10 ns apart. Two Pockels cells with three polarizers were used after the laser to select a single pulse out of the pulse train. The three polarizers were set up with their polarization axes perpendicular to each other. Two Pockels cells were controlled by a discriminator and a time delay system to select the central pulse with an extinction greater than 10^4 (the extinction was defined as the

ratio of the peak of the selected pulse to that of the pulse leaking through the Pockels cell system). This 1064-nm 30-ps pulse was then amplified by a second laser head to 400-600 μJ . Pulse energy was measured by an Rj-7200 Energy Ratio Meter (Laser Precision Corporation). The typical pulse energy fluctuation at 532 nm was $\pm 15\%$.

C. Detecting System

Two streak cameras were used in the experiment. One was a lab-built streak camera containing an image converter tube with a multi-alkali semi-transparent substrate of S-20 type photocathode (Delli Delti Limited, Picotron 100). The other was a Universal Temporal Disperser streak camera (Hamamatsu Photonics, Model C1587-01) with a model N2367 streak tube which had an S-1 photocathode. The two tubes work in a similar way. The main part of a streak camera is the photon-electron converter tube with a GaAs:Cr switching circuit (Fig. 3.4 [85]). Photons incident on the photocathode of the tube are converted into electrons. Those electrons are accelerated by the high voltage between cathode and anode. A focus cone is placed between the photocathode and anode to prevent electron beam dispersion. A time-dependent voltage applies to the deflecting plates changed the flight direction of the electrons to convert time information into spatial information. The arrival positions of the electrons at the phosphore screen then reflects the time course of the incident light. The sweep rate depends on the bias voltage and RC constant of the switching circuit. The starting time of the sweep voltage is controlled by the arrival of the one part of the laser pulse at the GaAs:Cr switch via an optical delay line. The signal on the phosphor screen of the streak tube amplified by the intensifier is then imaged on the vidicon detector. An optical multichannel analyzer (OMA) is coupled next to the detecting system to digitize the signal.

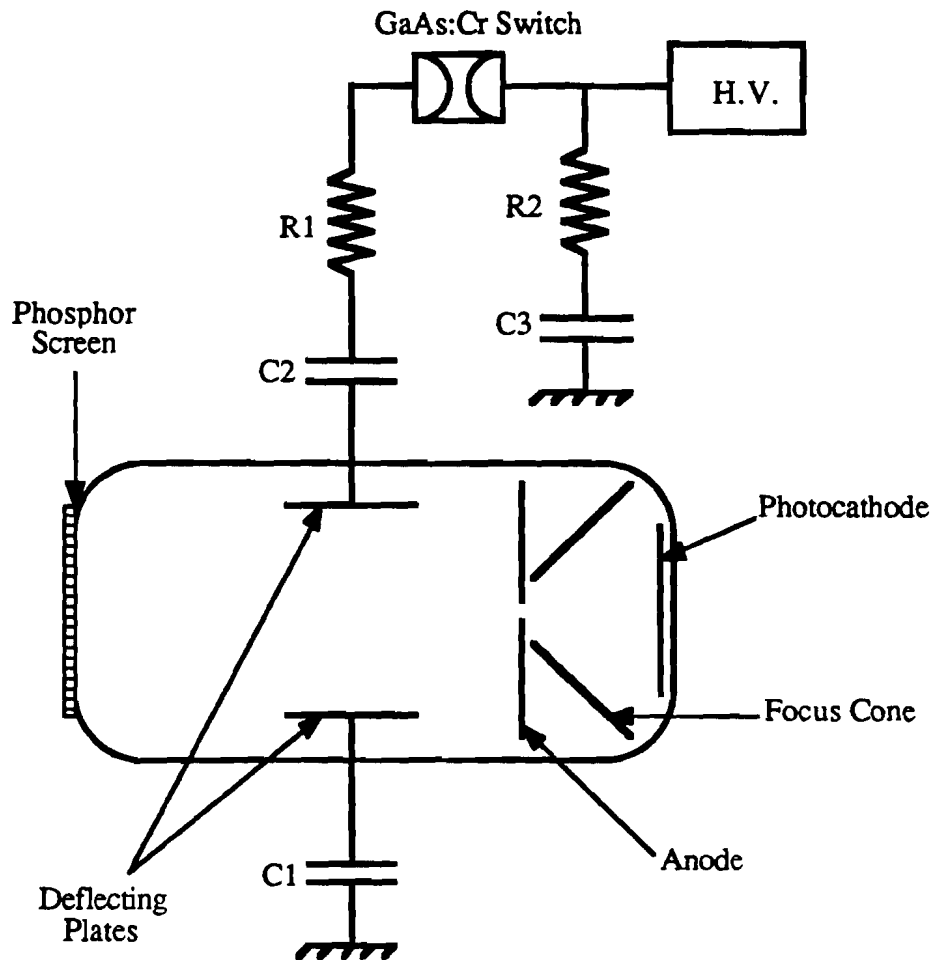


Fig. 3.4 Streak camera image converter tube with GaAs:Cr switching circuit. C1, C2 and C3 are capacitors. R1 and R2 are resistors. H.V. is a high voltage power supply.

D. Data Acquisition

After the signal emerging from the streak camera was amplified, it was imaged on a 500 by 500 two-dimensional diode array vidicon detector. A scanning electron beam was used to read out the signal from each diode. The charge required to recharge the diode elements was proportional to the signal intensity on the diode. Since the time required to recharge a diode depends on the level to which the diode is discharged, the recording of the signal by the system is not linear. The stronger the signal on a diode, the fewer scans were needed to read out the signal. Therefore the number of scans affected the system linearity response to the signal. Twenty scans were used for every shot in the measurement which was tested to provide reasonable response linearity and minimize further noise accumulation [85]. The process was controlled by an EG&G Princeton Applied Research System Controller (model 1216) and a System Processor (model 1215) computer. Data acquisition programs written in Forth [85] were used to control the experiment and record the data. For each data curve with 470 data points, 5 preshots were taken to initiate the system, then 100 to 400 shots were added up to improve the signal-to-noise ratio. The experimental data were stored on floppy disks right after each measurement then transferred to the VAX computer for corrections and analysis.

E. System Calibration

For each experiment, the system was calibrated as follows:

(i) Operating the streak camera in focus mode, i.e. with no sweep voltage on the deflecting plates of the streak camera tube, a narrow slit image scattered from a piece of paper was best imaged on the detector by adjusting the position of the paper and the focus of the fluorescence collecting lenses. Limited by the spatial resolution of the

streak camera tube, a 7-channel image from a 1 mm slit was accepted as the achievable result. Practically, however, the excitation beam was expanded until its image in focus mode was 10 to 13 channels wide to provide the maximum amount of fluorescence from the sample with an acceptable loss of time resolution.

(ii) To calibrate the time linearity of the system, a laser pulse was sent through an etalon which caused multi-reflections of the pulse spaced 125 ps apart. The system was set to work in a linear region by adjusting the offset voltage and sweep voltage of the deflecting plates of the streak camera tube, and the optical delay line which controlled the arrival time of the laser pulse. An etalon curve, shown in Fig. 3.5, was taken as a standard for time linearity and scale.

(iii) A fluorescence curve produced by excitation of rhodamine 6G in methanol, which has a lifetime much longer than the time scale of our detecting window, was taken as a reference for the channel-to-channel system response correction.

(iv) To correct for background light, a curve was taken by blocking the excitation beam after each data curve.

Fluorescence lifetimes of several dye solutions were measured for comparison with literature data (see Table 3.1). Fig. 3.6 shows one-exponential fits of fluorescence decay curves of malachite green in H_2O and rose bengal in H_2O .

Table 3.1 Fluorescence lifetimes of dyes. Comparison with previous work.

Dye	1-exponential fit lifetime	Previous results
Malachite green in H_2O	3.0 ± 1.0 ps	2.0 ± 1.0 ps [88]
Rose bengal in H_2O	85.0 ± 5.0 ps	90.0 ± 5.0 ps [89]

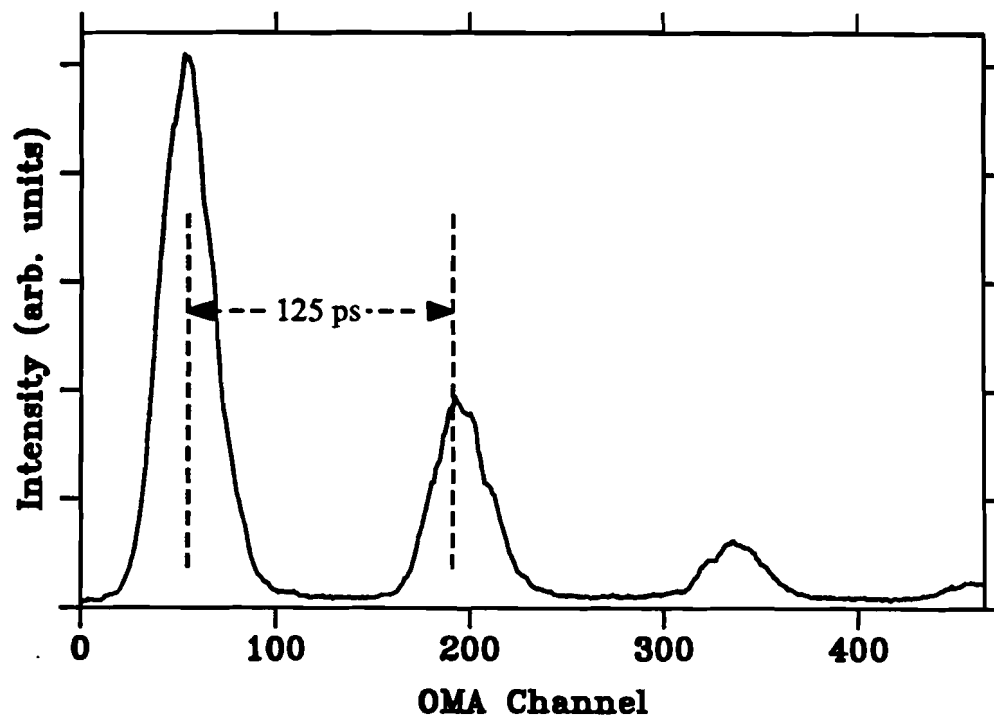


Fig. 3.5 Time-dependent intensity of an excitation pulse sent through an etalon. The curve was taken from the measurement of the scattering light of the excitation pulse from a piece of paper. An etalon causes multi-reflection of the pulse spaced 125 ps apart.

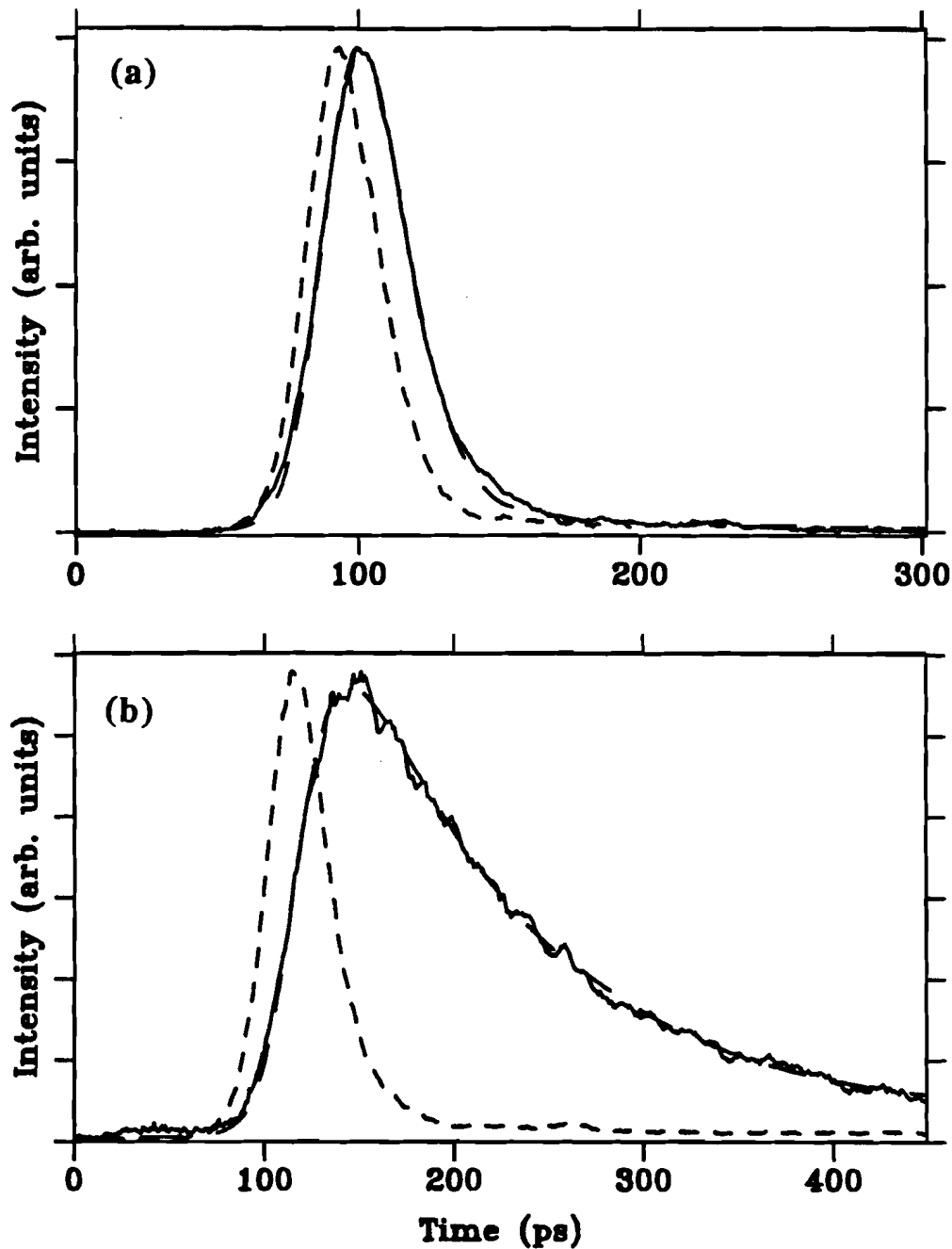


Fig. 3.6 Single-exponential fit of time-resolved fluorescence of (a) malachite green in methanol, $\tau = 5.7$ ps and (b) rose bengal in water, $\tau = 89.1$ ps. The experimental curve in each case is a sum of 100 shots. The long dashed line is the fit and the short dashed line is the profile of excitation pulse.

3.4 Data Analysis

A. Fourth-Derivative Analysis of Spectra

For the steady-state spectral analysis, a fourth-derivative method was used [90] to better resolve the emission bands. The fourth-derivative spectra were obtained by making four sequential differentiations of the fluorescence spectra. The differentiation intervals were varied to optimize the signal-to-noise ratio and resolution (a typical interval was 3-5 nm corresponding to 15 to 25 data points).

B. Data Correction

General: The time-resolved fluorescence was detected by an OMA II and digitized by a computer as described in part 3.3 D. There were 470 data points per curve, recording the intensity of the signal from 470 OMA channels. The regular routine for taking data in the experiment contained the following steps: (1) a time calibration curve was taken by sending a laser beam through an etalon to get a set of pulses separated by 125 ps, to check the linearity of the time axis and get the time-to-channel conversion factor (Fig. 3.5); (2) a rhodamine 6G fluorescence curve was taken for channel-to-channel response correction; (3) an excitation curve from the light scattered from a piece of paper was taken; (4) fluorescence curves from the sample were taken and (5) a background curve after each fluorescence curve was taken, by blocking the excitation beam.

Linearity correction: a particular error was caused by the electron beam scan. As described in part 3.3.D, when the electron beam scanned the vidicon to read out the signal, usually 20 scans were taken. There were differences among the signals with different intensities. The stronger the signal, the greater the efficiency of the scan. An

assumption was made to correct this system error. eq. 3.1 shows the relation between the real signal $S(i)$ and recorded fluorescence $F(i)$.

$$\{S(i)\} = \{F(i)^{1/\alpha}\} \quad (3.1)$$

In this equation “{...}” denotes an array and i denotes the i^{th} point of a data curve recorded by one OMA channel. α is the linearity factor determined as follows: for a fixed fluorescence intensity from the sample, the signal was detected at various intensity levels by adding neutral density filters in front of the streak camera, and then eq. 3.1 was used to determine α . It is assumed that α is independent of i , therefore an integrated value F over the whole range of i was used instead of $\{F(i)\}$. A set of F numbers was plotted as a function of the transmittance of the neutral density filter used in the measurement. The plot is on a log scale (Fig. 3.7). The slope of the straight line obtained from least-squares fitting gives value of α .

Residual background correction: the main source of the background was room light and the dark current of the streak tube. Fig. 3.8 shows a fluorescence curve $\{D(i)\}$ and a background curve $\{B(i)\}$.

Channel-to-channel response correction: we took a time dependent fluorescence curve $R(i)$ from a known long-lifetime dye (rhodamine 6G was used in our experiment) with its time zero displaced from the detecting window (Fig. 3.9). The fluorescence lifetime of rhodamine 6G in methanol is 3.5ns[91]. After the lifetime correction, shown in eq. 3.2, the corrected rhodamine curve $CR(i)$ gave a system channel-to-channel response correction.

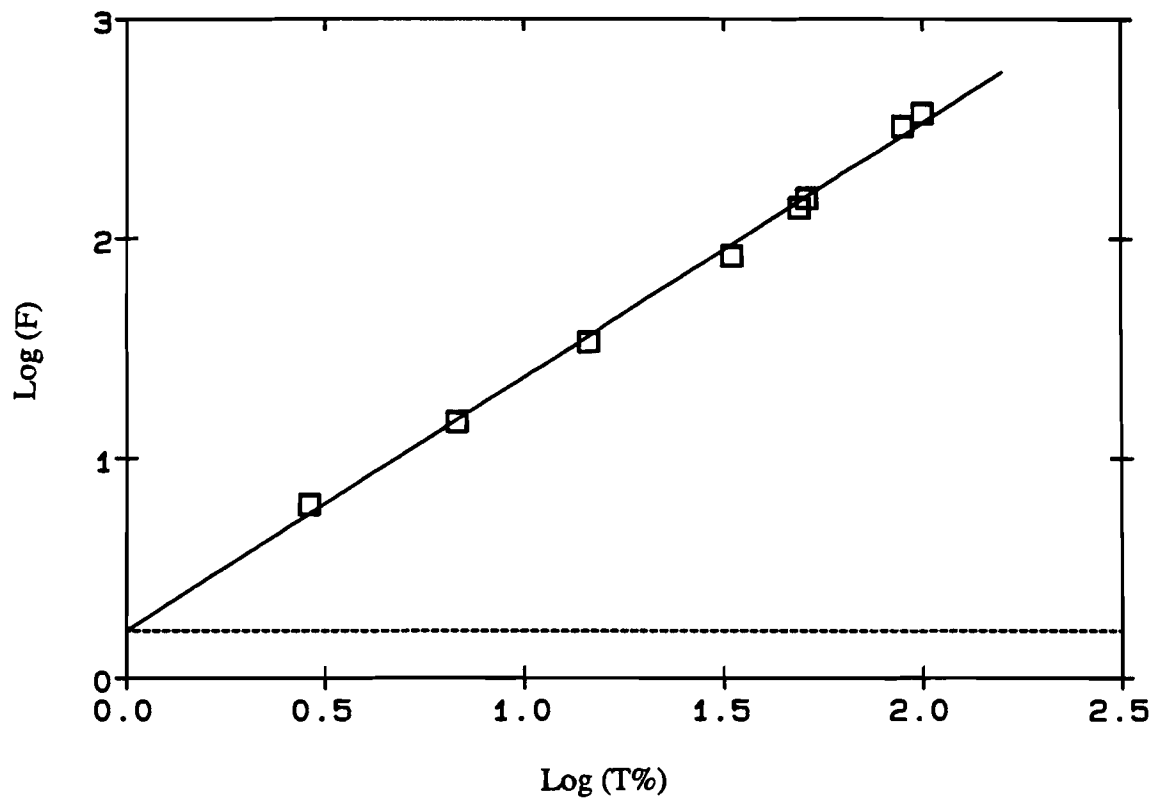


Fig. 3.7 Determination of linearity response factor of the detecting system to different level of the intensity of signal. Refer to the text for details.

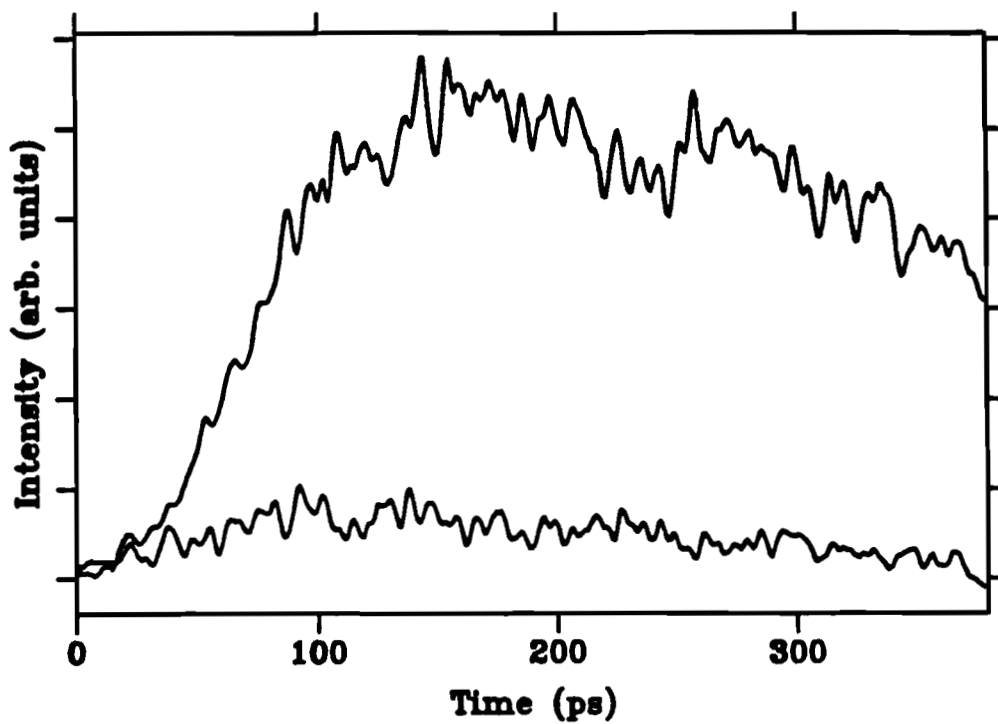


Fig. 3.8 Time-resolved fluorescence taken from a sample (upper curve) and the residual background (lower curve).

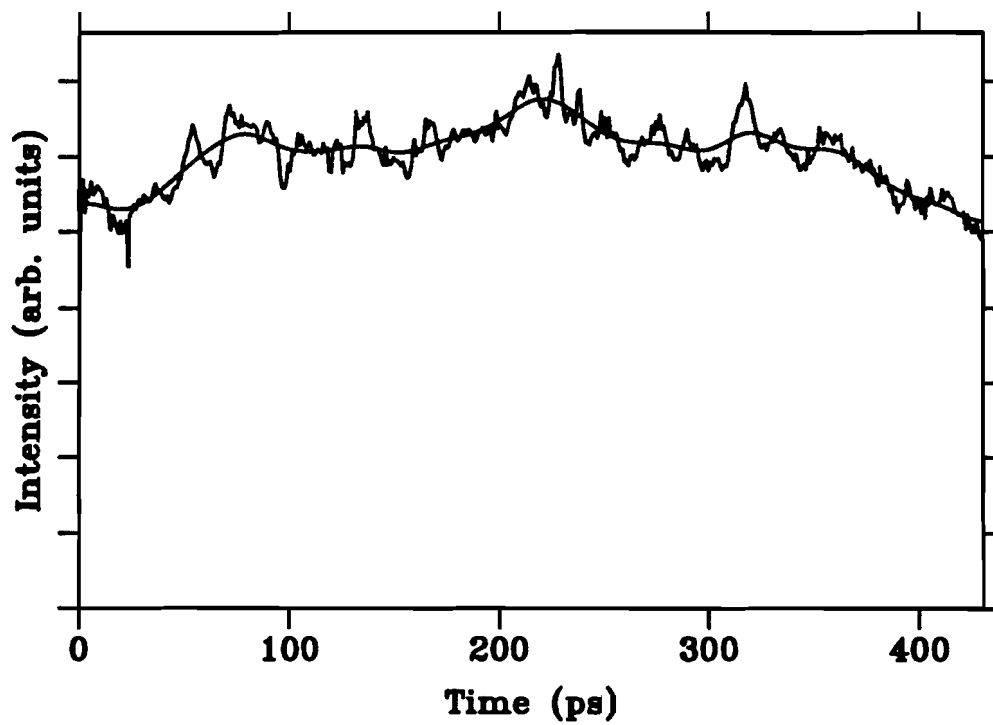


Fig. 3.9 The fluorescence decay curve of rhodamine 6G. The smooth curve was obtained after smoothing the experimental one.

$$\{CR(i)\} = \{[R(i)]^{1/\alpha}\} \exp(t/3.5ns) \quad (3.2)$$

Here t is the real time, its relation to an OMA channel being calculated from the measured etalon curve. The overall correction for a data curve $D(i)$ is:

$$\{CD(i)\} = N \frac{\{D(i)^{1/\alpha}\} - \{B(i)^{1/\alpha}\}}{\{CR(i)\}} \quad (3.3).$$

Here N is a normalization factor:

$$N = \frac{D(\text{peak}) - B(\text{peak})}{[D(\text{peak})]^{1/\alpha} - [B(\text{peak})]^{1/\alpha}} \quad (3.4).$$

C. Least-Squares Fitting

A nonlinear least-squares fitting program was used to fit corrected time-dependent fluorescence curves by a sum of up to 4 exponentials:

$$F(t) = \sum_{i=1}^n A_i \exp(-t/\tau_i) \quad (3.5).$$

Here A_i and τ_i are the amplitude and $1/e$ decay lifetime of the i th component, respectively. The sum of the squares of differences between measured and fitted data curves was used as the criteria for the best fitting. A typical result from the least-

squares fitting and the residual curve are shown in Fig. 3.10. This fitting provided the general characteristics of the time dependence of the sample fluorescence at decay level. Some of the parameters obtained from this fitting are used as references in the model calculation described in section D., which is the study in compartmental level.

D. Kinetic Modeling:

A three-component kinetic model, shown in Fig. 3.11, was used to simulate the experimental curves [92]. The following coupled kinetic equations were obtained according to the model.

$$\begin{aligned} \frac{dN_1(t)}{dt} = & [N_{10} - N_1(t)] [\sigma_1 I(t) + k_{12} N_2(t) + k_{13} N_3(t)] \\ & - N_1(t) \left\{ \frac{1}{\tau_1} + [N_{20} - N_2(t)] k_{21} + [N_{30} - N_3(t)] k_{31} + \gamma_1 N_1(t) + \sigma_1' I(t) \right\} \end{aligned} \quad (3.6)$$

$$\frac{dN_2(t)}{dt} = \left(\text{same as for } N_1 \text{ with cyclic permutation of labels } 1 \rightarrow 2 \rightarrow 3 \rightarrow 1 \right)$$

$$\frac{dN_3(t)}{dt} = \left(\text{same as for } N_1 \text{ with cyclic permutation of labels } 1 \rightarrow 3 \rightarrow 2 \rightarrow 1 \right)$$

Here $N_{i0} - N_i(t)$ is the number of molecules in the ground state of the component i ; σ_i and σ_i' are the ground and excited state absorption cross-section of component i , respectively (in cm^2); $I(t)$ is the excitation intensity in photons/ cm^2 per pulse; τ_i is the intrinsic decay lifetime of component i ; k_{ij} is the excitation transfer rate from component j to i and γ_i is the annihilation rate of component i .

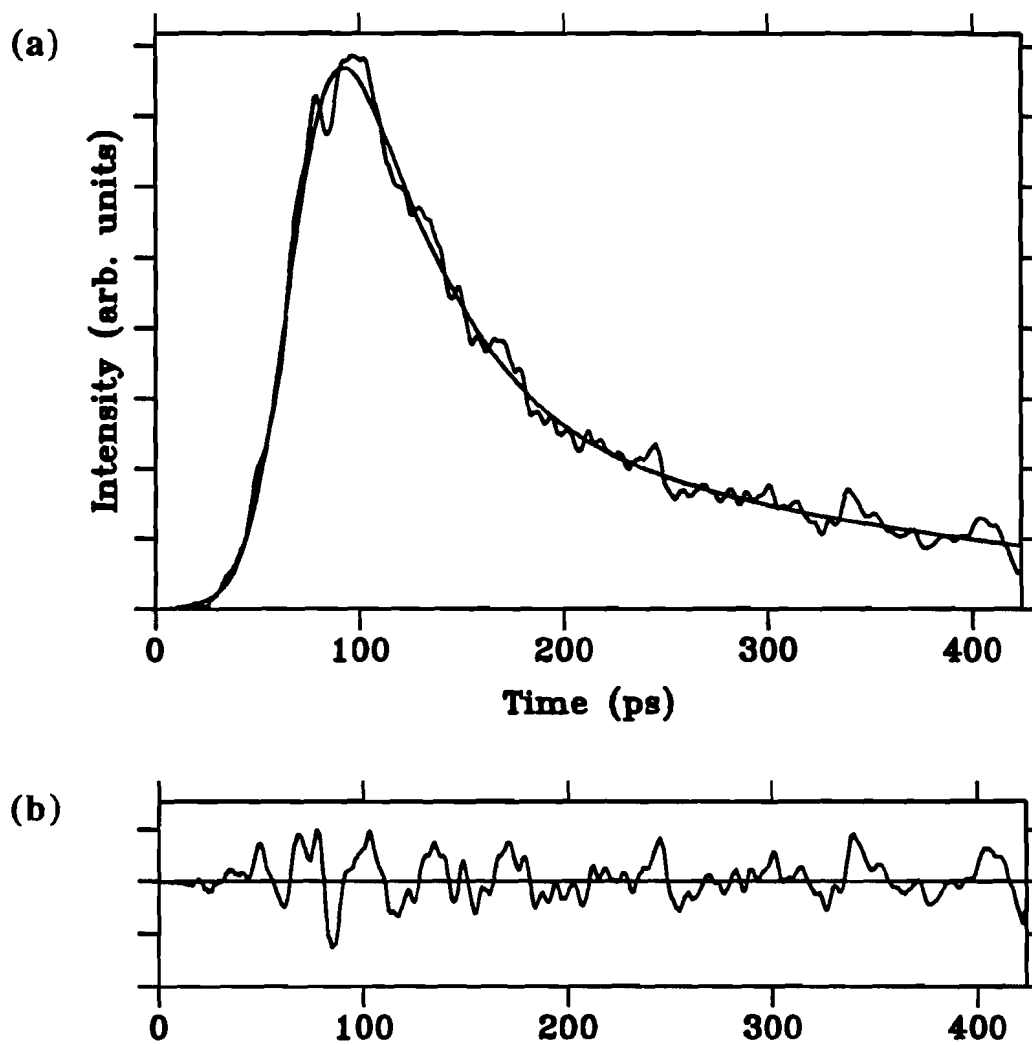


Fig. 3.10 (a) A typical least-squares fitting result and (b) its residual curve. The fitting parameters are: $A_1 = 77.1\%$; $\tau_1 = 35.5$ ps; $A_2 = 22.9\%$; $\tau_2 = 243.2$ ps.

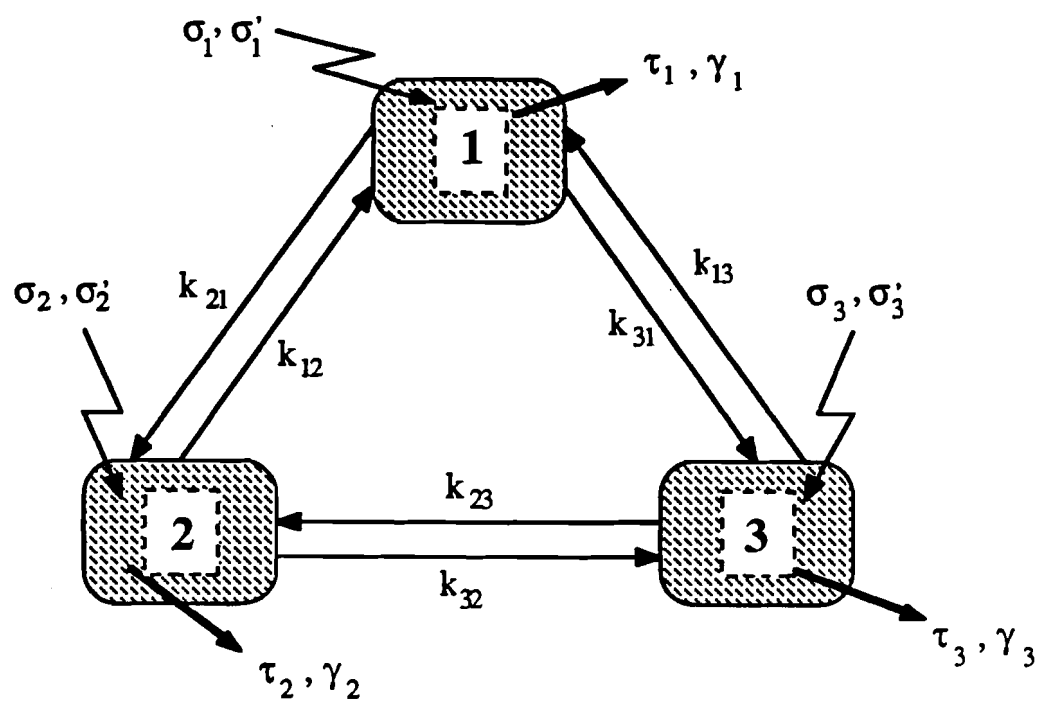


Fig. 3.11 Three-population kinetic model used in simulation of the experimental measurements. Refer to text for details.

During data simulation, some of the parameters were chosen from other independent experiments or literature and the others were varied until the best fit was obtained. The details will be mentioned in the data analysis part of each experiment.

Chapter 4. Low Temperature Time-Resolved Fluorescence Studies of F680 in Green Plant Chloroplasts

4.1 Overview

The spectral and kinetic heterogeneities of the fluorescence emission of green plant chloroplasts were reviewed in Chapter 2. The study reported here is to resolve and characterize a specific kinetic component which is involved in the energy transfer process in the green plant chloroplasts.

A. Spectral Characteristics of F680

Spectral studies of green plant chloroplasts at low temperatures show an emission band appearing as a weak shoulder at the short wavelength side of the well known band F685. F685 originates from PSII core antennae which are closely coupled to the PSII RCs. The peak of the short wavelength emission has been reported over a range of 675 to 681 nm [48,49,93]. In the measurement of the spectra at different stages of greening of maize leaves at 77 K, Garab *et al.* [93] found that the fluorescence yield of the band at 675 nm was higher when the leaf was in the earlier stage of greening, which was interpreted in terms of an unfavorable arrangement for energy transfer between the different chlorophyll forms at that stage. Butler proposed a three-component model (tripartite model) to describe the energy transfer and photochemical processes in PSII [94]. It was assumed in his model that the fluorescence band F680 at 77 K is representative of the fluorescence from the chlorophyll *a/b* complex. This assumption was upheld in their later experiment in which the isolated chlorophyll *a/b* complex has its main emission band centered at 681 nm [48]. Rijgersberg *et al.* investigated the

spectral properties of chloroplasts and subchloroplasts of various species of higher plants and algae in great detail between 100 and 4.2 K [49,95]. An emission band near 680 nm (F680) was clearly observed at temperatures below 15 K. Closer examination showed that F680 also exists at higher temperatures, and that its height was little effected by the temperature change [95]. The maximum of the F680 emission is reached when the excitation wavelength is at the carotenoid or the chlorophyll b absorption maxima. Carotenoid and chlorophyll b are pigments in LHC. F680 has not been detected in a chlorophyll b-less mutant which lacks LHC [49,55,95]. Purified LHC showing an emission maximum at 680 nm was also reported by other groups [53,96,97]. Therefore, F680 was tentatively attributed to LHC emission. A scheme for energy transfer in chloroplasts was proposed by Rijgersberg to explain the experimental results qualitatively. In his model F680 transfers its excitation energy to PSI and PSII even at 4 K. The temperature dependence of the emission bands was explained by changes in the thermal equilibrium between the energy levels of the emission bands upon cooling. The reproducibility of the F680 emission band and its absence in mutants without chlorophyll b showed that F680 was not simply a low temperature artifact. However, these assignments were obtained tentatively based on the spectral characteristics, and much less information was available on its kinetics.

B. Kinetics in the 680-685 nm Region

The kinetics of the two emission bands F680 and F685 have not been well established mainly because of the complexity of the spectral properties in this region. The fluorescence decay curves obtained by photon counting methods are usually detected at 685 nm or at wavelengths below 690 nm and fit by three decay components. The middle component, with a fluorescence decay lifetime of 200-300 ps and about

50% of the total amplitude at 77 K, was generally thought to originate from LHC [see review 7,45,65]. However, it was not clear how this component (obtained at the decay level) is related directly to the kinetic parameters of LHC at the compartmental level. Also, the fluorescence yield of this component seems much higher than the LHC emission observed in the steady-state spectra. A closer examination is necessary to find out the kinetics related to LHC emitting at 680 nm.

In the excitation-intensity-dependence study of F685 at 77 K, a three-population model was found to fit adequately the data successfully [40]. In this model, LHC (emitting at 680 nm) absorbs and transfers excitation energy to the proximal antenna of PSII where annihilation occurs. One problem with the model is that a short intrinsic lifetime of LHC had to be used in the data fitting which is expected to be on the order of nanoseconds according to the model. It is possible that the fast decay is the contribution from other emitters which can be clarified by measuring fluorescence over an extended wavelength region.

At 77 K, Mimuro [77] obtained time-resolved spectra of spinach chloroplasts and found an emission maximum appearing right after the excitation with a tendency to shift from 680 nm to 685 nm over a time period of 160 ps, and further to 695 nm within 350 ps. The understanding of this result is that excitation energy transfer occurs from LHC to the PSII antenna. Time-dependent fluorescence measurements will provide information to resolve the emission components.

C. About This Study

The study reported here was designed to answer the following questions: (1) What are the kinetic characteristics of the emission F680 at low temperatures? The question should be answered by examining the fluorescence decay rate. If the emitting

component is connected to the photosystems in the energy transfer chain, there must be an efficient energy transfer between them. In this case a strong fluorescence emission with a short decay lifetime should be observed. It is also possible that the emission originates from dissociated chlorophyll *a* molecules induced by low temperature damage. In this case a weak emission with a slow decay rate should be detected.

(2) Is F680 merely a low temperature effect? Or does it also reflect the kinetics under physiological conditions? A temperature-dependent study over a wide range of temperatures should provide information to answer the question.

By using picosecond streak camera and interference filter techniques, time-resolved fluorescence decay curves were measured at various temperatures and wavelengths. Special attention was paid to temperatures below 77 K.

4.2 Experimental Results

A. Spectral Properties of Spinach Chloroplasts at 77 K

Fig. 4.1 shows the fluorescence emission spectrum of spinach chloroplasts at 77 K. In the short-wavelength region two main emission bands are observed, at 685 nm (F685) and 695 nm (F695). The peak ratio of F685/F695 varied about 20% from sample to sample. By examining the second or fourth derivatives of the spectrum, a band around 680 nm (F680) was able to be resolved. In the long-wavelength region there was a broad band centered at 735 nm (F735). The spectrum is consistent with the measurements of other groups [95,98].

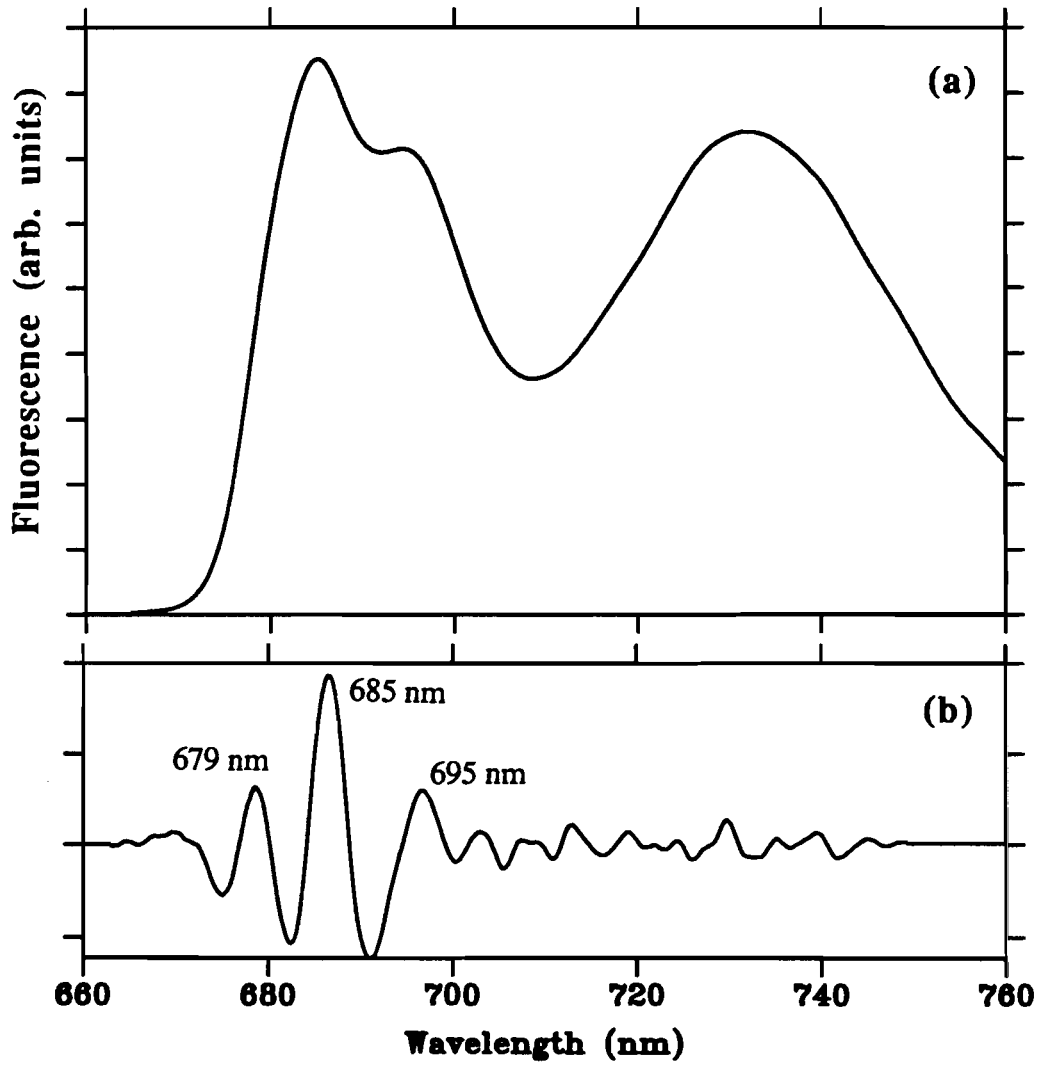


Fig. 4.1 (a) Steady-state fluorescence emission spectrum of spinach chloroplasts at 77 K. (b) The fourth derivative of the spectrum in (a).

B. Time-Resolved Fluorescence Measurements [99,100]

The emission spectrum of spinach chloroplasts at 77 K showed heavy overlapping of F680 and F685. In order to resolve the two components, time-dependent fluorescence was measured at various wavelengths. The idea was that if these two emission bands emitted with different decay lifetimes at slightly different wavelengths, contributions to a fluorescence decay curve from the two components would vary as the detection wavelength changed. In the experiment, fluorescence decay at 680 nm, 670 nm and 660 nm were recorded over a large temperature range (295 K - 20 K). Bandpass interference filters, IF680, IF670 and IF660 with bandwidths of 10 nm were used in the corresponding measurements. Emissions at 650 nm and shorter wavelengths were also checked at some temperatures. A very weak short-lived component could be seen at 650 nm, its decay profile was similar to that detected at 660 nm but with much lower intensity. No significant signal was detected at wavelengths shorter than 650 nm. The fluorescence decay curve measured at 690 nm showed more complicated rise, and decay profiles probably can be contributed to a combination of F685 and F695 emission. This is not considered in this study.

Fluorescence curves measured at 295 K, 77 K and 20 K are shown in Fig. 4.2. Differences among the room temperature time-dependent fluorescence at three wavelengths (the first row of Fig. 4.2) were not distinguishable within the signal to noise ratio. As the temperature dropped, a gradual change of the decay profile was observable, especially at the shortest detection wavelength. A fast decay component can be seen clearly at 20 K and 660 nm. By the simplest assumption, if there are two emission bands centered at slightly different wavelengths, the one emitting at shorter wavelength has a shorter fluorescence lifetime.

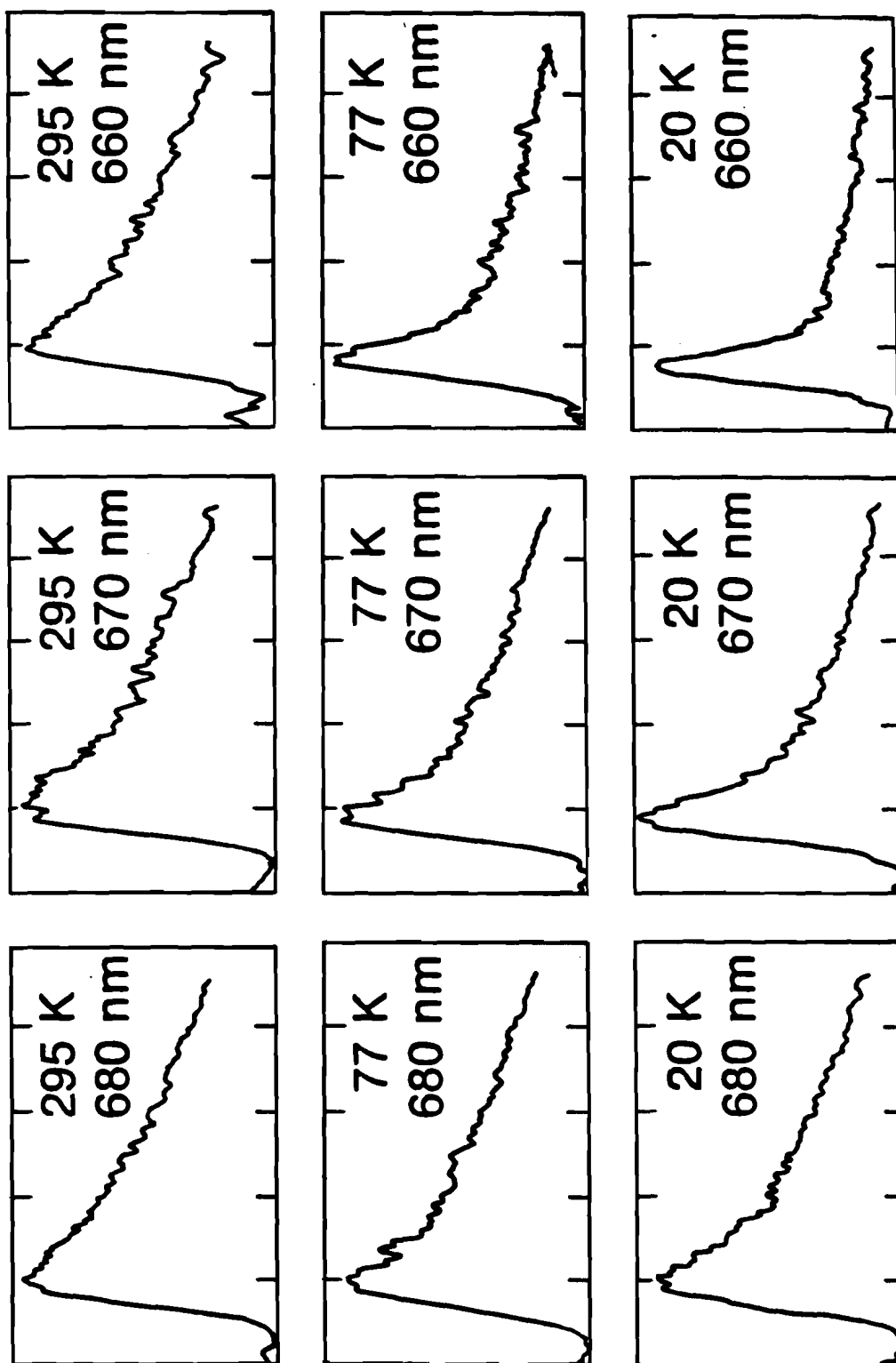


Fig. 4.2 Time-resolved fluorescence measured at various wavelengths and temperatures as marked in each frame. The data collected at 680 nm and 670 nm are the sum of 100 shots; 200 shots for those collected at 660 nm. Horizontal scale: 500 ps overall. Vertical scale: arbitrary units (reproduced from [99] with permission of the publisher).

In the experiments, the excitation pulse intensity was kept lower than 5×10^{13} photons/cm² so that exciton-exciton annihilation and other nonlinear effects could be neglected [40,87]. The fluorescence intensity at 650 nm was much weaker than the intensity at 660 nm even at higher excitation flux which excludes the possibility that the measured signal was due to Raman emission from the sample buffer (the Raman peak of the water excited at 532 nm is around 650 nm). In some of the measurements, the fast decay component did not show clearly, which may have been caused by several reasons. For example, seasonal changes in the Spinach; some uncontrolled difference in sample preparations, both of which may result in low emission intensity in the 680-685 nm region which can be seen in the steady-state spectra; sample cracking at low temperatures causes the scattering of the excitation light which may change the profile of the fluorescence decay curve.

C. Least-squares Fitting Results

A time-dependent fluorescence curve taken from spinach chloroplasts at 77 K is shown in Fig. 4.3. The fluorescence was collected at 685 nm by using an IF685 interference filter with a 14-nm bandwidth. The smooth curve was generated by using a set of parameters based on a photon counting result in reference [75] in which very low excitation intensity was used. The parameters used for both data fittings are listed in table 4.1. The two curves match reasonably well to within the noise. This provides a basis for comparison of the data taken by the photon counting methods and streak camera methods and shows that nonlinear effects can be neglected in our study even though a much higher excitation intensity was used.

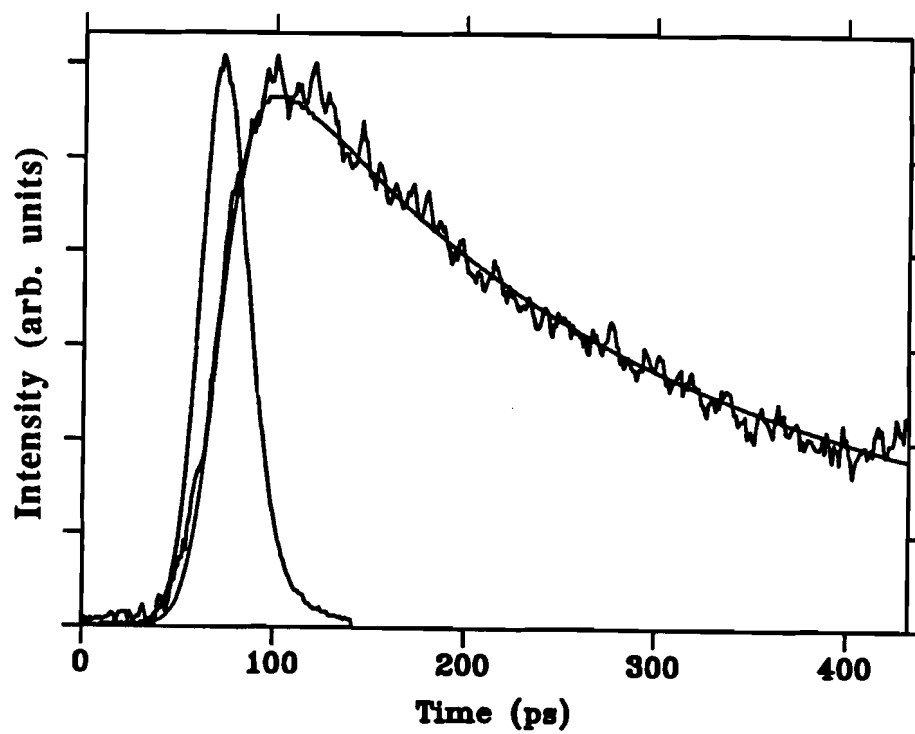


Fig. 4.3 Time-resolved fluorescence at 77 K from spinach chloroplasts measured at 685 nm. The curve is the sum of 200 shots. The smooth curve is calculated by adding three exponential decay components convolved with an excitation pulse (smooth line). For details about parameters used in the calculation, refer to the text.

Table 4.1 A comparison of fitting parameters from photon counting and streak camera data.

	A_1 (%)	τ_1 (ps)	A_2 (%)	τ_2 (ps)	A_3 (%)	τ_3 (ps)
photon counting data	13	1520	49	320	38	140
streak camera data	11.5	1520	49	320	39.5	140

Temperature-dependent measurements showed distinguishable fluorescence decay profiles of F660, F670 and F680 at temperatures below 110 K. The analysis here concentrates on the data collected at 77 K, 45 K and 20 K. At least two exponential decay components were required to fit the curves. Table 4.2 lists the results from a two-exponential nonlinear least-squares fitting of one group of data. Results from other experiments were on the same order with about 20% fluctuation.

For the results at 20 K, shown in table 4.2, one component of 9 ± 2 ps and another of about 220 ± 20 ps existed in all curves in various ratios. The shorter the detection wavelength, the larger was the portion contributed by the fast decay component. At higher temperature, the fast decay lifetime increased with temperature and the slow decay lifetime remained basically the same (the change in the slow lifetime was within 15% for most of the curves). The amplitude of the fast decay component was found to contribute more at shorter wavelength, as observed in the data measured at all temperatures. A third decay component could be added in some of the curve fittings. Its lifetime was basically in the nanosecond region with large variations and it had low amplitude. Since the fast decay lifetime is much less affected by adding the third slow decay component and our system has a limited

Table 4.2 Two-exponential nonlinear least-squares fitting results.

		τ_1 (ps)	τ_2 (ps)	A_1 (%)	A_2 (%)
20K	660 nm	8.94	228.7	91.1	8.9
	670 nm	10.5	185.3	76.2	23.8
	680 nm	9.39	234.4	63.5	36.5
30K	660 nm	9.67	164.5	89.6	11.4
	670 nm	11.94	190.8	71.0	29.0
	680 nm	12.18	214.9	58.2	41.8
45K	660 nm	11.18	303.7	87.4	12.6
	670 nm	12.27	233.7	72.9	27.1
	680 nm	11.97	220.9	54.5	45.5
77K	660 nm	14.32	218.0	78.5	21.5
	670 nm	13.33	218.4	65.0	35.0
	680 nm	15.81	254.7	47.7	52.3

ability to detect the long-time process, this slow decay was either averaged with the second component or neglected.

4.3 Kinetic Analysis

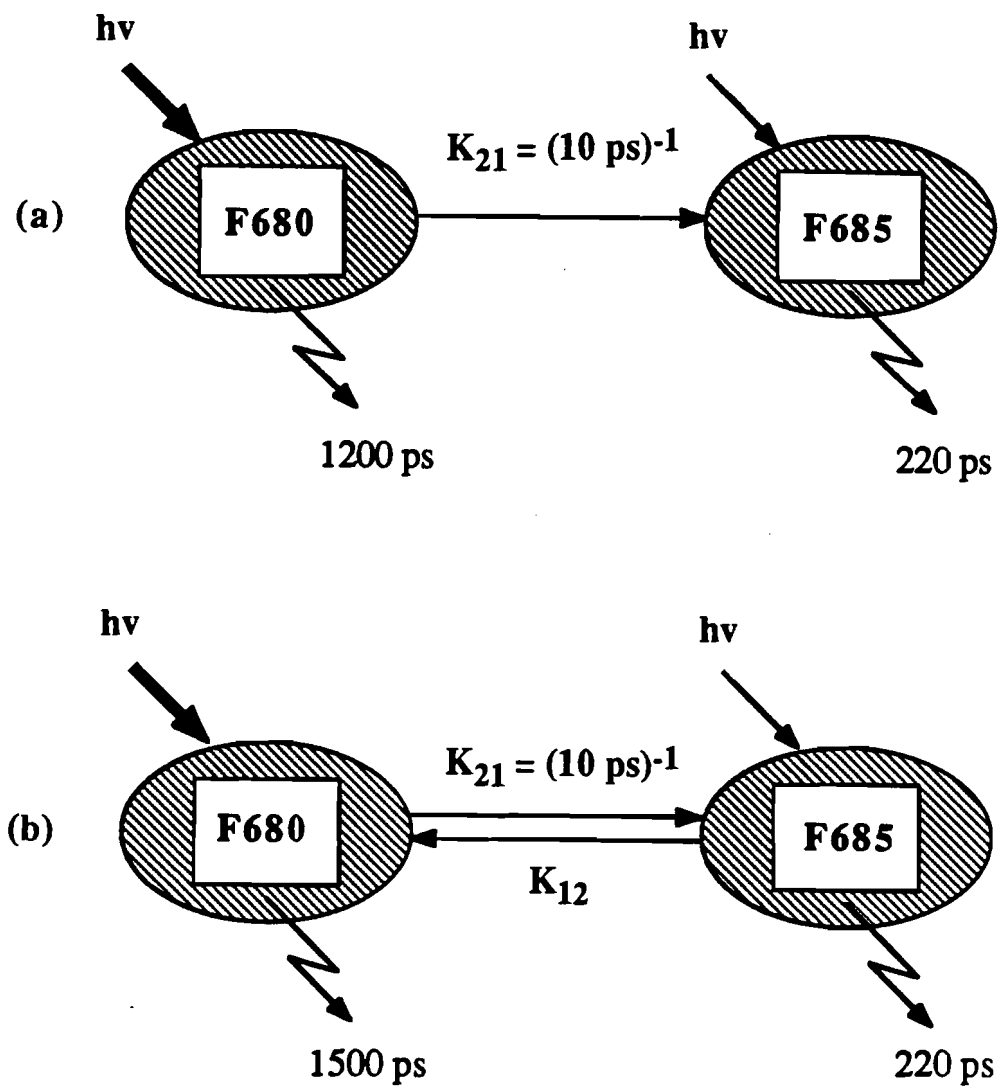
A. Fluorescence Decay kinetics at 20 K

Utilizing the information from the least-squares fitting, a two-population kinetic model (Fig. 4.4a) is proposed to explain the experimental results at 20 K. An assumption is first made that component 1 emits around 680 nm while component 2 emits around 685 nm. The excitation transfer rate K_{21} in the model corresponds to $k_{21}N_{20}$ in eq. 3.6 (in our case, $N_{10} \ll N_1$ and $N_2 \ll N_{20}$; for details see [87]). The kinetic equations 3.6 for describing the model then have the simple form

$$\begin{aligned} \frac{dN_1(t)}{dt} &= N_{10}\sigma_1 I(t) - \left[\frac{1}{\tau_1} + K_{21} \right] N_1(t) \\ \frac{dN_2(t)}{dt} &= N_{20}\sigma_2 I(t) - \frac{1}{\tau_2} N_2(t) + K_{21}N_1(t) \end{aligned} \quad (4.1)$$

For curves measured at the same temperature, the same set of parameters was used to generate the two curves $N_1(t)$ and $N_2(t)$ representing fluorescence decay from F680 ($F_{680}(t)$) and F685 ($F_{685}(t)$) respectively. The total fluorescence decay curve $F_\lambda(t)$ collected at wavelength λ was a linear combination of $F_{680}(t)$ and $F_{685}(t)$ expressed as:

$$F_\lambda(t) = A_\lambda F_{680}(t) + B_\lambda F_{685}(t) \quad (4.2)$$



$$K_{12} = K_{21} \exp(-\Delta E/kT)$$

Fig. 4.4 Two-population kinetic model used for simulating the time-resolved fluorescence measured at 20 K (a) and at higher temperatures (b).

The parameters used in the curve simulation were obtained as follows: N_{10} and N_{20} , as well as σ_1 and σ_2 were chosen from literature first [80] and later adjusted so that A_λ and B_λ were about equal when fitting 680 nm data at 20 K; τ_1 was the intrinsic fluorescence decay lifetime which was on the order of nanosecond [99-101]; the parameters K_{21} , τ_2 , A_λ and B_λ were varied until a good simulation was obtained.

All curves measured at 20 K at emission wavelengths 650 nm, 660 nm, 670 nm and 680 nm could be fit by the same group of parameters with different linear combinations of $F_{680}(t)$ and $F_{685}(t)$. This supports the idea of the two-component model, i.e. component 1 absorbs light and transfers its excitation energy to component 2 very rapidly (the transfer rate is about 10 ps) and fluoresces at shorter wavelengths; component 2, emitting at 685 nm, obtains most of its excitation energy from component 1. Its lifetime is affected by other transfer and photoconversion processes.

Fig. 4.5 shows calculated fluorescence decay curves used to simulate the data at 20 K. The short dashed line and long dashed line represent the F_{680} and F_{685} components, respectively, and the solid line is the combination of the other two which fits the fluorescence decay curve measured at 660 nm at 20 K.

The integrated fluorescence intensity I from a decay component was calculated in a given time interval from the curves shown in Fig. 4.5 according to

$$I_{680}(\lambda, t_1, t_2) = A(\lambda) \int_{t_1}^{t_2} F_{680}(t) dt$$

$$I_{685}(\lambda, t_1, t_2) = B(\lambda) \int_{t_1}^{t_2} F_{685}(t) dt$$
(4.3)

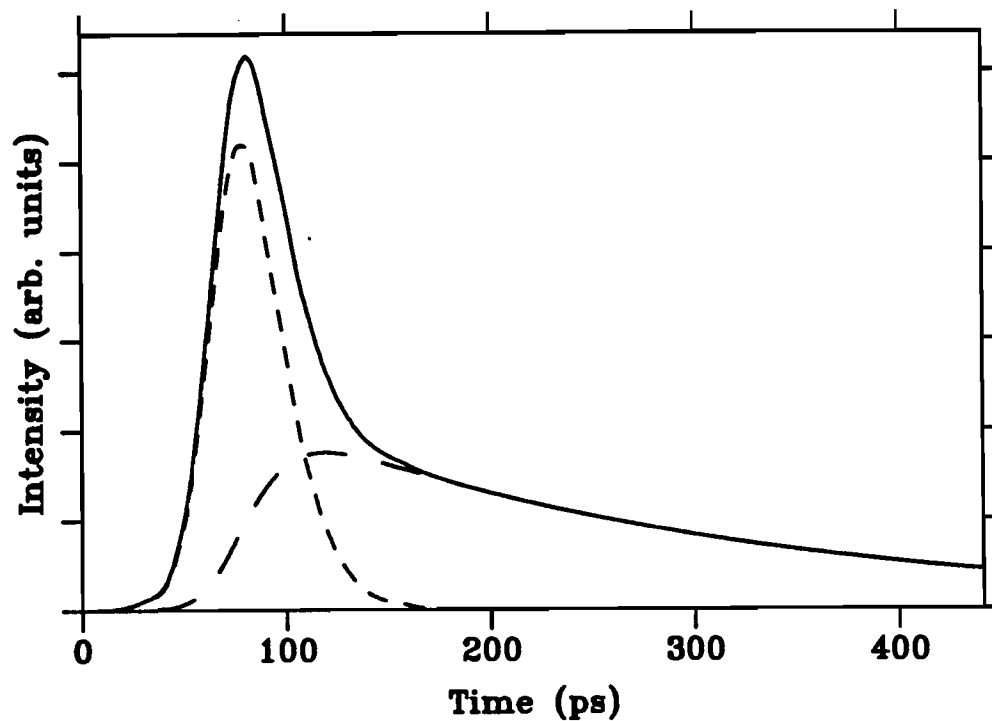


Fig. 4.5 Curves generated from the kinetic model in Fig. 4.4a. The parameters used are from the data simulation result of the fluorescence at 20 K collected through IF660. The fast decay component (short dashed line) and the slow component (long dashed line), and a sum of the two components (solid line) which fits the profile of the experimental curve.

Here λ is the detection wavelength at which a fluorescence decay curve was collected; t_2-t_1 is the time interval during which fluorescence intensity was integrated. Time-resolved emission spectra at 20 K were constructed from the time-integrated fluorescence intensity. Two curves were obtained, one contributed by the emission of the fast decay component and the other by the slow component. At the early time, i.e. shortly after the excitation, F680 (circles) emits strongly as shown in Fig. 4.6a. It diminishes when integrated over a long time period (Fig. 4.6b) compared with the slow decay emission (squares). This shows that the spectrum in this wavelength region is composed of at least two strongly overlapping bands. The two emission bands were fit by gaussians with their amplitudes, peak positions and band widths freely varying. The gaussian curves and the fitting parameters are also shown in Fig. 4.6. The solid line is for the fast component and the dashed line is for the slow component. The fast component is centered at 677 ± 2 nm with a band width of 19 ± 1 nm and the longer lived component is centered at 683 ± 2 nm with a band width of 21 ± 1 nm. For convenience of comparison with others' results, the terms F680 and F685 are still used in the following discussion.

B. Kinetics at Higher Temperatures

Data analysis at 20 K suggests a two-population kinetics. Naturally one asks whether this kinetic model can also be used to explain the data at higher temperatures. The results from the least-squares fitting showed a longer apparent lifetime as the temperature increased. The increase in lifetime seems to indicate a slower forward transfer rate. However, one would expect the energy transfer to be faster at higher temperatures.

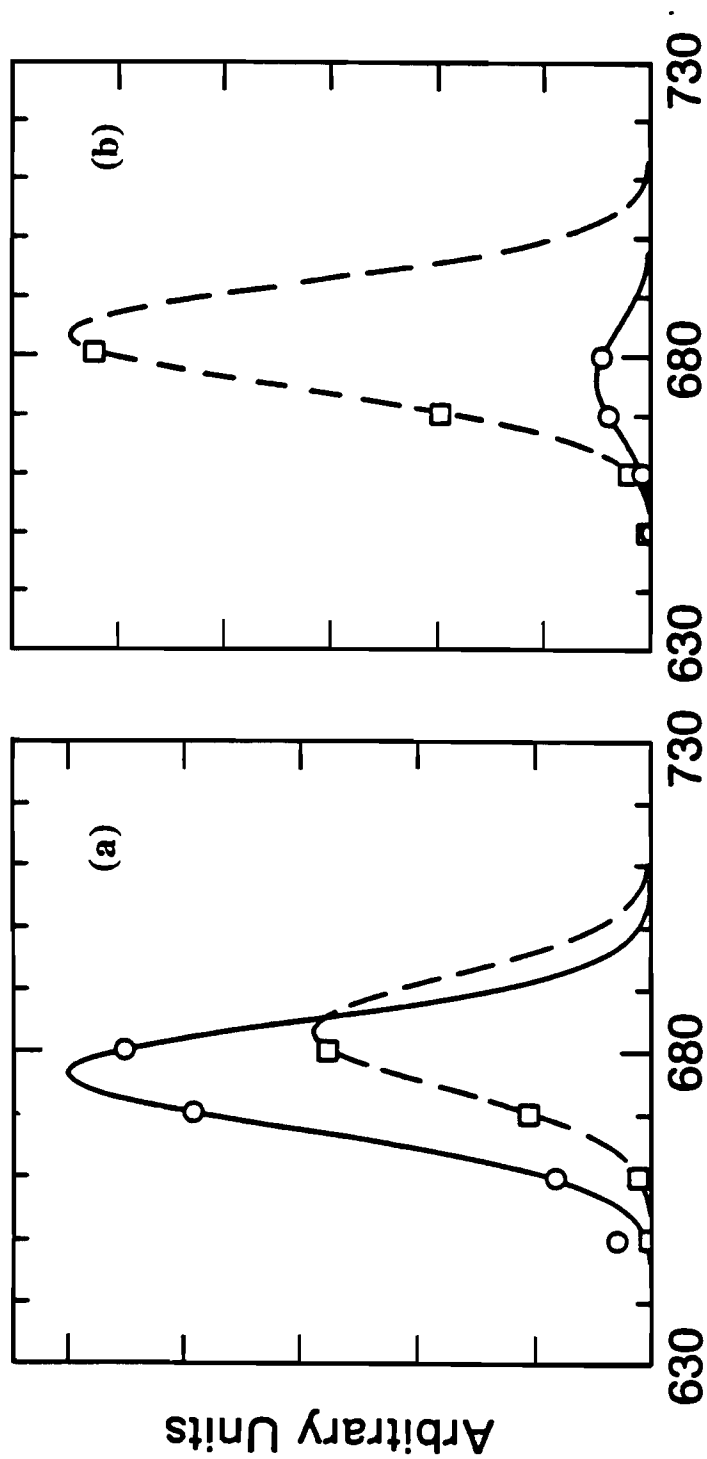


Fig. 4.6 Fluorescence emission bands F680 and F685 reconstructed from the time-resolved fluorescence data at 20 K. The band at shorter wavelength (squares) is from the integrated fluorescence of the fast decay components and the one at longer wavelength (circles) is from the slow decay. The integration time period is ~ 0 ps for (a) and $0 \sim 375$ ps for (b). Time zero is set at the maximum of the excitation pulse. Two emission bands are fitted by Gaussians. For the fast decay component, the emission maximum is at 677 nm with a FWHM of 20 nm. For the slow decay component, the emission maximum is at 683 nm and its FWHM is 21 nm (reproduced from [99] with permission of the publisher).

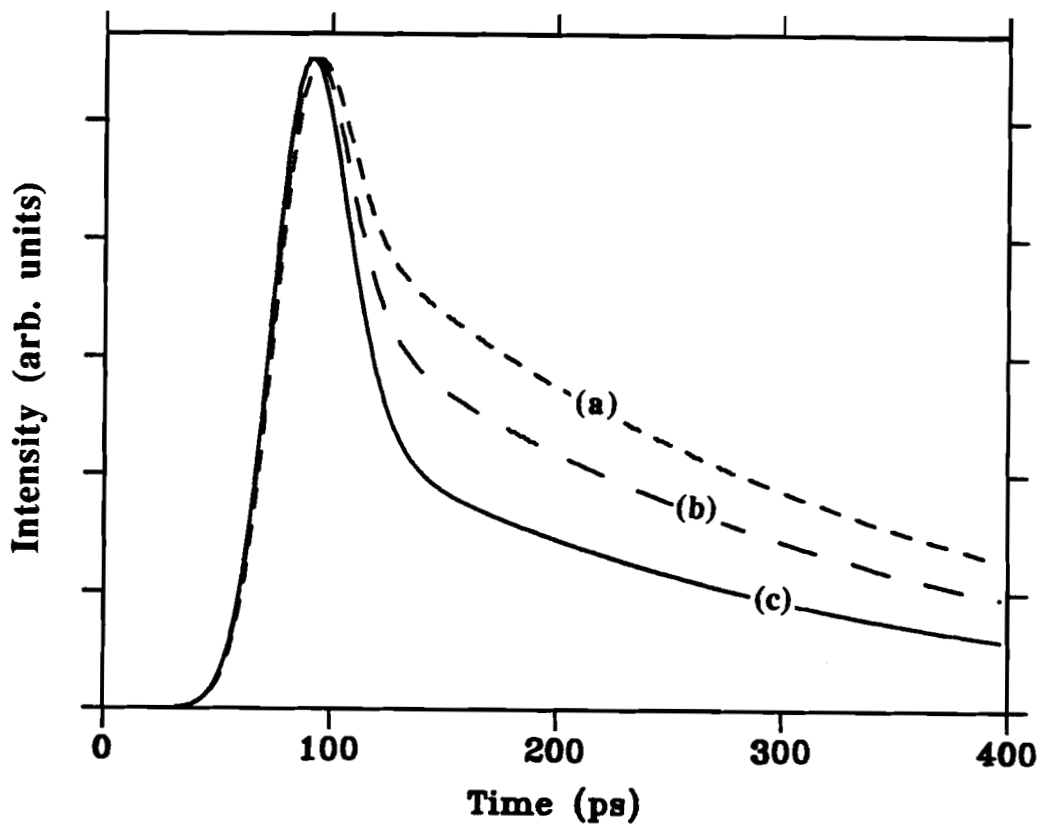
This conflict can be resolved by introducing a back transfer rate which varies with temperature according to the Boltzmann factor. The relation between forward and backward transfer rates is [102]

$$K_{12}/K_{21} = \exp(-\Delta E/kT) \quad (4.4)$$

Here K_{21} and K_{12} are the forward and backward energy transfer rate respectively; ΔE is the energy difference between the two components, $\Delta E = E_1 - E_2$ in our case; k is the Boltzmann constant and T is the absolute temperature. Considering the two emission bands at 677 nm and 683 nm, the energy difference between the two energy levels is only 0.016 eV which gives a K_{12} to K_{21} ratio of 0.088 at 77 K. This back transfer affects the fluorescence decay profile considerably. A set of fluorescence decay curves are shown in Fig. 4.7, calculated based on the parameters in the kinetic model in Fig. 4.4a with an additional energy back transfer rates varying with temperature. This indicates that inclusion of back transfer may yield good fits for higher temperature data.

Under the trial assumption that the forward transfer rate and other parameters remained the same as at 20 K, an extension of the kinetic model (Fig. 4.4b) was used for data simulation for the fluorescence measured at 77 K. The whole set of decay curves can be fit fairly well. Then the 45 K data were predicted from the known parameters. Therefore, the trial assumption was accepted and used in the following studies.

Fig. 4.8 shows the experimental curves with the theoretical fitting at various wavelengths and temperatures. An excitation pulse profile is illustrated only in the



- (a) $T = 100 \text{ K}$, $K_{12}/K_{21} = 0.13$
(b) $T = 77 \text{ K}$, $K_{12}/K_{21} = 0.088$
(c) $T = 20 \text{ K}$, $K_{12}/K_{21} = 0.0002$

Fig. 4.7 Simulated time-resolved fluorescence decay curves at various temperatures calculated from the kinetic model in Fig. 4.4b. Parameters are from the fitting of 20 K 680 nm data except K_{12} which is calculated according to eq. 4.4.

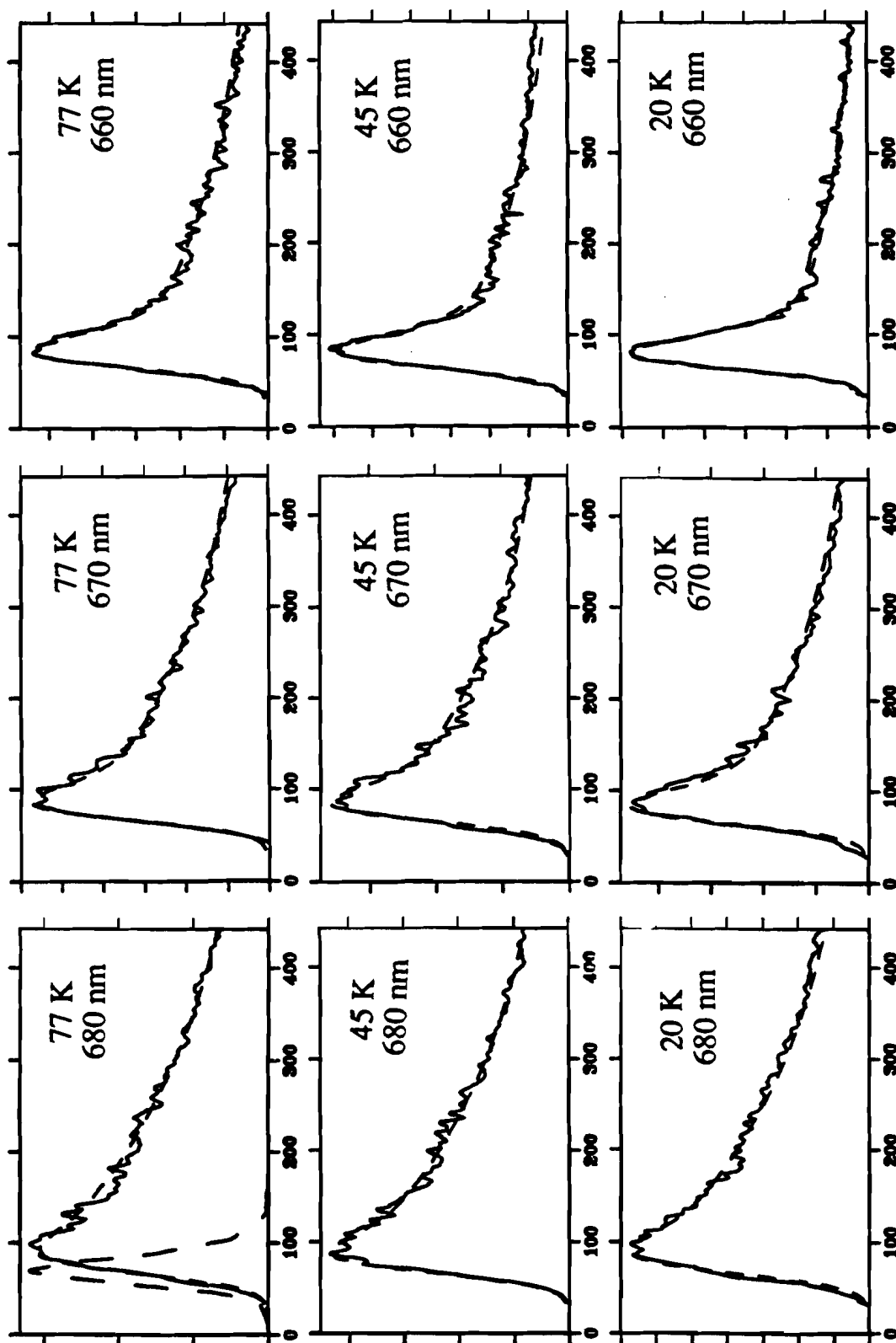


Fig. 4.8 Time-resolved fluorescence from spinach chloroplasts and the fitting curves. The detection wavelengths and temperature are marked in each frame. An excitation pulse profile is shown with the 680-nm 77-K data. Horizontal scale: 100 ps per division. Vertical scale: arbitrary units.

680-nm, 77-K decay curve frame. The theoretical fitting at higher temperatures and longer wavelengths is not quite as good as those at 20 K. Two reasons could be considered: (1) the data at 680 nm may include some of the emission from longer wavelength components, for example F695 and at higher temperatures more complicated processes should be involved; and (2) emission bands shift as temperature changes, a fact which was not considered in the calculation. The reconstructed spectra at higher temperatures gave profiles similar to those at 20 K. The results of the fitting reconstructed emission bands at 45 K and 77 K show a 2 to 3.5 nm red shift of the peaks of F680 and F685 and a band width 24 ± 6 nm. The accuracy of the spectral curves at higher temperature is not as good as that of at 20 K, therefore, is insufficient to provide the emission peak and bandwidth changes with temperature.

Rijgersberg's study showed that the difference between absorption and emission peaks of Bchl of *P. aestuarii* increased as temperature dropped and the bands became narrower [95]. The emission peak of F827 shifted to longer wavelength less than 2 nm as the temperature changed from 80 K to 4 K. The effect has not been observed in the spectra of green plant chloroplasts and green algae because of the complexity of the structures. However, an assumption was made in our study that the blue shift of the emission peak in our case should be of the same order of magnitude, which could induce a 1.5% error in the transfer rate calculation.

The fluorescence intensities of the two components were plotted as a function of temperature (Fig. 4.9). The intensity of F680 shows a change which is less than 10% in the temperature region 110 K to 20 K.

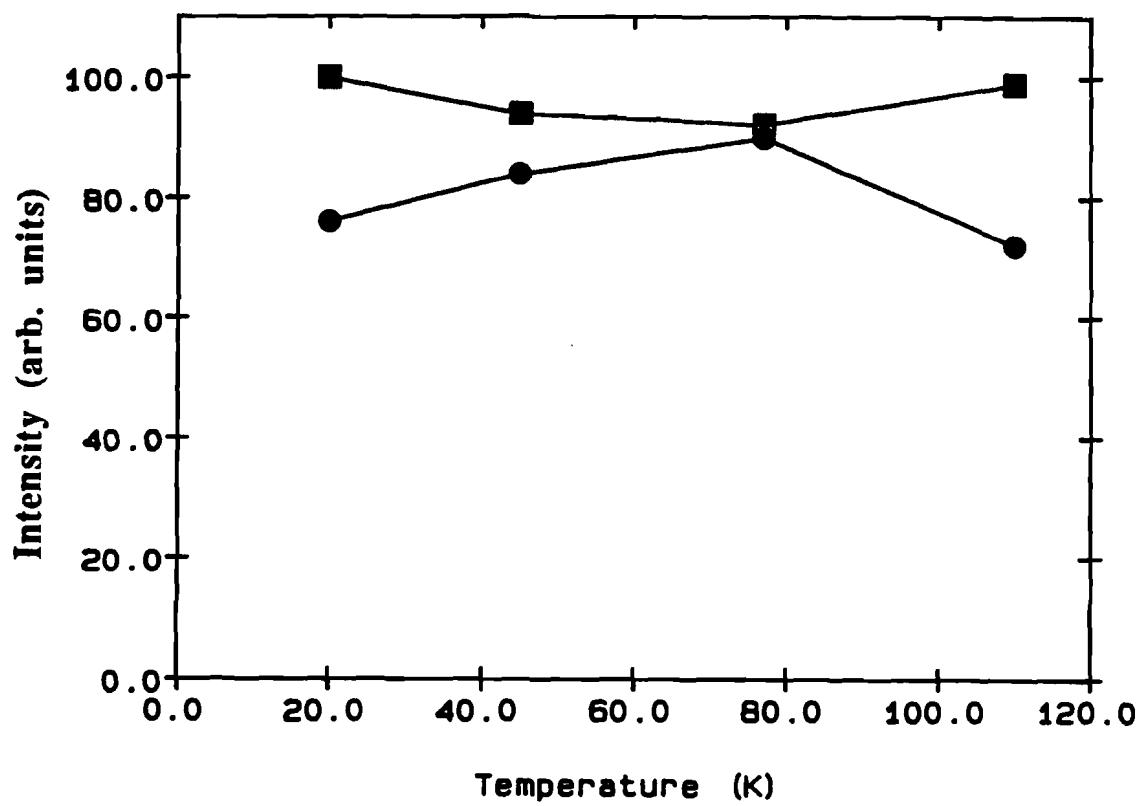


Fig. 4.9 Fluorescence intensity of F680 at different temperatures. Squares and circles represent two different sets of data.

4.4 Summary and Discussion

Low temperature time-resolved fluorescence of spinach chloroplasts was measured at 660 nm, 670 nm and 680 nm in the temperature region 110 K to 20 K. As the temperature dropped, a fast decay component became obvious which could be seen clearly in the 660 nm decay curve taken at 20 K. A two-population kinetic model, with the consideration of temperature-dependent transfer process, can explain the experimental data very well in a temperature range of 20 K to 77 K. At 20 K, the fluorescence lifetime of the short lived component is about 9 ps and the slow decay component has a lifetime of 220 ps. The fast decay component still exists at higher temperatures (30-110 K) but the apparent fluorescence lifetime increases which is explained by an increase of energy back transfer and more spectral overlapping. The emission bands reconstructed from the two fluorescence decay components at 20 K are centered at 677 nm and 683 nm respectively with a bandwidth of about 20 nm. The short-wavelength band with a fast fluorescence decay which emits strongly at early time. The fluorescence yield of the fast decay component is much lower than the slow one. The reconstructed emission bands at higher temperatures show similar profiles as those at 20 K. The fluorescence intensity of F680 has a minor change with temperature.

The analysis shows that the fast decay component of the time-resolved fluorescence corresponds to the emission band "F680" originally identified at low temperature by Satoh and Butler [48] and Rijgersberg *et al.* [49]. The high transfer rate between F680 and F685 implies good coupling between the two emission components. The spectral and kinetic properties of F680 in this study supports the proposed kinetic model [40] in which F680 is attributed to LHC emission and F685 is from PSII core

antenna. Therefore, it is concluded that LHC, as the system antenna, absorbs light and transfers energy to PSII core antenna with high efficiency (the transfer rate is about 10 ps). The transfer processes and excitation distribution are affected by temperature. The forward transfer process can be taken to be insensitive to the temperature at least in the temperature region studied, so it is possible that similar transfer occurs at room temperature. The signal-to-noise ratio of the data was not good enough to examine the detailed changes of the forward transfer rate as the temperature varied.

In our study, F680 emits strongly at early time and diminishes in the spectrum when integrated over a long time period. This explains why a low fluorescence yield at 680 nm has always been observed in steady-state emission spectra. Excitation transfer from F680 to F685 is very fast showing the same tendency of energy flow as that in Mimuro's experiment but with a different time scale. F680 shifted to F685 "within 100 ps" as reported recently in his more detailed study and analysis [103]. A recent time-dependent anisotropy absorption recovery measurement on PSII particles shows an efficient transfer between photosynthetic pigments in PSII particles with an 8 ps rate constant at room temperature [104]. This fast process was assigned to energy transfer from LHCII to PSII core antenna. LHCII, in their definition, is part of the LHC which are closely associated with PSII. The fluorescence decay time of F680 in the study is much shorter than that reported in [40]. It is possible that the fluorescence collected at 685 nm has some F680 component but is not well resolved at that wavelength, therefore the short intrinsic lifetime (75 ps) in their case is effectively shortened by this 10 ps decay. How this fast decay relates to the middle decay component from photon counting measurements is still not clear. One possible explanation is that the very fast transfer is from LHC to PSII as we proposed in the model and that there is another part of LHC which transfers energy to PSI at different rate (similar to the middle component

from the photon counting data, for example). The idea that LHC serves as the antenna for both photosystems is also suggested in the other studies [40,105]. Therefore, a study on structurally modified systems which lack one or more parts of the system is necessary to provide information for testing the idea. In the next chapter, we report the results of studies on the green alga C. reinhardtii and its photosynthetic mutants using the same methods.

Chapter 5 Studies of the Green Alga Chlamydomonas reinhardtii and its Mutants at 77 K

5.1 Overview

As reported in the preceding chapters, a fast energy transfer process related to LHC was found in the kinetic study of green-plant chloroplasts and was tentatively attributed to transfer of excitation from LHC to PSII. Studies on C. reinhardtii and its mutants were designed to provide further information about energy transfer pathways between LHC and other photosynthetic pigments. The results reported in this chapter support the picture obtained from the study on spinach chloroplasts in the 680-685 nm wavelength region. Furthermore, time-resolved fluorescence at long wavelengths which is thought to be partly related with the energy transfer process from LHC was extensively measured. Kinetic models are suggested to explain the results at the PSI emission wavelengths.

A. Chlamydomonas reinhardtii

C. reinhardtii is a unicellular green alga containing a single chloroplast. Studies have shown that the molecular organization of chlorophyll in C. reinhardtii is essentially similar to that in higher plants [106,107]. About 50% of the chlorophylls in C. reinhardtii chloroplasts are in the form of chlorophyll a/b protein complexes which serve as system antennae. Other chlorophylls are associated with PSI and PSII, acting as core antennae and RCs [108]. The energy transfer kinetics of C. reinhardtii chloroplast can be described by a model similar to that of the green-plant chloroplast [27,45].

Because of the complexity of molecular organization and heavy overlapping of emission bands of green-plant and green-alga chloroplasts, it is difficult to get a complete and detailed picture about excitation distribution and transfer in such systems. Thus properties of the photosynthetic pigments of higher plants are often derived from investigations of detergent isolated subchloroplast particles. However, the fragment isolation may cause lesions and disconnection of photosystem components, which in turn certainly changes energy transfer processes. Particular attention has therefore been paid to the study of photosynthetic mutants which are deficient in one or more chlorophyll-protein complexes and show part of the activities being suppressed. Because of the ease of handling cultures of algal cells, C. reinhardtii and its mutants have proved to be excellent systems for study [for example, see references 50,51,59,104]. Various mutants have been used to reduce the complexity of the system and to allow assignment of fluorescence components consistently to parts of the system. Those studies can also provide useful information for elucidating similar processes in higher plants.

B. Spectral Studies of C. reinhardtii and its Mutants at Low Temperatures

Fluorescence emission spectra of wild type and all mutant strains of C. reinhardtii at 295 K are similar, containing a main emission band around 685 nm, while their spectra show significant differences among different mutants at low temperatures [51]. Absorption, linear dichroism, fluorescence excitation and emission spectra at low temperatures were studied by several groups in an attempt to identify the different photosynthetic pigments and their functions [51,59,109-111]. The emission spectrum of wild type C. reinhardtii at 77 K usually exhibited three bands, F685, F695 and F717 corresponding to the emissions F685, F695 and F735 of higher-plant chloroplasts

respectively. F680 can be resolved by closer examination and attributed to LHC emission [112].

The relationship between low-temperature fluorescence emission bands of whole cells and chlorophyll-protein complexes was studied in detail by Garnier *et al.* [51]. Fluorescence spectra of wild type *C. reinhardtii* and eight mutants, as well as some isolated particles, were measured at 77 K. Emission bands were resolved and assigned to the different chlorophyll-protein complexes. The results are summarized in table 5.1.

Table 5.1 The components and functions of chlorophyll-protein complexes of *C. reinhardtii* and their emission bands at 77 K [51].

chlorophyll-protein complex	composition	function as	emission peak at 77 K (nm)
CP0	chl a, chl b	LHCI	707
CP0a	chl a	PSI	703
CPI	chl a	PSI core	715
CPII	chl a, chl b	LHC	682
CPIII	chl a	PSII	696
CPIV	chl a	PSII	686
(CPV	unknown)		

Two energy flow pathways were proposed to describe the excitation transfer from antennae to RCs of photosystems. The pigment called CPII, corresponding to LHC in green-plant chloroplasts, transfers part of its excitation energy to PSII core antenna (CPIV and CPIII) and then to RCs of PSII. CPII also provides excitation to CP0, i.e. LHCI, the peripheral antenna of PSI. The energy from CP0 is further transferred to

CP0a then to the core antenna of PSI (CPI) which is directly associated with RCs of PSI. Karapetyan *et al.* had a different conclusion about energy transfer from LHC to other components [109]. In their experiment, the fluorescence spectra of those samples with an active PSII exhibited a band at 685-688 nm which was assigned to the emission of antenna chlorophyll of PSII. A strong emission band with a maximum at 680 nm was observed in the spectrum of the mutant missing PSII. Therefore they concluded that F680 is the emission of the chlorophyll that is not energetically associated with PSI.

C. Time-Resolved Fluorescence Studies at Low Temperatures

Although much work has been done to identify the origin of each of its emission bands, not much is known about the kinetics of *C. reinhardtii* at low temperatures. Room-temperature picosecond fluorescence decay measurement in the 680 nm region indicated heterogeneity of the kinetics similar to that of green-plant chloroplasts [113,114]. At least three exponential decay components were required to fit fluorescence decay from wild type *C. reinhardtii*. Studies of PSI and PSII mutants (lacking PSI and PSII respectively) provided more information about the fast decay (89 ps) in wild type, i.e., it turned out to be an average of two fast components (53 ps and 152 ps) arising from excitation transfer and trapping related to PSI and PSII. Moya and Garcia studied phase fluorimetric lifetime spectra of green algae at 77 K [74]. Emission spectra and the mean value of the lifetime at each emission wavelength were measured. Up to seven emission bands were resolved, each of them with a single exponential decay time. An interesting result was that the band at 689 nm, corresponding to F685 of green-plant chloroplasts and having a 530-ps lifetime, was assigned to PSII emission rather than the LHC. The assignment disagrees with the one

in green plants (see chapter 4.1). The band emitting at 714.4 nm was attributed to a component directly associated with P700. Recently, a low-temperature picosecond-decay-kinetics study and other spectral properties of C. reinhardtii mutants lacking both PSI and PSII was reported [115]. These studies agreed with the existence of at least two types of LHCP, each of them connecting with one photosystem [109,110]. An efficient energy transfer was found within the complex while the transfer between different LHCPs seemed to be absent or very weak which is in contrast with the model of Garnier [51].

D. About This Study

In the fluorescence kinetic study of green plant chloroplasts at low temperatures described in chapter 4, the fast fluorescence decay was assigned to LHC emission (F680) which was tentatively related to an efficient energy transfer from LHC to PSII. The remaining questions were: is this fast transfer between LHC and PSII only, or is it also related to PSI? and how is it affected by the change of different parts of the system? The spectral properties of the wild type and three kinds of mutant strains of C. reinhardtii were studied at 77 K. The mutants used in our experiments included those with PSI deficiency, PSII deficiency and a double mutant strain missing both PSI and LHC. Based on the large amount of available spectral information, the time-resolved fluorescence was selectively measured at various wavelengths and analyzed using a proposed kinetic model. The results show that the emission band around 680 nm also exists in C. reinhardtii and has a short fluorescence lifetime similar to that of green plant chloroplasts. This fast decay is related to an efficient energy transfer from LHC to PSII core antenna. LHC also transfers excitation to LHCI but at a different rate.

5.2 Characteristics and Spectral Properties of Mutant Strains of C. reinhardtii [116]

The photosynthetically deficient mutants of C. reinhardtii used in the experiments were acetate-requiring and photosensitive, showing normal growth in the dark [117]. The measurements of steady-state fluorescence spectra were described in section 3.2B. The biogenetic characteristics and our measurements of fluorescence spectral properties of various strains at 77 K are described as follows.

DES15: a wild type strain of C. reinhardtii which is the progenitor for the mutants B4, B1 and LM15-4D1C described below. Its fluorescence spectrum at 77 K is shown in Fig. 5.1a. The emission bands F685 and F695 are clear while only a shoulder around 717 nm is seen. F680 can be resolved in a fourth-derivative spectrum (Fig.5.1b).

B4: a nuclear PSI deficient mutant which produces PSII and LHC even when grown in the dark. The spectrum (Fig. 5.2) shows a dramatic increase of a broad band around 707 nm compared with the spectrum of DES15. Other emission bands at shorter wavelengths are difficult to distinguish; only the 685 nm band can be seen.

B1: a chloroplast mutation with a deletion of psbA, the gene encoding the D1 protein of PSII [118]. This mutant does not contain PSII. As shown in Fig. 5.3, there is a very strong emission band at 681 nm and a shoulder at longer wavelengths. The emission F685 and F695 have disappeared.

LM15-4D1C: a double mutant carrying the B4 mutation causing PSI deficiency and also a mutant called DS521 that causes deficiency in most of the LHC complexes. The emission bands F685 and F695 can be seen in the spectrum (Fig. 5.4). There is an emission band centered at 719 nm which probably originates from the remaining PSI particles since the fluorescence intensities of all bands in this spectrum are much

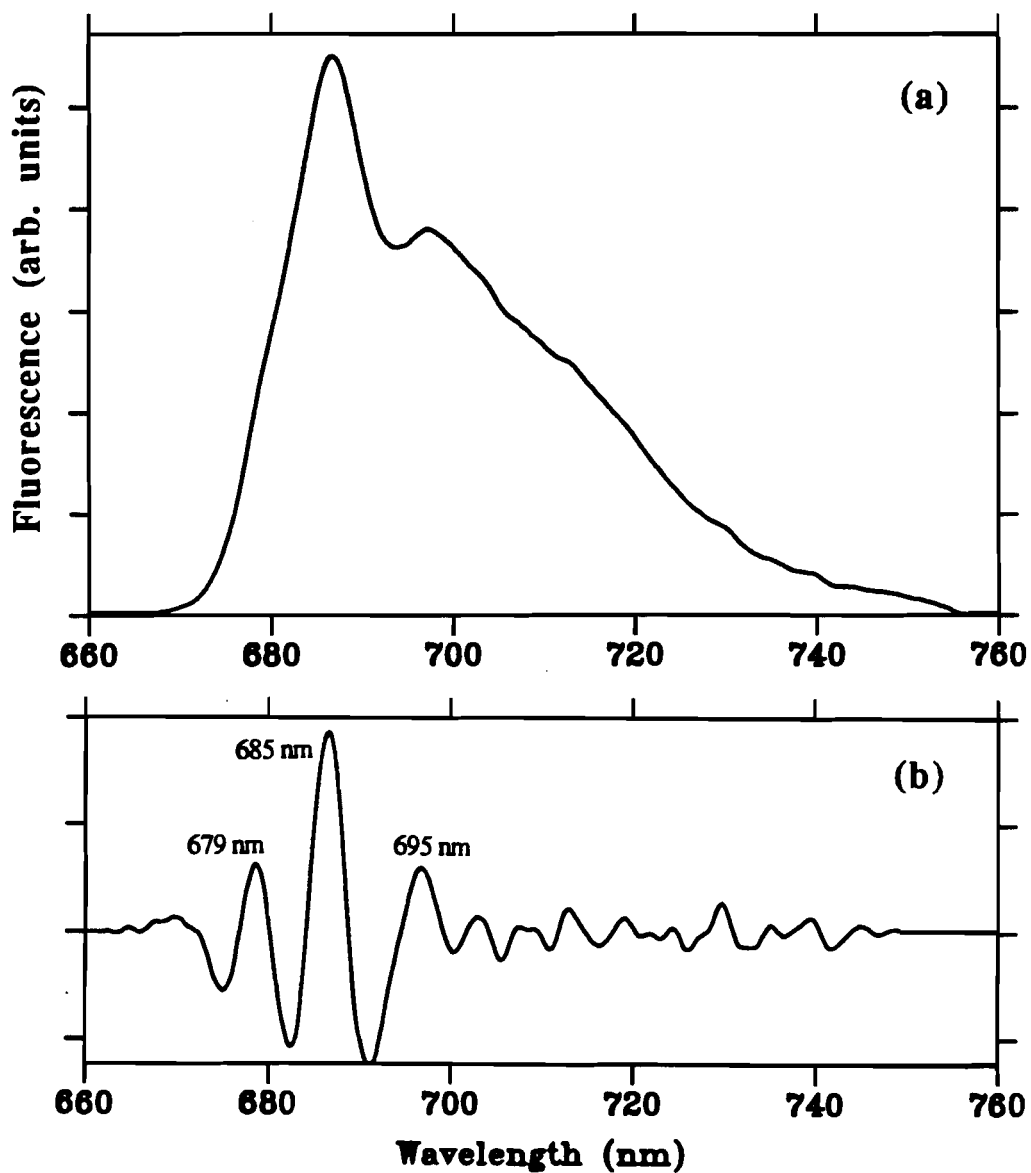


Fig. 5.1 (a) Steady-state fluorescence emission spectrum of DES15 at 77 K and (b) the fourth derivative of the spectrum in (a). The wavelength resolution of the spectrum is 0.2 nm.

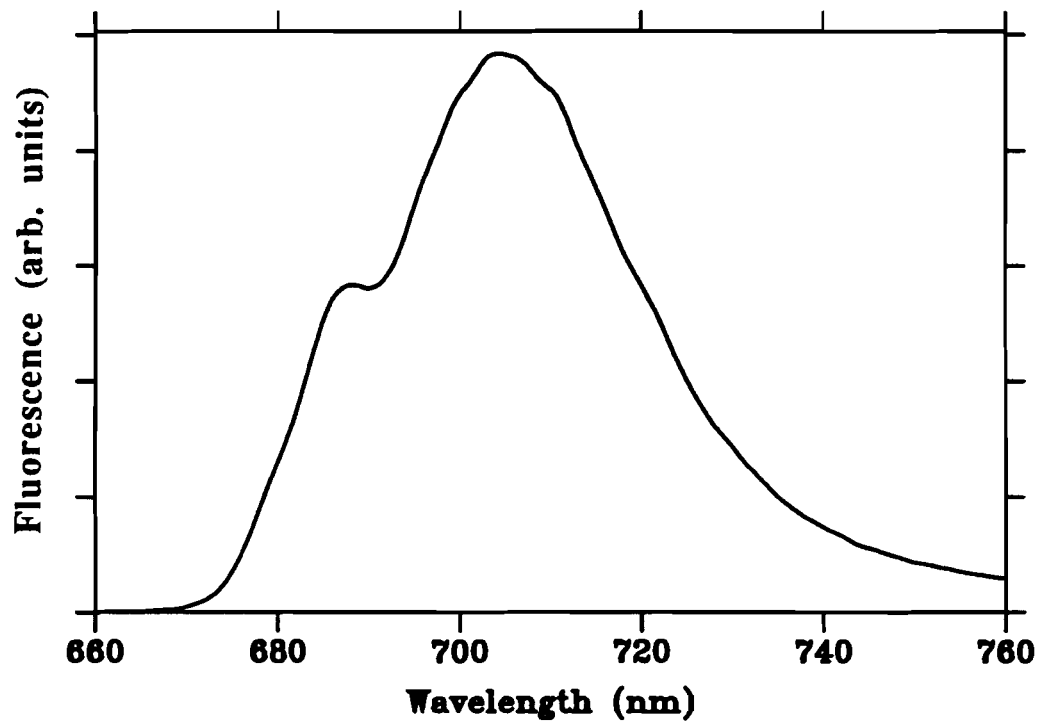


Fig. 5.2 Steady-state fluorescence emission spectrum of B4, a PSI deficient mutant, at 77 K. The wavelength resolution of the spectrum is 0.2 nm.

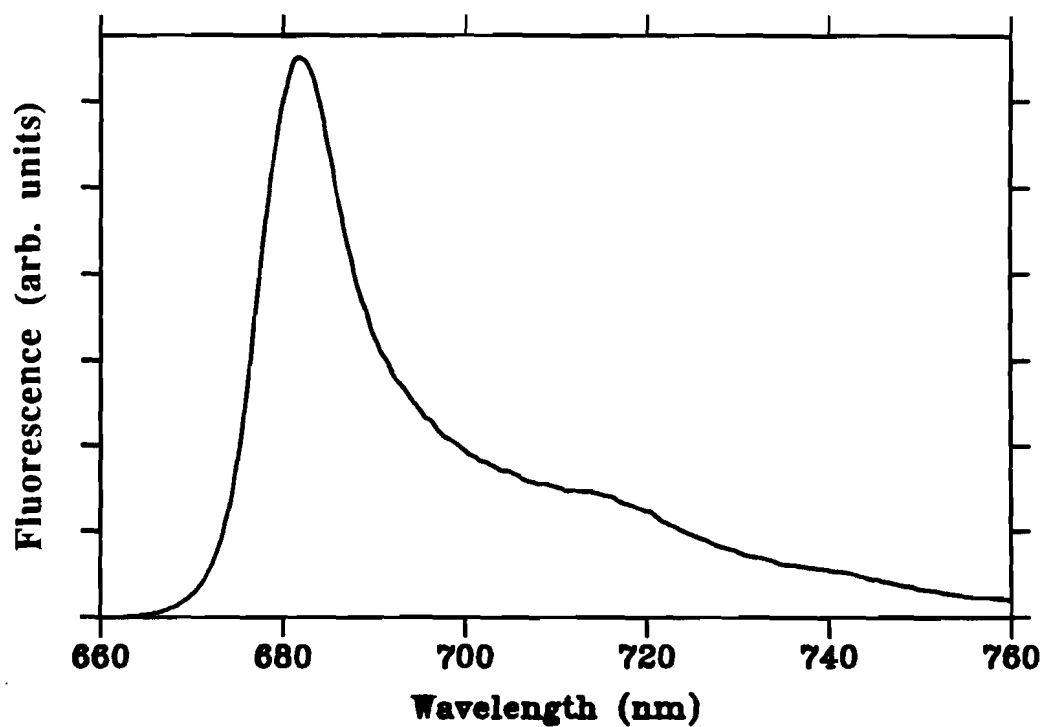


Fig. 5.3 Steady-state fluorescence emission spectrum of B1, a PSII deficient mutant, at 77 K. The wavelength resolution of the spectrum is 0.2 nm.

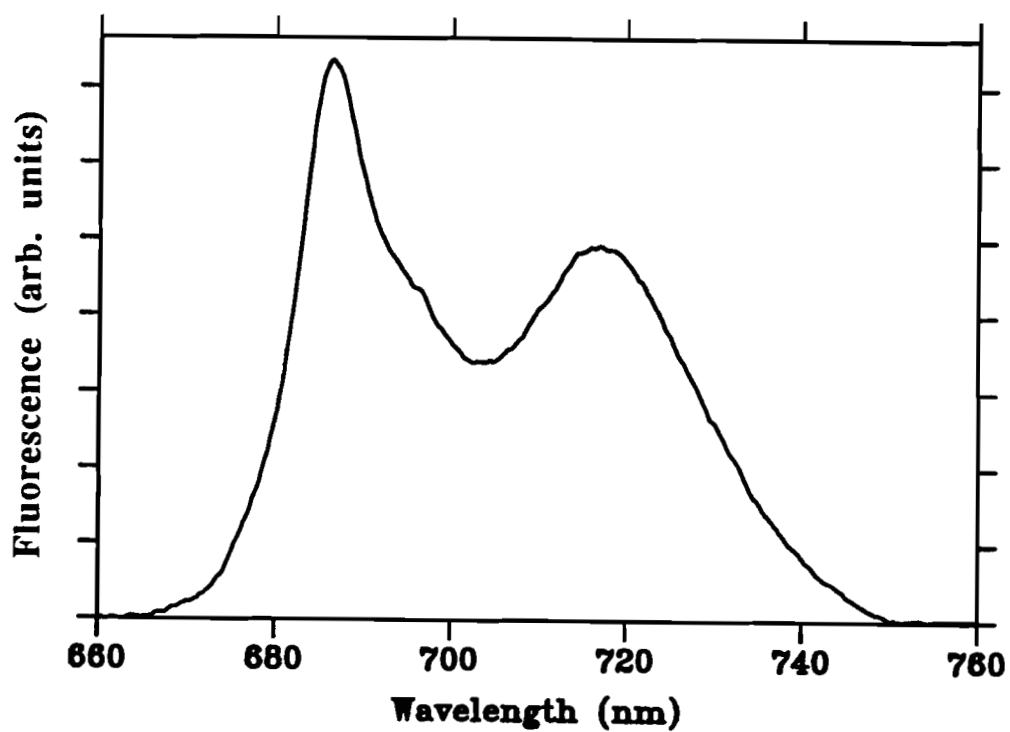


Fig. 5.4 Steady-state fluorescence emission spectrum of LM15-4D1C, a double mutant which lacks LHC and PSI, at 77 K. The wavelength resolution of the spectrum is 0.2 nm.

lower than those of wild type emission.

10-3C: a mutant missing PSI. The spectrum (Fig. 5.5) shows emission at 685 nm and 707 nm, similar to that of B4. F680, F695 can be distinguished from its derivative spectrum.

Although mutant strain 10-3C were derived from slightly different wild type cells, this should not effect the results relevant to our analysis [116].

The chlorophyll-protein complex contents of wild type and mutant C. reinhardtii used in the measurements are listed in Table 5.2. The protein-complex pigments are classified in the same terms as for green-plant chloroplasts.

Table 5.2 Complexes content of the wild type and mutant strains of C. reinhardtii.

	LHC	PSII	LHCI	PSI
DES15	+	+	+	+
B4	+	+	+	-
B1	+	-	+	+
LM15-4D1C	-	+	+	-
10-3C	+	+	+	-

The spectra of DES15, B4, B1, and 10-3C at 77 K exhibit characteristics similar to those of spectra observed with C. reinhardtii by several groups [51,109-111] with minor differences in relative intensities of emission bands. No published data have been found to be compared with the spectrum of LM15-4D1C at 77 K. The emission bands shown in most of the spectra are consistent with the properties of the mutants excepted the F719 in LM15-4D1C spectrum.

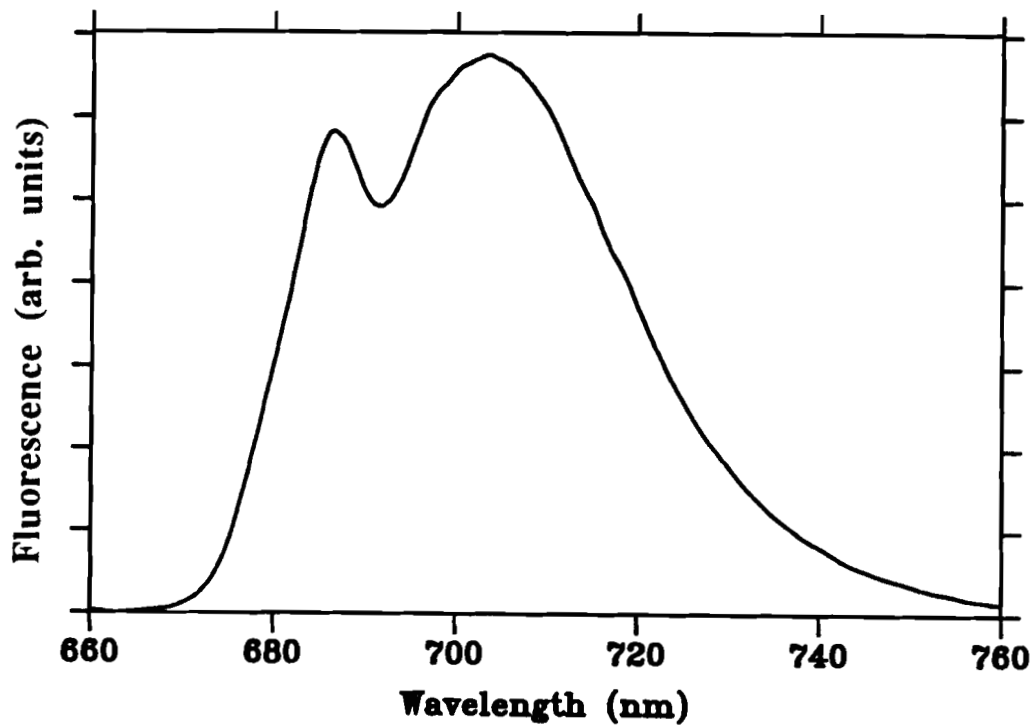


Fig. 5.5 Steady-state fluorescence emission spectrum of 10-3C, a PSI deficient mutant, at 77 K. The wavelength resolution of the spectrum is 0.2 nm.

The spectra of wild type and the PSI mutant 10-3C are normalized at 685 nm (Fig. 5.6). Two spectra have the same profile at wavelengths shorter than 685 nm. The increasing emission at 707 nm in the spectrum of 10-3C is due to the deficiency of PSI traps, i.e., LHCI fluoresces strongly when the PSI core complex is missing from the system. Similar results are also observed from the comparison of spectra of wild type with that of B4 (Fig. 5.7).

The emission spectrum of B1 contains a strong band at 681 nm and a shoulder at about 717 nm. A comparison of spectrum of B1 with that of DES15 is shown in Fig. 5.8. F685 and F695 are not seen in the spectrum of B1. The measurement indicated that at least a major part of excitation energy in LHC flows into PSII pigments in cells which have functional PSII.

Fig. 5.9a shows spectra of 10-3C and LM15-4D1C normalized at 685 nm. The difference spectrum of 10-3C and LM15-4D1C (Fig. 5.9b) has two bands at 680 and 706 nm which represents the emissions from LHC and LHCI respectively. Spectra of other LHC-containing sample also show the existence of LHC emission, i.e., F680 (Fig. 5.10). The fluorescence yield of F685 and F695 of LM15-4D1C are low, which indicates that the absorption cross-section of PSII core antenna is small and LHC is the major pigment to harvest light energy in the wild type cells.

By investigating the low-temperature fluorescence spectra of the wild type and different mutant strains, assignments and statements were made according to the characteristics of the samples. (1) LHC, the origin of F680, is mostly connected with PSII core antennas. However, its relation with LHCI is not clear. (2) The pigment emitting at 707 nm is LHCI which transfers excitation energy to PSI. In the case that the PSI core complex is deficient, the intensity of F707 increases dramatically.

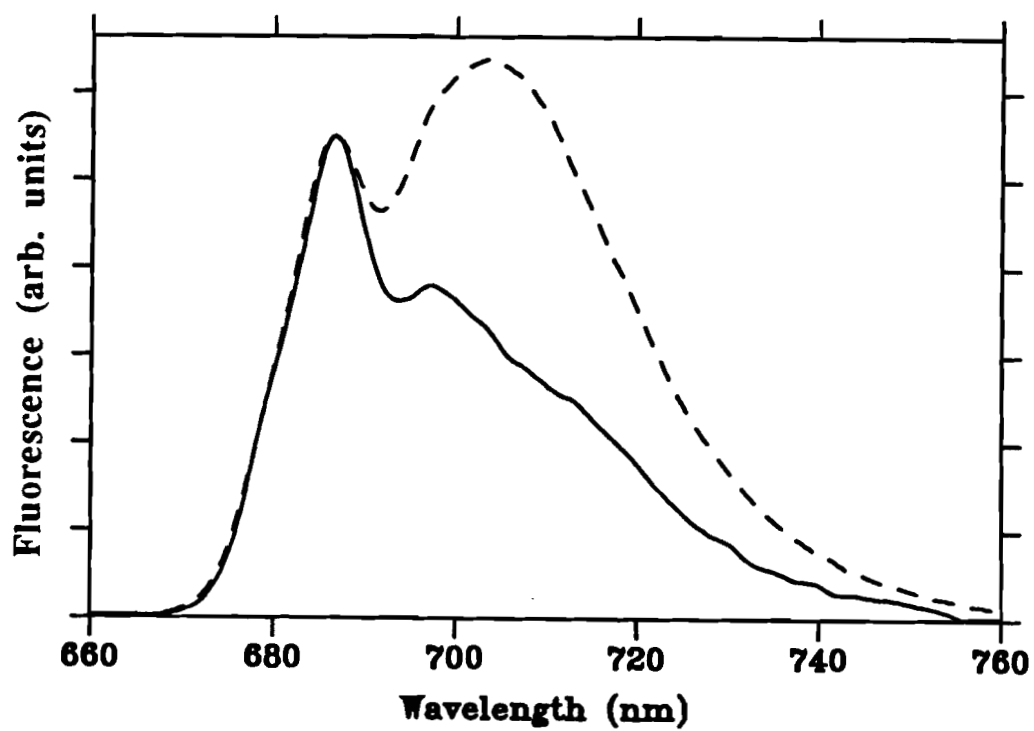


Fig. 5.6 A comparison of steady-state fluorescence emission spectra of DES15 (solid line) and 10-3C (dashed line) at 77 K. Spectra are normalized at 685 nm.

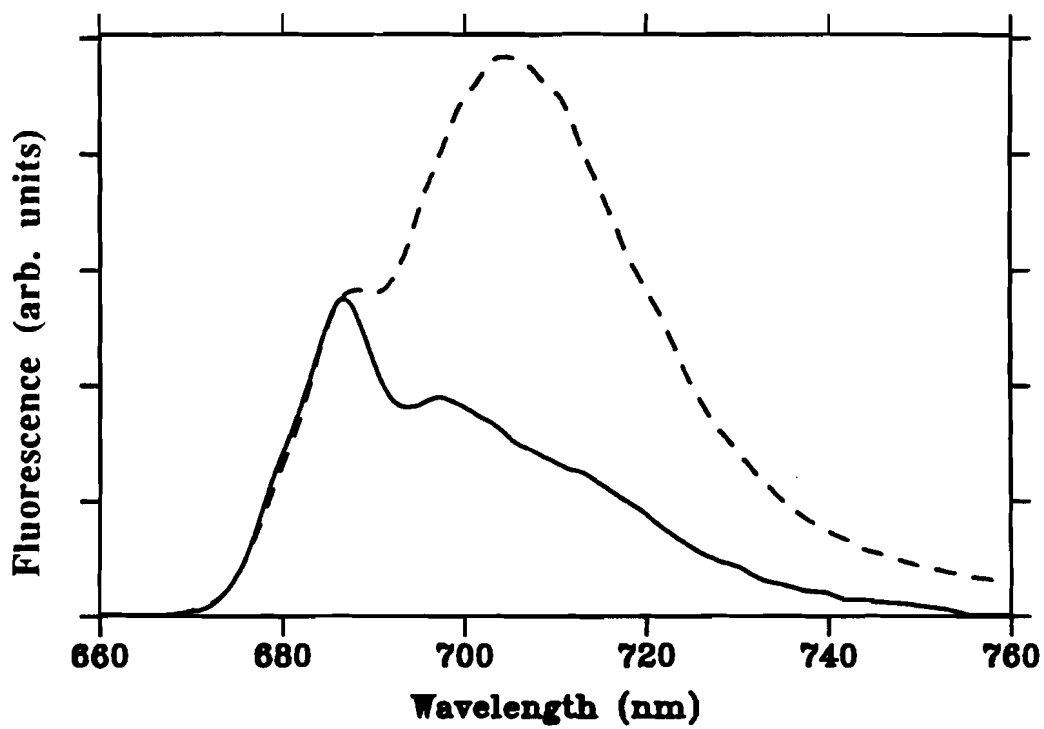


Fig. 5.7 A comparison of steady-state fluorescence emission spectra of DES15 (solid line) and B4 (dashed line) at 77 K. Spectra are normalized at 685 nm.

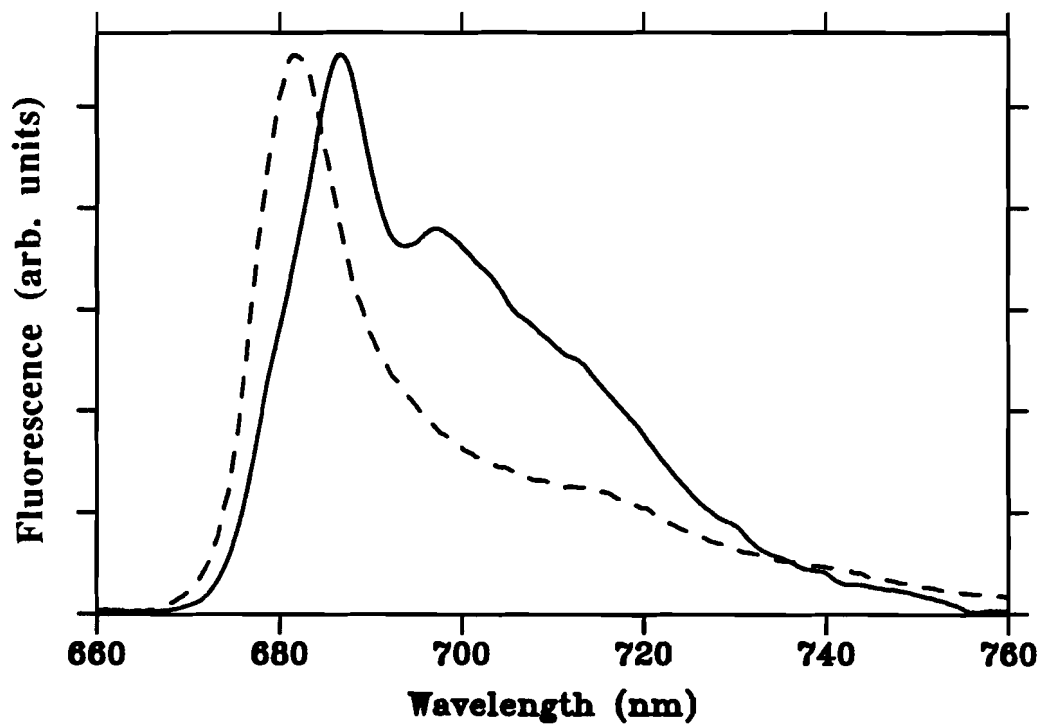


Fig. 5.8 A comparison of steady-state fluorescence emission spectra of DES15 (solid line) and B1 (dashed line) at 77 K normalized at the peak.

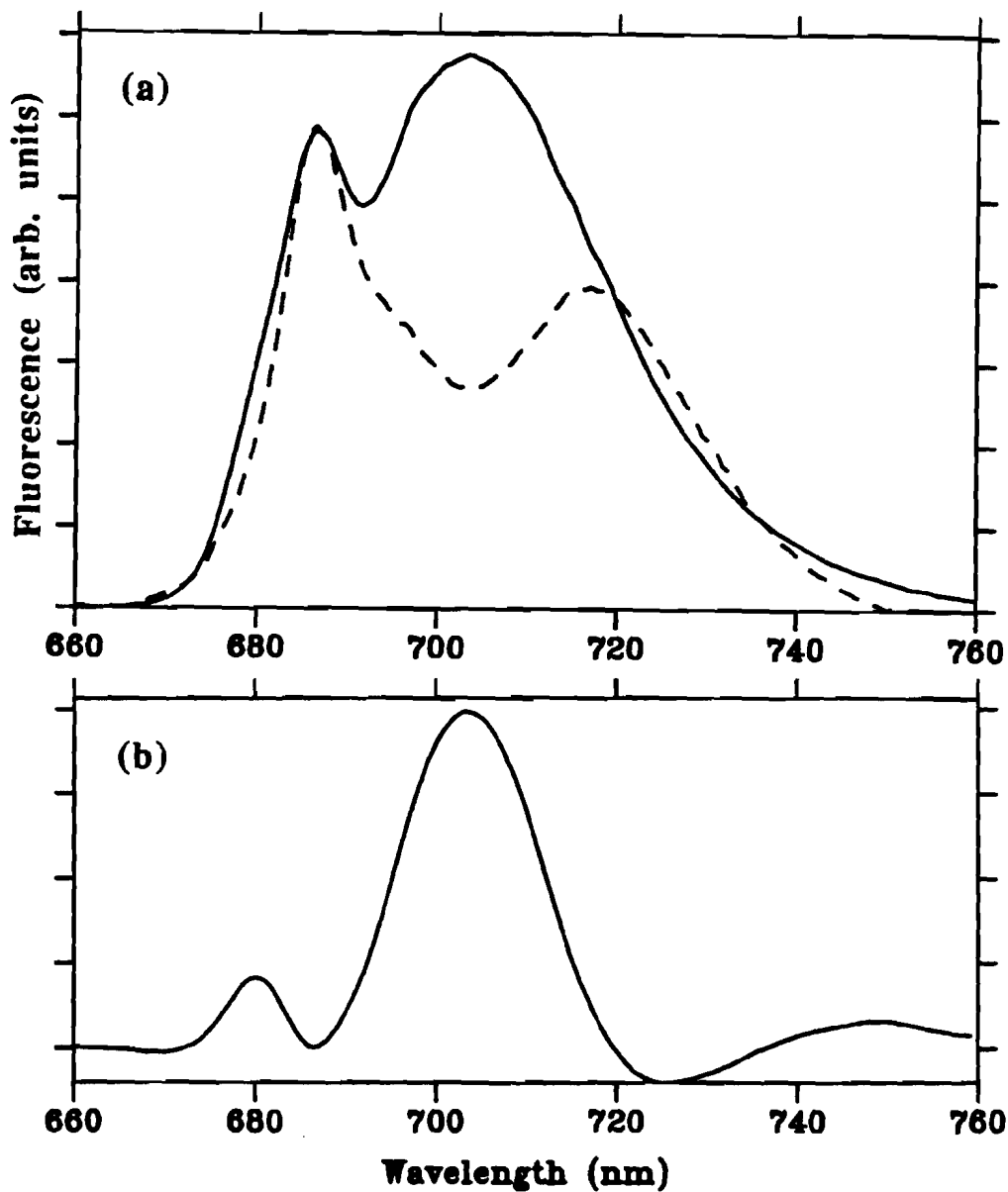


Fig. 5.9 (a) A comparison of steady-state fluorescence emission spectra of 10-3C (solid line) and LM15-4D1C (dashed line) at 77 K normalized at 685 nm. (b) The difference of the two curves in (a).

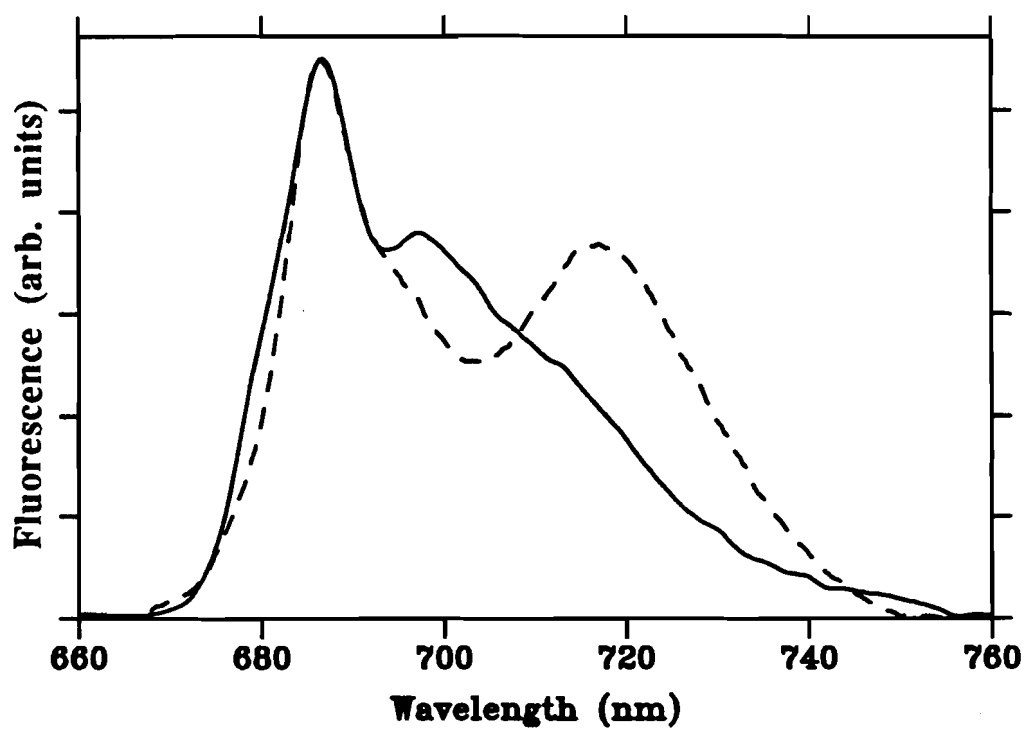


Fig. 5.10 A comparison of steady-state fluorescence emission spectra of DES15 (solid line) and LM15-4D1C (dashed line) at 77 K normalized at the peak.

5.3 Time-Resolved Fluorescence at 77 K

The question remaining in the spectral studies is that of whether LHC (the 680 nm emitting species) serves as the system antenna delivering excitation energy to both PSII and PSI. If the answer is "yes," what are the energy transfer rates? This question can be answered by examining the excitation kinetics of those pigments. Several measurements have been made here to provide information about energy transfer pathways between LHC and photosynthetic pigments. If the fast transfer in the short-wavelength region can be found in both wild type and PSI deficient mutants and it disappears in the mutants lacking LHC or lacking PSII, its relationship with LHC and PSII is confirmed. The existence of transfer from LHC (F680) to LHCI (F707) can be investigated by measuring the decay kinetics of F680 in the PSII deficient mutant and the rise phase of F707, to see whether LHCI is directly excited or gets excitation from other pigments.

A. The F680 Region

Time-resolved fluorescence of DES15, B4, 10-3C, B1 and LM15-4D1C was measured at 660 nm, 670 nm and 680 nm at 77 K. A preliminary data analysis was done by using two-exponential least-squares fitting routine. The results from DES15, B4 and 10-3C contained components with decay times of about 15 ps and 160 to 200 ps. The ratio of the amplitudes of the two components varied with detection wavelength. The fast decay contributes a larger portion of the total fluorescence at shorter wavelengths. This analysis shows characteristics similar to those observed in the same type of measurement of green-plant chloroplasts. There is no significant

difference between the data on wild type and the PSI-deficient mutants (i.e., B4 and 10-3C) at the wavelengths measured.

In contrast, the fluorescence decay curves collected at 660 nm, 670 nm and 680 nm from LM15-4D1C, a double mutant missing LHC and PSI, have the same rise and decay profiles at early time. Two-exponential fitting gives decay times of 110 ps and 500 ps. The 100 ps-decay component contributes more on the longer wavelength side. The fast decay resolved from wild type and PSI mutant data (on the order of 15 ps) was not found in this measurement. In fact, a nanosecond decay component was seen at shorter wavelengths with a very low amplitude, probably originating from dissociated chlorophyll *a* molecules.

Fig. 5.11 shows a comparison of the rise and decay of fluorescence detected at 660 nm, 670 nm and 680 nm from the various samples. The wild type and PSI mutant (DES15 and 10-3C respectively) show a significant wavelength-dependent change of the rise and decay profiles, while LM15-4D1C does not.

The fluorescence decay curves of B1 at 660 nm and 670 nm only show one exponential decay with a lifetime of about 650 to 780 ps. An additional component with a 40 ps lifetime is needed for the 680 nm-data. A time-resolved fluorescence curve of B1 measured at 670 nm at 77 K is shown in Fig. 5.12. Note that at room temperature, the decay lifetime of LHC in solvent is about 0.8 to 6 ns [105,112]. At low temperatures, the similar decay lifetime is assumed. The single exponential decay of B1 in 660 nm to 780 nm region in our measurement is a little shorter than the lifetime of dissociated LHC. It is possible that there is still some part of LHC which still involved in the energy transfer process, for example to PSI, and because of the signal-to-noise ratio, it cannot be resolved. In the next section, the study in the longer wavelength region will give aspect to this point.

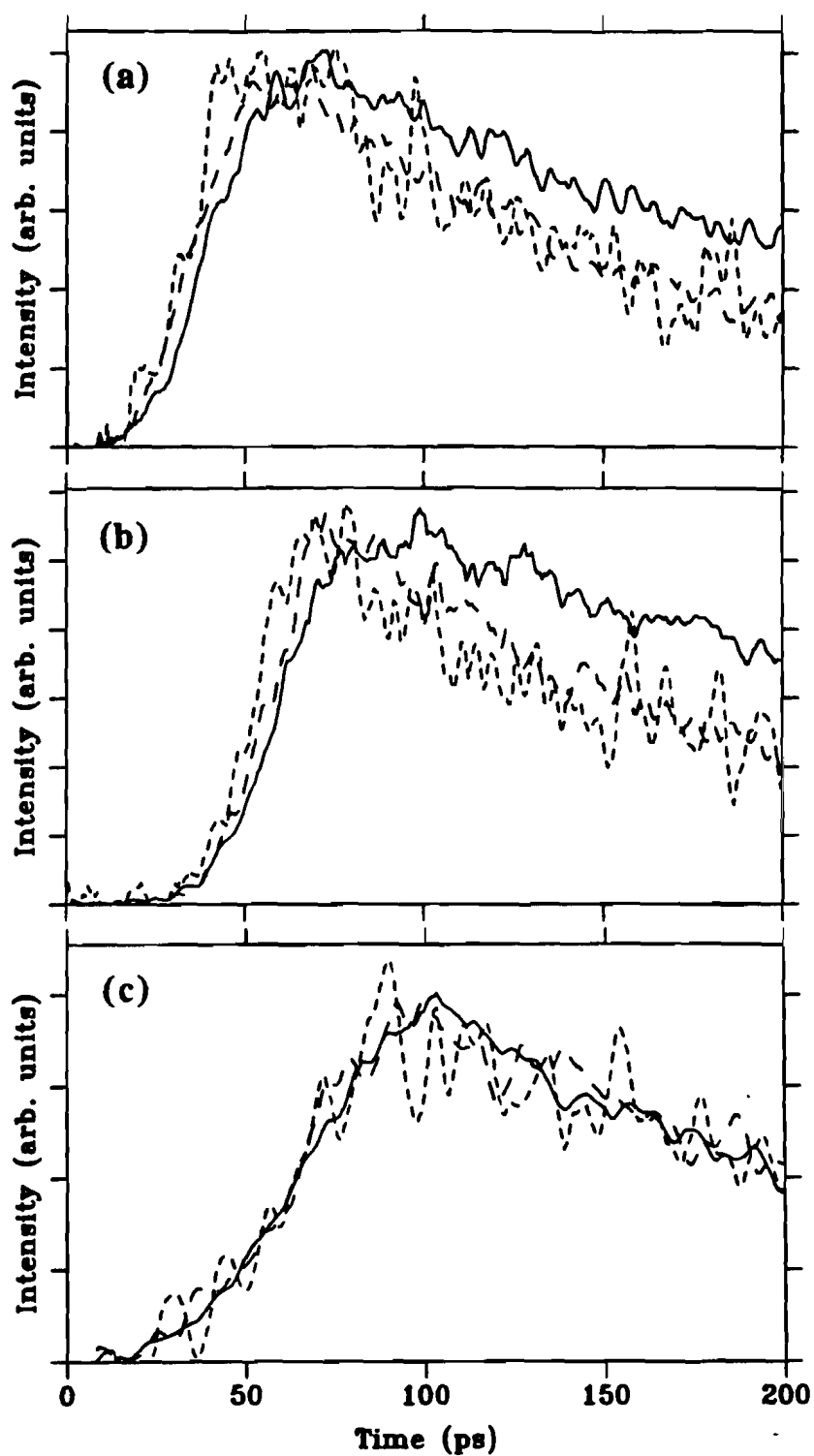


Fig. 5.11 Time-resolved fluorescence rise and decay profiles at 77 K from (a) DES15, (b) 10-3C and (c) LM15-4D1C. In each case, fluorescence measured at various wavelengths are plotted as short dashed line (F660), long dashed line (F670) and solid line (F680) and normalized at the peak.

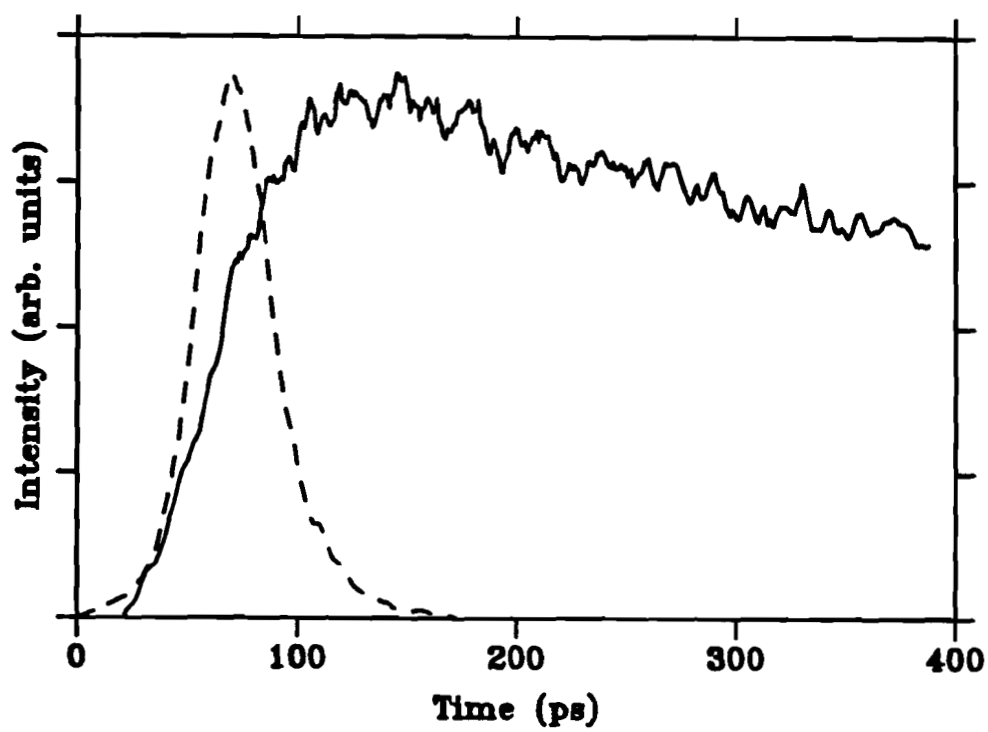


Fig. 5.12 Time-resolved fluorescence of B1 at 77 K measured at 670 nm. The dashed line is the profile of the excitation pulse.

B. The F715 Region

Time-resolved fluorescence was recorded at 700 nm, 710 nm and 720 nm from various mutant strains. The results for DES15 and one of the PSI mutants, 10-3C, measured at 720 nm, are shown in Fig. 5.13. A complicated rise phase which changed with detection wavelength was observed for DES15 and PSI-deficient mutants. The fluorescence decay of the PSI-deficient mutants is slower than that of the wild type. Two-exponential least-squares fitting showed a lifetime about 100 ps with a negative amplitude and a longer decay, on the order of several hundred picoseconds, with positive amplitude. The decay curves of B1, a PSII-deficient mutant, in this region show similarity to those of DES15. A fitting component with a negative amplitude usually indicates a delayed rise of fluorescence. No rise delay was found from the time-resolved fluorescence of LM15-4D1C in this region.

5.4 Kinetic Analysis

A. The F680 Region

The same kinetic model as the one used for green plant chloroplasts data in the same wavelength region (Fig. 4.5) was used to simulate the decay curves. The results are listed in Table 5.3. For each group of data, i.e. fluorescence detected at 660 nm, 670 nm and 680 nm from one sample, the same parameters could be used except the weights (A_1 and A_2) of fluorescence contributed by different populations.

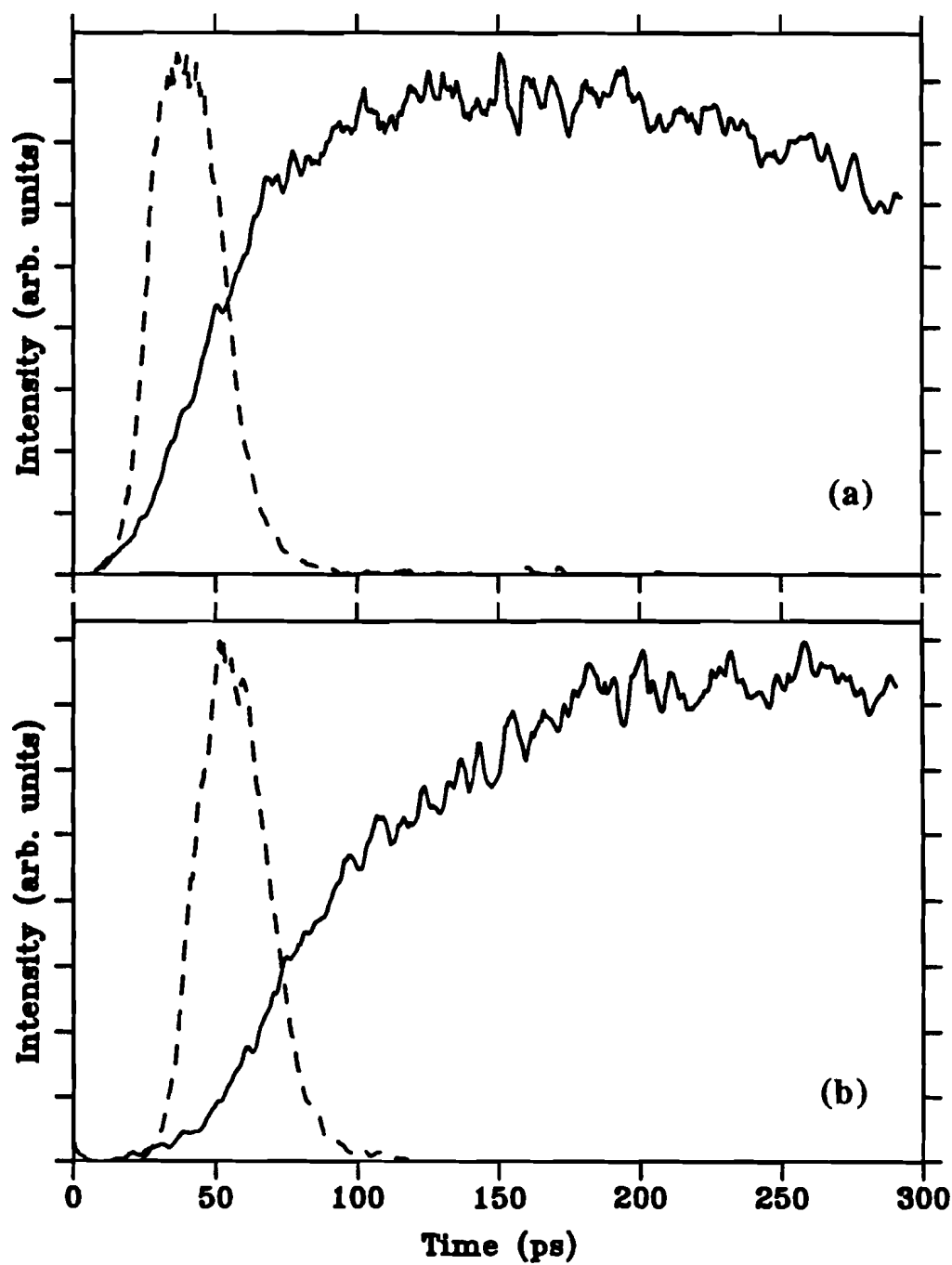


Fig. 5.13 Time-resolved fluorescence measured at 710 nm at 77 K from (a) DES15 and (b) 10-3C. Each curve is a sum of 100 shots. One OMA channel corresponds to 0.665 ps.

Table 5.3 Parameters used in kinetic model simulations in the F680 region.

sample	N_{10} ($1/\text{cm}^3$)	N_{20}	σ_1 (cm^2)	σ_2	τ_1 (ps)	k_{21} (1/ps)	τ_2 (ps)	k_{12} (1/ps)
wild type	10^{20}	10^{19}	10^{-17}	10^{-18}	1500	1/15	180	1/140
PSI-minus	10^{20}	10^{19}	10^{-17}	10^{-18}	1600	1/15	210	1/140

Time-resolved fluorescence and the theoretical fitting curves of DES15 and 10-3C at 660 nm, 670 nm and 680 nm are shown in Fig. 5.14 and Fig. 5.15 respectively.

The intensity ratio of the two emissions varied at different wavelengths. Population one contributed more at shorter wavelength. The fast decay of population one is mainly determined by the transfer rate k_{21} . The two lifetimes τ_1 and τ_2 are less dependent on both the detecting wavelength and the sample. Fig. 5.16 shows a plot of integrated fluorescence intensities of the fast decay and the slow decay at different wavelengths from DES15 and 10-3C integrated over a time period from 0 ps to 100 ps.

The results indicate that the energy transfer rates between the two populations are essentially the same within the wild type and PSI mutants and also agree with the data obtained from chloroplasts of higher plants. The fast component in the decay curves did not show as clearly compared with that in the green plant chloroplasts data, probably because of stronger scattering in the sample.

Based on kinetic analysis similar to that of green-plant chloroplast case and the fact that the fast decay disappears from the sample missing either PSII or LHC, the origin of the fast decay is clear, i.e. it is related to energy transfer between LHC and PSII core antenna. The excitation generated in LHC migrates among the chlorophylls

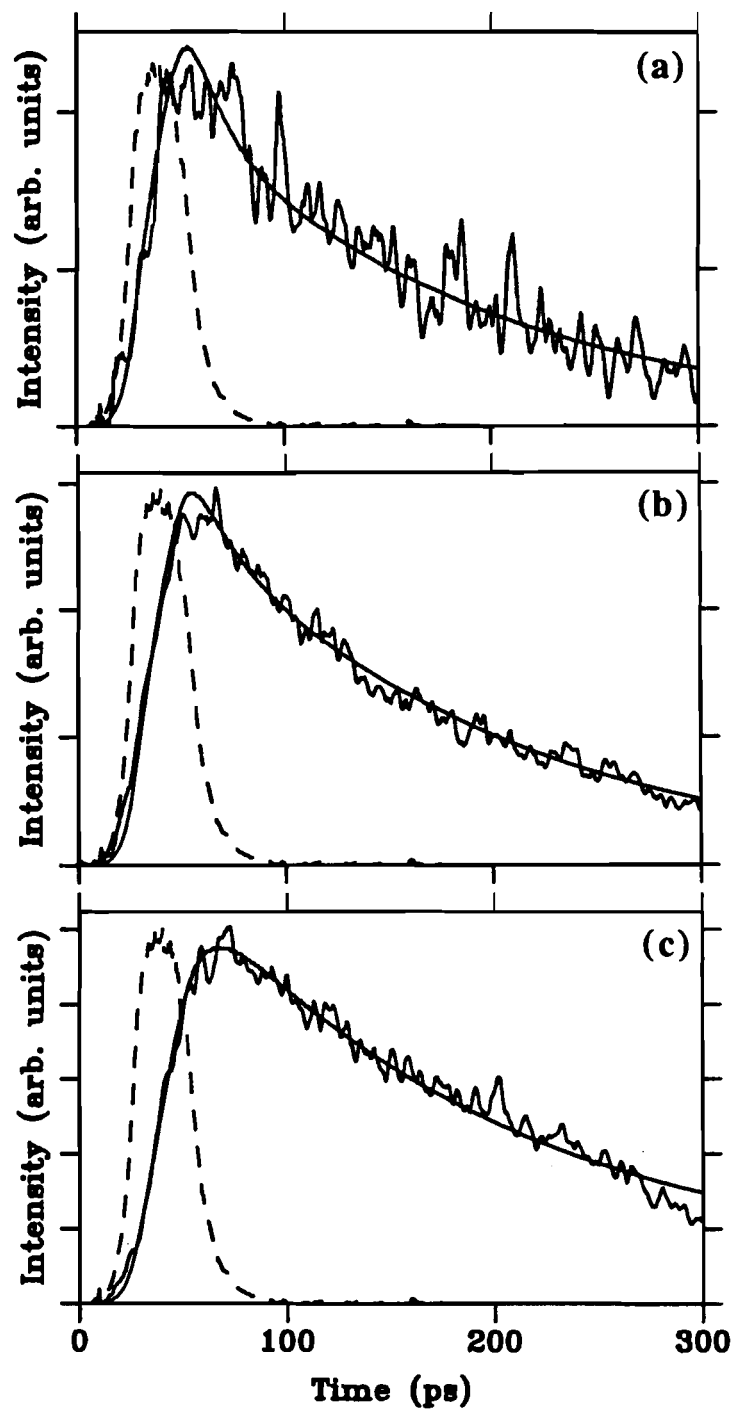


Fig. 5.14 Time-resolved fluorescence of DES15 at 77 K measured at (a) 660 nm, (b) 670 nm and (c) 680 nm with the theoretical fit. The dashed line in each frame is the profile of the excitation pulse. One OMA channel corresponds to 0.862 ps.

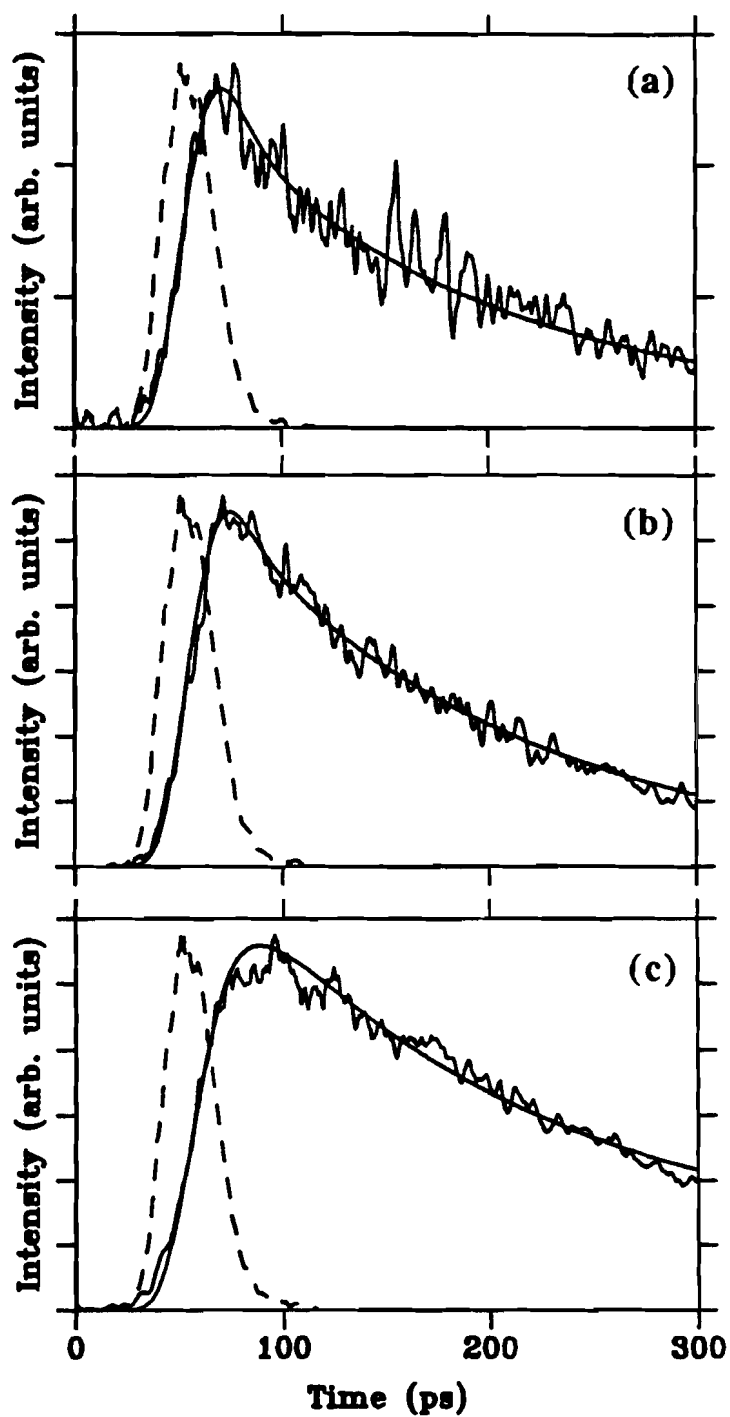


Fig. 5.15 Time-resolved fluorescence of 10-3C at 77 K measured at (a) 660 nm, (b) 670 nm and (c) 680 nm with the theoretical fit. The dashed line in each frame is the profile of the excitation pulse. One OMA channel corresponds to 0.862 ps.

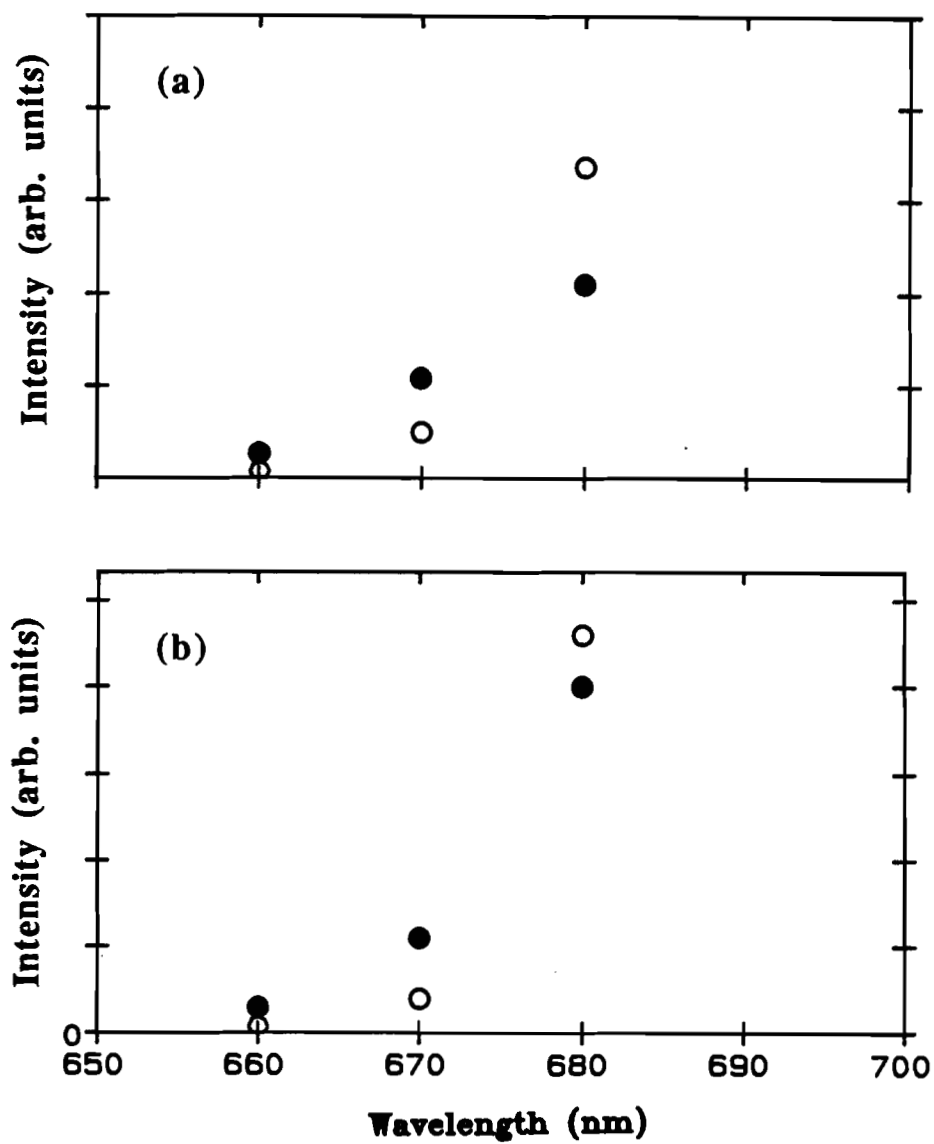


Fig. 5.16 Integrated fluorescence intensity of the fast (full circles) and the slow (open circles) components in the model simulation. Time interval: 0 ps – 10 ps. (a) DES15, (b) 1C3C.

within the LHC complex and transfers through the boundary of LHC to PSII, the overall process taking place with an average rate of $(15 \text{ ps})^{-1}$.

B. The F715 region

Time-resolved fluorescence measured in this region showed different rise and decay profiles changing with detection wavelength and sample, indicating a complicated energy transfer kinetics involving many components. Based on the knowledge of the contents of the photosynthetic components and their spectral characteristics, two kinetic models were used in the model simulation (shown in Fig. 5.17). It was assumed in the data fitting that LHCI, CP0a and PSI core antenna are the major emitters contributing to the fluorescence in the 700 to 720 nm region and that the emission bands of LHCI, CP0a and PSI core antenna are centered at 707 nm, 703 nm and 715 nm respectively. In model a, the system antenna LHC transfers its excitation energy to both PSII and LHCI then PSI. The latter also absorbs excitation directly. LHCI provides excitation to both CP0a and the PSI core antenna. In model b, only part of LHC is associated with LHCI, and excitation flows through an energy transfer chain: LHC \rightarrow LHCI \rightarrow CP0a \rightarrow PSI core.

The fitting parameters used in the simulation of the fluorescence decay curves of various samples are listed in table 5.4. Populations 1 to 4 represent LHC, LHCI, CP0a and the PSI core antenna, respectively. The parameters for the consistent part of the sample were kept the same whenever possible. In model a, τ_1 was chosen to be 15 ps for wild type and the PSI-deficient mutant, as the energy transfer rate from LHC to PSII obtained from the previous studies is $(15 \text{ ps})^{-1}$. It was set equal to 1000 ps for the case of B1 since PSII is missing from this mutant. The population of the PSI core antenna was set to zero in the case of PSI-deficient mutant. The back transfer rates

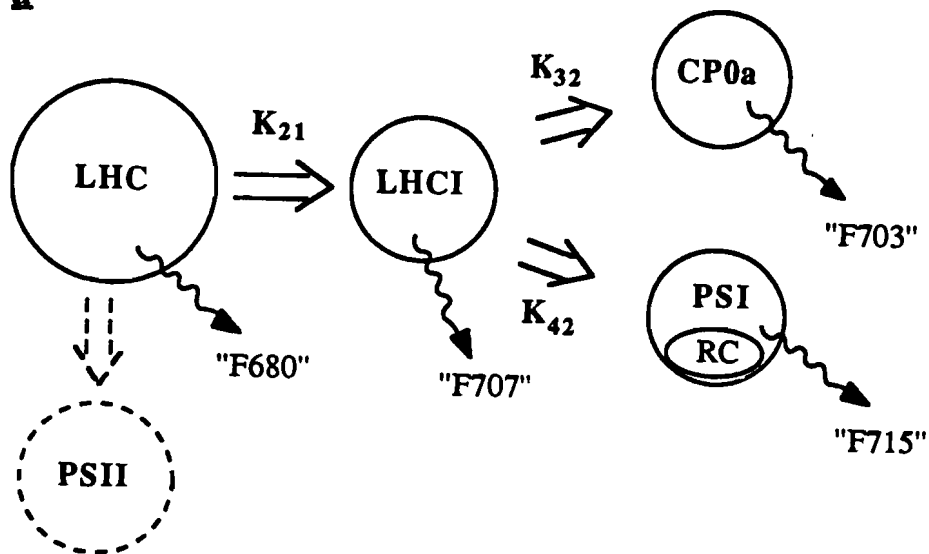
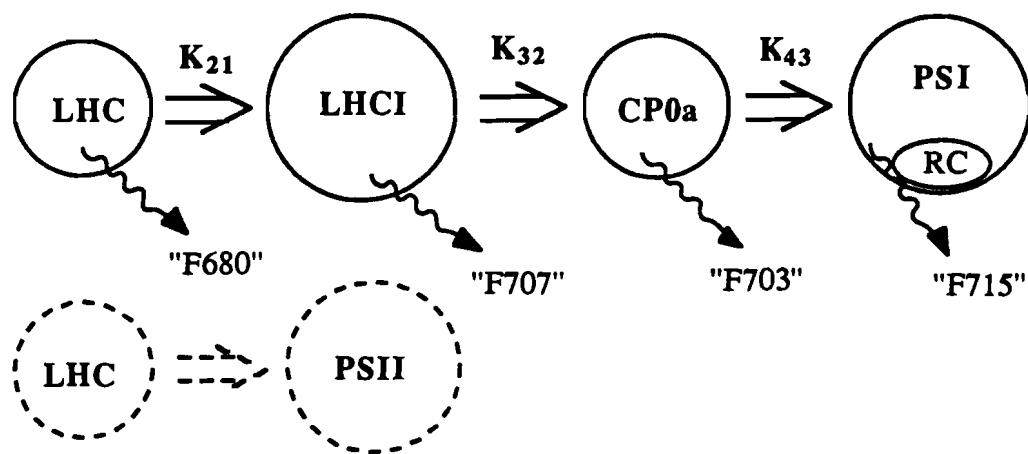
model a**model b**

Fig. 5.17 Kinetic models proposed to fit experimental curves measured in the wavelength region where PSI emits. The arrows indicate excitation transfer pathways and K_{ij} s are the transfer rate constants. Back transfer paths are not labelled and are discussed in the text. Numbers in quote marks represent emission peak wavelengths of hypothesized component fluorescence bands.

Table 5.4 Parameters used in kinetic model simulation of fluorescence in PSI emission region.

Symbol	model a			model b		
	DES15	10-3C	B1	DES15	10-3C	B1
N_{10} (10^{16})	10000	10000	7000	1500	1500	1500
N_{20} (cm^{-3})	3000	3000	3000	3000	3000	3000
N_{30}	500	500	500	300	300	300
N_{40}	500	0	500	300	3	300
σ_1 (10^{-19})	100	100	100	100	100	100
σ_2 (cm^2)	100	100	100	100	100	100
σ_3	1	1	1	1	1	1
σ_4	1	0	1	1	1	1
τ_1 (ps)	15	15	1000	1000	1000	1500
τ_2	2000	2000	2000	2000	2000	2000
τ_3	2000	1500	2000	2000	2000	2000
τ_4	15		15	75	100	100
k_{21} (ps^{-1})	$(100)^{-1}$	$(100)^{-1}$	$(150)^{-1}$	$(60)^{-1}$	$(60)^{-1}$	$(60)^{-1}$
k_{32}	$(150)^{-1}$	$(150)^{-1}$	$(150)^{-1}$	$(33)^{-1}$	$(33)^{-1}$	$(33)^{-1}$
k_{42}	$(100)^{-1}$	0	$(100)^{-1}$	0	0	0
k_{43}	0	0	0	$(75)^{-1}$	$(75)^{-1}$	$(75)^{-1}$

required in this model were much smaller than values calculated according to the Boltzmann factor. Comparison of the experimentally-deduced back transfer rates with the rates from model simulations are shown in table 5.5. With model b, the population of LHC was less than that in model a which suggests that only part of LHC transfers excitation to LHCI and this part of LHC is not associated with PSII. The model b back transfer rates used in the data fitting were very close to those estimated by the Boltzmann distribution (see table 5.5). The major difference from model a is that a smaller number of LHC had to be used; the fluorescence decay lifetime of this part of LHC does not depend on the existence of PSII. Time-resolved fluorescence of DES15, 10-3C and B1 with their theoretical curves from model b are shown in Fig. 5.18 to Fig. 5.20. The fitting curves using model a are quite similar to those of from model b, so they are not shown here.

Table 5.5 Ratio of energy transfer and back transfer rates used in the model simulation at 77 K.

	K_{23}/K_{32}	K_{24}/K_{42}	K_{34}/K_{34}
calculated according to the Boltzmann factor	4.506	0.052	0.011
obtained from model <u>a</u>	0.745	0.025	
obtained from model <u>b</u>	4.4		0.03

Both models can be used to obtain reasonable results. The fitting in model a is sensitive to the change of transfer rates between LHCI and CP0a, while in model b, the ratio of LHC to LHCI and the decay lifetime of the PSI core antenna are the main factors which effect the fluorescence profiles. The fitting parameters used in the

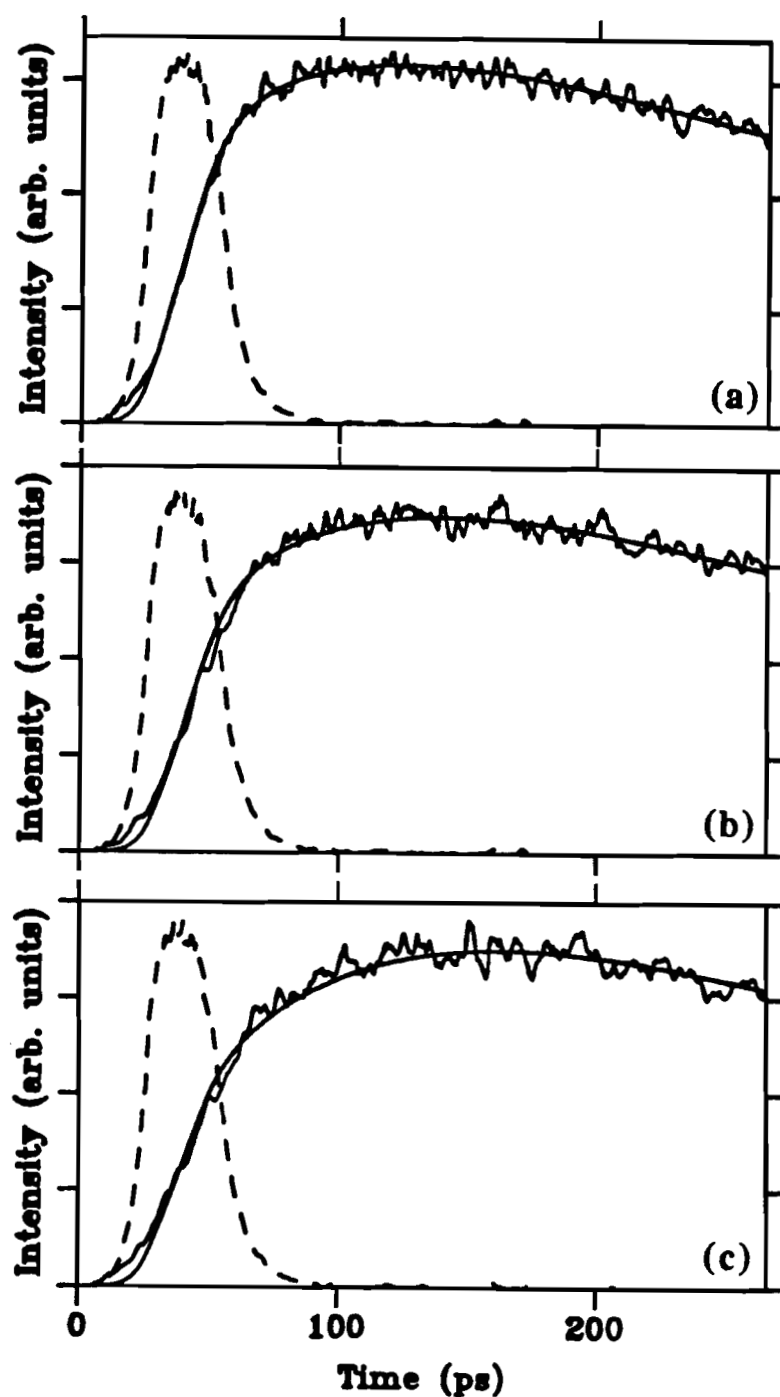


Fig. 5.18 Time-resolved fluorescence of DES15 at 77 K measured at (a) 700 nm, (b) 710 nm and (c) 720 nm with the theoretical fit using model **b** in Fig. 5.17. The dashed line in each frame is the profile of the excitation pulse. One OMA channel corresponds to 0.665 ps.

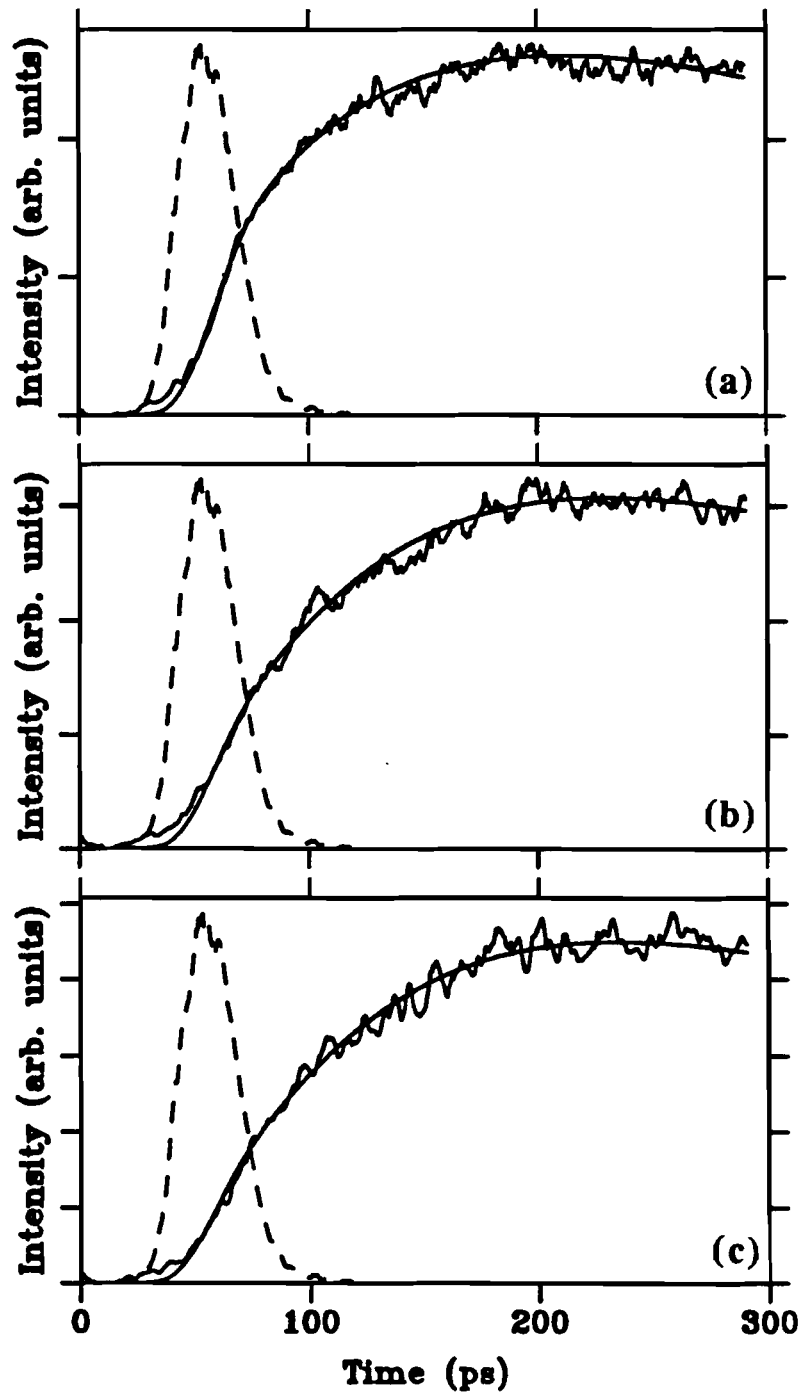


Fig. 5.19 Time-resolved fluorescence of 10-3C at 77 K measured at (a) 700 nm, (b) 710 nm and (c) 720 nm with the theoretical fit using model b in Fig. 5.17. The dashed line in each frame is the profile of the excitation pulse. One OMA channel corresponds to 0.665 ps.

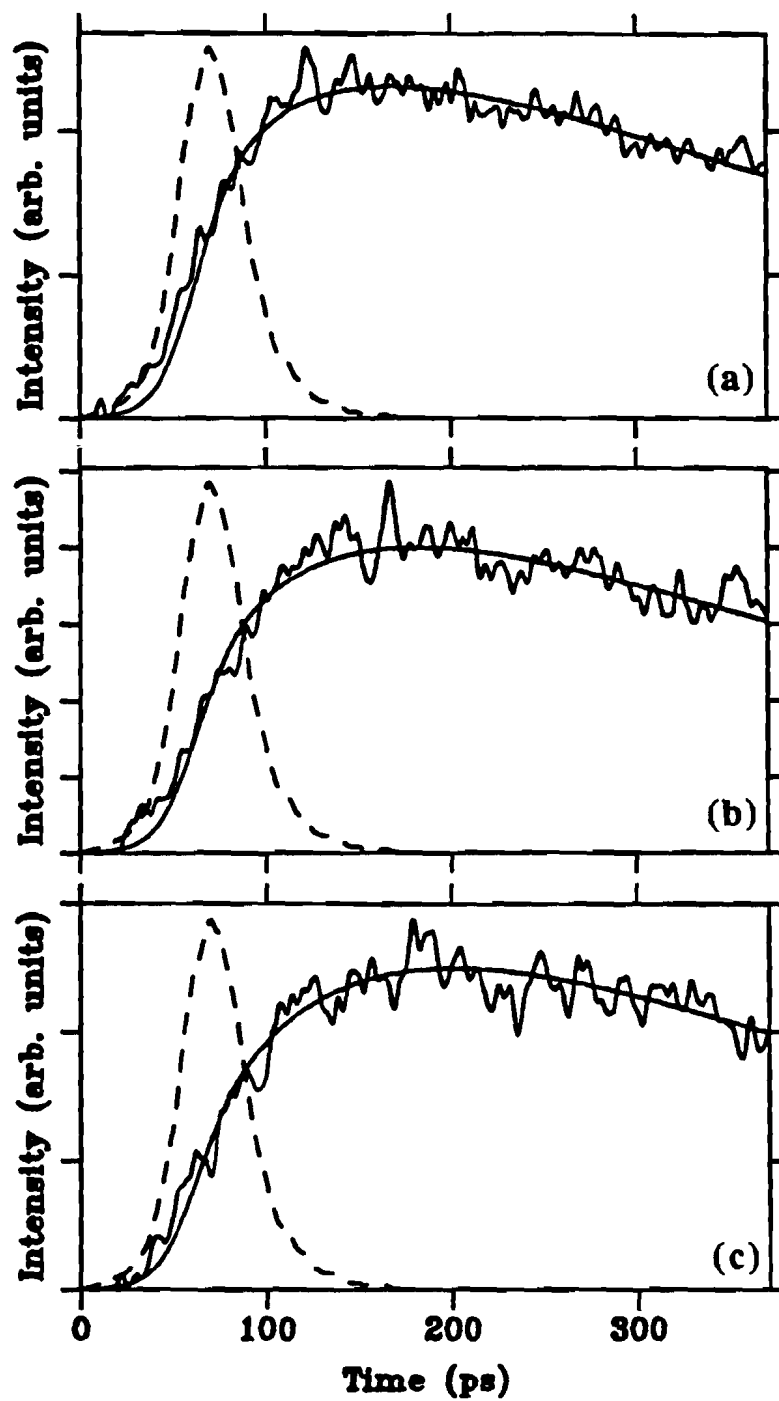


Fig. 5.20 Time-resolved fluorescence of B1 at 77 K measured at (a) 700 nm, (b) 710 nm and (c) 720 nm with the theoretical fit using model **b** in Fig. 5.17. The dashed line in each frame is the profile of the excitation pulse. One OMA channel corresponds to 0.862

calculation were highly hypothetical. However, one thing is clear: that an energy transfer to LHCI is necessary. It is this transfer which causes the rise delay of the F707 component. It is reasonable to assign LHC as the pigment which provides excitation energy to LHCI with a rate of $(60 \text{ ps})^{-1}$ in model a and $(100 \text{ ps})^{-1}$ in model b.

5.5 Summary and Discussion

Time-resolved fluorescence of wild type and mutant C. reinhardtii was measured at various wavelengths at 77 K. Particular attention was paid in two regions: the wavelengths around 680 nm where LHC emits and the wavelengths from 700 nm to 720 nm where PSII and its associated parts emit. The goal was to find energy transfer pathways and transfer rates between LHC and other part of the system.

At short wavelengths, a fast decay was resolved from the fluorescence decay of those samples which contain both LHC and PSII. Kinetic analysis shows that this short-lived component originates from LHC emission which transfers its excitation energy to PSII core antenna with a high efficiency. This transfer was not seen in the mutant strains missing either PSII or LHC. The steady-state emission spectrum of B1, a PSII-deficient mutant, shows a strong band at 681 nm which arises from the increase of the fluorescence lifetime of F680 from 15 ps to 700 ps. F685 and F695 in the spectrum of LM15-4D1C, a mutant without LHC, have much lower fluorescence yields than they have in the spectrum of wild type. These facts indicate that LHC and PSII core antenna are closely coupled and the PSII core antenna gets most of its excitation from LHC. The experimental results on wild type C. reinhardtii at 77 K generally agree with those obtained from green-plant chloroplasts (in chapter 4). The studies of various mutant strains provide further information about the kinetic connection between

LHC and PSII. The tentative assignment in chapter 4 that the short-lived component originates from LHC which transfers excitation to PSII efficiently is therefore confirmed.

The fluorescence at long wavelengths showed a rise delay in all samples containing LHC. Its apparent rise time was found to be 120 ± 20 ps. Deficiency of PSI mainly affects the decay time in this region. Two kinetic models were proposed to simulate fluorescence decay curves. Model **a** was proposed upon analogy with the F735 emission in PSI of green-plant chloroplasts [40]. In model **a**, LHC which provides excitation to LHCI originates from the same photosynthetic pigment as the one providing excitation to PSII, but at different rate. And CP0a is an alternative trap of antenna excitation energy that competes with the PSI reaction center and core antenna closely associated with it. All the energy back transfer rates obtained from this model fitting are very small, therefore negligible. Model **b** was based on a chain-model proposed by Garnier *et al.* [51]. A rather small amount of LHC is required to supply the excitation to LHCI. This supports the model that LHC has two kinetically distinguishable parts which provide excitation to PSI and PSII separately. The transfer rates which are faster than in model **a** were obtained and the back transfer rates between different components are needed with values close to the calculation according to the Boltzmann factor. The results indicated that LHCI, the peripheral antenna of PSI, obtains at least part of its excitation from LHC. The transfer rate from LHC to LHCI is in a range of $(60 \text{ ps})^{-1}$ to $(100 \text{ ps})^{-1}$. Both models support the view that there exists a large amount of LHC, the origin of the F680, which provide excitation to both photosystems. Further distinction between the model **a** and **b** can be made by studying a mutant which lacks the CP0a species.

A delayed and multiphasic rise of the fluorescence was observed in the PSI emission region at 77 K. Its apparent rise time of 120 ± 20 ps agrees very well with the results from green-plant chloroplasts at 735 nm where PSI emits. In the latter case, a 50–150 ps rise time was found from multi-exponential least-squares fitting of photon counting data [75,78]. It was resolved into a biphasic rise in a higher time resolution measurement [40]. The delayed rise was related to the rate-limiting step of transfer from LHC to PSI antenna with subsequent rapid transfer to C705, the emitter at 735 nm.

The transfer kinetics at room temperature are quite different. Recent studies by Holzwarth *et al.* [119] on green-plant chloroplasts and by Owens *et al.* [120] on green algae show different fluorescence characteristics than those from low temperature measurements. The fluorescence rise and decay from PSI do not depend on the excitation wavelength which is in contrast with the result at 77 K [64], explained by rapid excitation equilibration among the various pigments. No rise time longer than 20 ps was observed in the room temperature data. We can easily understand this major difference by assuming that one of the forward transfer steps is “uphill” [121]. In either model *a* or *b* the emitter of F707 precedes that of F703 in the sequence. Their energy level difference can be taken to be only 0.01 eV and the ratio of forward and backward transfer rate is about 0.68 at room temperature, so thermal equilibrium can be reached in a short time. Since the forward transfer is an uphill transfer, the transfer rate could be much smaller at 77 K than at room temperature which will effect the rise time of fluorescence. This aspect helps us to understand the difference between room temperature and 77 K results from both green algae and green-plant chloroplasts. It also shows the importance of a detailed kinetic study over a wide temperature range.

It is suggested for further studies that (1) in the F715 region, the investigation of a mutant which lacks CP0a would be very interesting. This should be able to distinguish the two kinetic models introduced in this chapter. Such a study will tell whether CP0a acts as the middle component delivering excitation from LHCI to the PSI core antenna or as an alternative trap competing with the PSI core antenna. (2) A temperature dependence study in the long wavelength PSI-emission region will be very informative. Both time-resolved and steady-state fluorescence of green-plant chloroplasts and green algae show marked differences between room temperature and low temperature data. Some steady-state measurements have been done over a wide temperature region (for example, see [64,95]), however, most of the time-resolved fluorescence measurements have only been done at room temperature and at 77 K. It is clear that a temperature dependence study will be helpful to understand the changes and provide information about the connection between kinetics at different temperatures.

REFERENCES

1. Govindjee and R. Govindjee, "Introduction to photosynthesis", (1975) in: *Bioenergetics of Photosynthesis* (Govindjee, ed.), Academic Press, New York, 1-50.
2. Clayton, R.K., "Photosynthesis, Physical Mechanisms and Chemical Patterns", (1980) Cambridge University Press, Cambridge, UK, 165-262.
3. Thornber, J.P., "Biochemical characterization and structure of pigment-proteins of photosynthetic organization", (1986) in *Photosynthesis III: Photosynthetic Membranes and Light Harvesting Systems*. Vol.19 of the *Encyclopedia of Plant Physiology*, new series, 98-142, (L.A. Staehelin and C.J. Arntzen, eds.), Springer-Verlag Press, Berlin.
4. Staehelin, L.A., "Chloroplast structure and supramolecular organization of photosynthetic membranes", (1986) in [3] chapter 1, 1-84.
5. See, e.g., various articles in: *Primary Processes of Photosynthesis*. (1977) (J. Barber ed.) Elsevier/North Holland Biomedical Press, Amsterdam.
6. Karukstis, K.K. and K. Sauer, "Fluorescence decay kinetics of chlorophyll in photosynthetic membranes", (1983) *J. of Cellular Biochemistry* **23**, 131-158.
7. Geacintov, N.E. and J. Breton, "Energy transfer and fluorescence mechanisms in photosynthetic membranes", (1987) in *Critical Reviews in Plant Sciences*, Vol. 5 Issue 1, 1-44, CRC Press.
8. Sauer, K. and H. Scheer, "Excitation transfer in C-phycoyanin. Förster transfer rate and exciton calculations based on new crystal structure data for C-phycoyanins from *Agmenellum quadruplicatum* and *Mastigocladus laminosus*", (1988) *Biochem. Biophys. Acta* **936**, 157-170.
9. Satoh, K. and W.L. Butler, "Competitions between the 735 nm fluorescence and the photochemistry of photosystem I in chloroplasts at low temperature", (1978) *Biochem. Biophys. Acta* **502**, 103-110.
10. Knox, R.S., "Excitation dynamics in biomolecular systems", (1987) In: *Excited-State Spectroscopy in Solids*, 31-Rendiconti S.I.F.-XCVI Corso, Soc. Italiana di Fisica-Bologna-Italy, 481-509.
11. Hooper, K.J., "Chloroplasts", (1984) Plenum Press, New York.
12. Breton, J., "Molecular orientation of the pigments and the problem of energy trapping in photosynthesis", (1986) in [3] section 7.4, 319-326.
13. Robertson, R.N., "The Lively Membrane", (1983) Cambridge University Press, Cambridge, UK.

14. Geacintov, N.E. and J. Breton, "Topology dimensions of antenna pigment system probed by exciton annihilation", (1986) in [3] section 7.3, 310-328.
15. Miller, K.R., "The photosynthetic membrane", (1979) *Sci. Am.* **241**(4), 102-113.
16. Peter, G.F. and J.P. Thornber, "The antenna components of photosystem II with emphasis on the major pigment-protein, LHC IIb", in *Proc. Intl. Workshop, Photosynthetic Light-Harvesting Systems: Structure and Function*, 175-186, Freising, FRG, Oct 12-16, 1987 (Scheer, H. and Schneider, S. eds) De Gruyter, Berlin.
17. Michel, H. and J. Deisenhofer, "X-Ray diffraction studies on a crystalline bacterial photosynthetic reaction center: a progress report and conclusions on the structure of photosystem II reaction centers", (1986) in [3] section 8.4 371-387.
18. Golbeck, J.H., "Structure, Function and organization of the photosystem I reaction center complex", (1987) *Biochem. Biophys. Acta* **895**, 167-204.
19. Markwell, J.P., J.P. Thornber and R.T. Boggs, "Higher plant chloroplasts: evidence that all the chlorophyll exists as chlorophyll-protein complexes", (1979) *Proc. Natl. Acad. Sci. USA* **76**, 1233-1235.
20. Matthews, B.W., R.E. Fenna, M.C. Bolognesi, M.F. Schmid and J.M. Olson, "Structure of a bacteriochlorophyll *a*-protein from the green photosynthetic bacterium *Prosthecochloris aestuarii*", (1979) *J. Mol. Biol.* **131**, 259-285.
21. Kühlbrandt, W., "Three-dimensional crystals of the light-harvesting chlorophyll *a/b* protein complex from pea chloroplasts", (1987) *J. Mol. Biol.* **194**: 757-762.
22. Kühlbrandt, W., "Structure of the light-harvesting chlorophyll *a/b*-protein complex from chloroplast membranes", (1988) in [16], 211-215.
23. Zuber, H., "Structure and function of light-harvesting complexes and their polypeptides", (1985) *Photochem. Photobiol.* **42**, 821-844.
24. Butler, P.J.G. and W. Kühlbrandt, "Determination of the aggregate size in detergent solution of the light-harvesting chlorophyll *a/b* protein complex from chloroplast membranes", (1988) *Proc. Natl. Acad. Sci. USA* **85**, 3797-3801.
25. Breton, J. and N.E. Geacintov, "Picosecond fluorescence kinetics and fast energy transfer processes in photosynthetic membranes", (1980) *Biochem. Biophys. Acta* **594**, 1-31.
26. Holzwarth, A.R., "Excited state kinetics of chlorophyll antenna pigments", (1986) in [3] section 7.2, 299-309.

27. Van Grondelle, R., "Excitation energy transfer, trapping and annihilation in photosynthetic systems", (1985) *Biochem. Biophys. Acta* **811**, 147-195.
28. Rabinowitch, E. and Govindjee, "Photosynthesis", (1969) J. Wiley and Sons, Inc., New York.
29. Danks, S.M., E.H. Evans and P.A. Whittaker, "Photosynthetic Systems: Structure, Function and Assembly", (1983) J. Wiley and Sons, Inc., New York.
30. Kenkre, V.M. and R.S. Knox, (a) "Theory of fast and slow excitation transfer rates", (1974) *Phys. Rev. Lett.* **33**, 803-806. (b) "Optical spectra and exciton coherence", (1976) *J. Lum.* **12/13**, 187-192.
31. Förster, Th.W., "Transfer mechanisms of electronic excitation", *Faraday Soc. Disc.* **27**, 7-17.
32. Weidner, R. and Georghiou S., "Global computational techniques", (1988) In: *Time-Resolved Laser Spectroscopy in Biochemistry, Proceedings of SPIE* **909**, 402-410.
33. Knox, R.S., "Excitation energy transfer and migration: theoretical considerations", (1975) In: *Bioenergetics of Photosynthesis*, (Govindjee, ed.), Academic Press, New York, 183-221.
34. Knox, R.S., "Photosynthetic efficiency and exciton trapping", (1977) In: *Primary processes of Photosynthesis, Vol. 2*, (J. Barber ed.), Elsevier Press, Amsterdam, 55-97.
35. Pearlstein, R.M., "Chlorophyll singlet excitons", (1982) In: *Photosynthesis: Energy Conversion by Plants and Bacteria, Vol. 1*, (Govindjee, ed.), Academic Press, New York, 293-330.
36. Paillotin, G., "Transport and capture of electronic excitation energy in the photosynthetic apparatus", (1972) *J. Theor. Biol.* **36**, 223-235.
37. Paillotin, G., "Capture frequency of excitations and energy transfer between photosynthetic units in the photosystem II", (1976) *J. Theor. Biol.* **58**, 219-235.
38. Pearlstein, R.M., "Exciton migration and trapping in photosynthesis", (1982) *Photochem. Photobiol.* **35**, 835-844.
39. Freiberg, A., V.I. Godik and K. Timpmann, "Excitation energy transfer in bacterial photosynthesis studies by picosecond laser spectrochronograph", (1984) in: *Advances in Photosynthesis Research, Vol. 1*, 45 (C. Sybesma ed.) M. Nijhoff/Dr. W. Junk Publisher, The Hague, Netherlands.

40. Wittmershaus, B., T.M. Nordlund, W.H. Knox, R.S.Knox, N.E. Geacintov, and J. Breton, "Picosecond studies at 77 K of energy transfer in chloroplasts at low and high excitation intensities", (1985) *Biochem. Biophys. Acta* **806**, 93-106.
41. Geacintov, N.E., J. Breton and R.S. Knox, "Excitation transfer and exciton trapping in green plant photosynthesis", (1986) *Photosynthesis Research* **10**, 233-242.
42. Schatz, G.H., H. Brock and A.R. Holzwarth, (a) "Picosecond kinetics of fluorescence and absorbance changes in photosystem II particles excited at low photon density", (1987) *Proc. Natl. Acad. Sci., USA* **84**, 8414-8418.
(b) "Kinetics and energetic model for the primary processes in photosystem II", (1988) *Biophys. J.* **54**, 397-405.
43. Klimov, V.V., A.V. Klevamik, V.A. Shuvalov and A.A. Krasnysky, "Reduction of pheophytin in the primary light reaction of photosystem II", (1977) *FEBS Lett.* **82**, 183-186.
44. Goedheer, J., "Fluorescence bands and chlorophyll forms", (1964) *Biochem. Biophys. Acta* **88**, 403-431.
45. Bose, S., "Chlorophyll fluorescence in green plants and energy transfer pathways in photosynthesis", (1982) *Photochem. Photobiol.* **36**, 725-731.
46. Brody, S.S., "New excited state of chlorophyll", (1958) *Science* **128**, 838-839.
47. Butler, W.L. and K.H. Norris, "Lifetime of the long-wavelength chlorophyll fluorescence", (1963) *Biochem. Biophys. Acta* **66**, 72-77.
48. Satoh, K. and W.L. Butler, "Low temperature spectral properties of subchloroplast fractions purified from spinach", (1978) *Plant Physiol.* **61**, 373-379.
49. Rijgersberg, C.R., J. Amesz, A.P.G.M. Thielen and J.A. Swager, "Fluorescence emission spectra of chloroplasts and subchloroplast preparations at low temperature", (1979) *Biochem. Biophys. Acta* **545**, 473-482.
50. Karapetyan N.V., M.G. Rakhimberdieva, N.G. Bukhov and I. Gyurjan, "Characterization of photosystems of Chlamydomonas reinhardtii mutants differing in their fluorescence yield", (1980) *Photosynthetica* **14**, 48-54.
51. Garnier J., J. Maroc and D. Guyon, "Low-temperature emission spectra and chlorophyll-protein complexes in mutants of Chlamydomonas reinhardtii: evidence for a new chlorophyll-a-protein complex related to PSI", (1986) *Biochem. Biophys. Acta* **851**, 395-406.

52. Doukas, A.G., V. Stefancic, J. Buchert, R.R. Alfano and B.A. Zilinskas, "Exciton annihilation in the isolated phycobiliproteins from the blue-green alga Nostoc sp. Using picosecond absorption spectroscopy", (1981) Photochem. Photobiol. **34**, 505-510.
53. Mullet, J.E. and C.J. Arntzen, "Simulation of grana stacking in a model membrane system mediated by a purified light-harvesting pigment-protein complex from chloroplasts", (1980) Biochem. Biophys. Acta **589**, 100-117.
54. Nairn, J.A., W. Haehnel, P. Reisberg and K. Sauer, "Picosecond fluorescence kinetics in spinach chloroplasts at room temperature. Effects of Mg^{2+} ", (1982) Biochem. Biophys. Acta **682**, 420-429
55. Burke, J.J., K.E. Steinback and C.J. Arntzen, "Analysis of the light-harvesting complex of wild type and a chlorophyll-*b*-less mutant of barley", (1979) Plant Physiol. **63**, 237-243.
56. Kramer, H.J.M., J. Amesz and C.P. Rijgersberg, "Excitation spectra of chlorophyll fluorescence in spinach and barley chloroplasts at 4 K", (1981) Biochem. Biophys. Acta **637**, 272-277.
57. Mullet, J.E., J.J. Burke and C.J. Arntzen, "A developmental study of photosystem I peripheral chlorophyll proteins", (1980), Plant Physiol. **65**, 823-827.
58. Diner, B.A. and F.A. Wollman, "Functional comparison of the photosystem II center-antenna complex of a phycocyanin-less mutant of Cyanidium caldarium with that of Chlorella Pyrenoidosa", (1979) Plant Physiol. **63**, 20-25.
59. Tapie, P., Y. Choquet, F-A. Wollman, B. Diner and J. Breton, "Orientation of the pigments in photosystem II: a low-temperature-linear dichroism and polarized fluorescence emission study of chlorophyll-protein complexes isolated from Chlamydomonas reinhardtii", (1986) Biochem. Biophys. Acta **850**, 156-161.
60. Van Dorssen, R.J., J.J. Plijter, J.P. Dekker, A. den Ouden, J. Amesz and H.J. Van Gorkom, "Spectroscopic properties of chloroplast grana membranes and of the core of photosystem II" (1987) Biochem. Biophys. Acta **890**, 134-143.
61. Breton, J. and S. Katoh, "Orientation of the pigments in photosystem II: low temperature linear-dichroism study of a core particle and of its chlorophyll-protein subunits isolated from Synechococcus sp.", (1987) Biochem. Biophys. Acta **892**, 99-107.
62. Nechushtai, R., S.D. Nourizadeh and J.P. Thornber, "A reevaluation of the fluorescence of the core chlorophylls of photosystem I", (1986) Biochem. Biophys. Acta **848**, 193-200.

63. Mullet, J.E., J.J. Burke and C.J. Arntzen, "Chlorophyll proteins of photosystem I", (1980), *Plant Physiol.* **65**, 814-822.
64. Mukerji, I. and K. Sauer, "Temperature dependent steady state and picosecond kinetic fluorescence measurements of a photosystem I preparation from spinach", (1988) *Proc. C.S. French Symposium on Photosynthesis*, Stanford, CA, July, 1988, Alan. R. Liss Inc. Publisher.
65. Holzwarth, A.R., "Fluorescence lifetimes in photosynthetic systems", (1986) *Photochem. Photobiol.* **43**, 707-726.
66. Van Grondelle, R. and V. Sundstrom, "Excitation energy transfer in photosynthesis", (1988) in [16], 403-438.
67. Haehnel, W., J.A. Nairn, P. Reisberg and K. Sauer, "Picosecond fluorescence kinetics and energy transfer in chloroplasts and algae", (1982) *Biochem. Biophys. Acta* **680**, 161-173.
68. Güllöty, R.J., G.R. Fleming and R.S. Alberte, "Low-intensity picosecond fluorescence kinetics and excitation dynamics in barley chloroplasts", (1982) *Biochem. Biophys. Acta* **682**, 322-331.
69. Magde D., S.J. Berens and W.L. Butler, "Picosecond fluorescence in spinach chloroplasts", (1982) *Proc. SPIE-Int. Soc. Opt. Eng* **322**, 80-86.
70. Berens S.J., J. Scheele, W.L. Butler and D. Magde, "Kinetic modeling of time-resolved fluorescence in spinach chloroplasts", (1985) *Photochem. Photobiol.* **42**, 59-68.
71. Hodges, M., I. Moya, J-M. Briantais and R. Ramy, "Time resolved chlorophyll fluorescence studies of photosynthetic pigment protein complexes: characterization of five kinetic components", (1987) in: *Progress in Photosynthesis Research* (J. Biggins ed.) Vol. 1, 115-118. Martinus Nijhoff Publishers, Dordrecht, The Netherlands.
72. Wendler, J. and A.R. Holzwarth, "State transitions in the green alga *Scenedesmus obliquus* probed by time-resolved chlorophyll fluorescence spectroscopy and global data analysis", (1987) *Biophys. J.* **52**, 717-728.
73. Hodges, M. and I. Moya, " Time-resolved chlorophyll fluorescence studies of photosynthetic membranes: resolution and characteristics of four kinetic components" (1986), *Biochem. Biophys. Acta* **849**, 193-202.
74. Moya, I. and R. Garcia, "Phase fluorimetric lifetime spectra. I. In algal cells at 77 K", (1983) *Biochem. Biophys. Acta* **722**, 480-491.
75. Reisberg P., Nairn J.A. and Sauer K., "Picosecond fluorescence kinetics in spinach chloroplasts at low temperature", (1982) *Photochem. Photobiol.* **36**, 657-661.

76. Avarmaa R.A., Kochubey S.M. and Tamkivi R.P., "Low-temperature decay and energy transfer in photosynthetic units", (1979) FEBS Lett. **102**, 139-142.
77. Mimuro, M., N.Tamai, T. Yamazaki and I. Yamazaki, "Excitation energy transfer in spinach chloroplasts", (1987) FEBS Lett. **213**, 119-122.
78. Butler, W.L., C.J. Tredwell, R. Malkin and J. Barber, "The relationship between the lifetime and yield of the 735 nm fluorescence of chloroplasts at low temperatures", (1979) Biochem. Biophys. Acta **545**, 309-315.
79. Pellegrino, F.A., P.S.Dagen and R.R.Alfano, "Temperature dependence of the 735 nm fluorescence kinetics from spinach measured by picosecond laser-streak camera system", (1983) Photobiochem. Photobiophys. **6**, 15-23.
80. Wittmershaus, B.P., "Measurements and kinetic modeling of picosecond time-resolved fluorescence from photosystem I and chloroplasts", (1987) in [71], 75-82.
81. Owens, T.G., S.P.Webb, L.Mets, R.S.Alberte and R.G.Fleming, "Antenna size dependence of fluorescence decay in the core antenna of photosystem I: estimates of charge separation and energy transfer rates", (1987) Proc. Natl. Acad. Sci, USA **84**, 1532-1536.
82. Breton, J., E. Roux and J. Whitmarsh, "Dichroism of chlorophyll a: absorption change at 700 nm using chloroplasts oriented in a magnetic field", (1975) Biochem. Biophys. Res. Comm. **64**, 1272-1274.
83. Gorman, D.S. and R.P. Levine, "Cytochrome f and plastocyanin: their sequence in the photosynthetic electron transport chain of Chlamydomonas reinhardtii", (1965) Proc. Natl. Acad. Sci. USA **54**, 1665-1669.
84. Seka, W. and W. Bunkenburg, "Active-passive modelocked oscillators at 1.054 μm ", (1978) J. Appl. Phys. **49**, 2277-2280.
85. Knox, W., "Picosecond time-resolved spectroscopic study of vibrational processes in alkali halides", (1983) Ph.D. Thesis, University of Rochester.
86. Knox, W. and G. Mourou, "A simple jitter-free picosecond streak camera", (1981) Opt. Comm. **37**, 203-206.
87. France, L., N.E. Geacintov, S. Lin, B.P. Wittmershaus, R.S. Knox and J. Breton, "Fluorescence decay kinetics and characteristics of bimolecular exciton annihilation in chloroplasts", (1988) Photochem. Photobiol. **48**, 333-339.
88. Ippen, E.P., C.V. Shank and A. Bergman, "Picosecond recovery dynamics of malachite green", (1976) Chem. Phys. Lett. **38(3)**, 611-614.

89. Fleming, G.R., A.W.E. Knight, J.M. Morris, R.J.S. Morrison and G.W. Robinson, "Picosecond fluorescence studies of xanthene dyes", (1977) *J. Amer. Chem. Soc.* **99**(13), 4300-4308.
90. Butler, W.L. and D.W. Hopkins, "An analysis of fourth derivative spectra", (1970) *Photochem. Photobiol.* **12**, 451-456.
91. Penzkofer, A. and Y. Lu, "Fluorescence quenching of rhodamine 6G in methanol at high concentration", (1986) *Chem. Phys.* **103**, 399-405.
92. Wittmershaus, B.P., "Excitation transfer in photosystem I and chloroplasts: a picosecond time-resolved fluorescence study", (1986) Ph.D. Thesis, University of Rochester.
93. Garab, G.I., G. Horvath and A. Faludi-Daniel, "Resolution of the fluorescence bands in greening chloroplasts of maize", (1974) *Biochem. Biophys. Res. Comm.* **56**, 1004-1009.
94. Butler, W.L. and R.J. Strasser, "Tripartite model for the photochemical apparatus of green plant photosynthesis", (1977) *Proc. Natl. Acad. Sci. USA* **74**, 3382-3385.
95. Rijgersberg, C.P., "Fluorescence and photochemistry at low temperature in photosynthetic systems", (1980) Ph.D. Thesis, Leiden.
96. Öquist, G. and G. Samuelsson, "Sequential extraction of chlorophyll from chlorophyll-protein complexes in lyophilized pea thylakoids with solvents of different polarity", (1980) *Physiol. Plant* **50**, 57-62.
97. Hayden, D.B., N.R. Baker, M.P. Percival and P.B. Beckwith, "Modification of the photosystem II LHC *a/b* protein complex in maize during chill-induced photoinhibition", (1986) *Biochem. Biophys. Acta* **851**, 86-92.
98. Rijgersberg, C.P., A. Melis, J. Amesz and J.A. Swager, "Quenching of chlorophyll fluorescence and photochemical activity of chloroplasts at low temperature", (1979) in "Chlorophyll Organization and Energy Transfer in Photosynthesis", Ciba Foundation Symposium 61, 305-318, Excerpta Medica, Amsterdam.
99. Lin, S. and R.S. Knox, "Time resolution of a short-wavelength chloroplast fluorescence component at low temperature", (1988) *J. Lum.* **40/41**, 209-210.
100. Knox, R.S. and S. Lin, "Time resolution and kinetics of 'F680' at low temperatures in spinach chloroplasts", (1988) in [16], 567-577.
101. Searle, G.F.W. and C.J. Tredwell, "Picosecond fluorescence from photosynthetic system *in vivo*", (1979) in [98], 257-277.
102. Kittel, C. "Elementary Statistical Physics", (1958) John Wiley and Sons, Inc., New York.

103. Mimuro, M., "Analysis of excitation energy transfer in thylakoid membranes by time-resolved fluorescence spectra", (1988) in [16], 589-600.
104. Pålsson, L-O., T. Gillbro, P. Svensson and P-Å. Albertsson, "Interaction between LHC-II antenna and PSII core in thylakoid vesicles", (1989) The VIII international Congress in Photosynthesis, Stockholm, Sweden, August 6-11, Poster 413.
105. Brecht, E., "The light-harvesting chlorophyll *a/b*-protein complex II of higher plants: results from a twenty-year research period", (1986) *Photobiochem. Photobiophys.* **12**, 37-50.
106. Rubin, L.B., B.N. Korvatovskii, O.V. Braginskaya, V.Z. Pashchenko, K.H. Pershke and V.B. Tosov, "Dynamics of electronic excitation in the photosynthetic pigment apparatus", (1980) *Molekul Biologiya (English translation)* **14**, 538-545.
107. Litvin, F.F. and V.A. Sineshchekov, "Molecular organization of chlorophyll and energetics of the initial stages in photosynthesis", (1975) in [98], 619-661.
108. Kan, K-S. and J.P. Thornber, "The light-harvesting chlorophyll *a/b*-protein complex of *Chlamydomonas reinhardtii*", (1975) *Plant Physiol.* **57**, 47-52.
109. Picaud, A. and G. Dubertret, "Pigment protein complexes and functional properties of tetratype resulting from crosses between CP₁ and CP₂ less *Chlamydomonas* mutants", (1986) *Photosynthesis Res.* **7**, 221-236.
110. Wollman, F-A. and P. Bennoun, "A new chlorophyll-protein complex related to photosystem I in *Chlamydomonas reinhardtii*", (1982) *Biochem. Biophys. Acta* **680**, 352-360.
111. Tapie, P., Y. Choquet, J. Breton, P. Delepelaire and F.-A. Wollman, "Orientation of photosystem-I pigments: investigation by low-temperature linear dichroism and polarized fluorescence emission", (1984) *Biochem. Biophys. Acta* **767**, 57-69.
112. Güloty, R.J., L. Mets, R.S. Alberte and G.R. Fleming, "Picosecond fluorescence study of photosynthetic mutants of *Chlamydomonas reinhardtii*: origin of the fluorescence decay kinetics of chloroplasts", (1985) *Photochem. Photobiol.* **41**, 487-496.
113. Haehnel, W., A.R. Holzwarth and J. Wendler, "Picosecond fluorescence kinetics and energy transfer in the antenna chlorophylls of green algae", (1983) *Photochem. Photobiol.* **37**, 435-443.
114. Hodges, M. and I. Moya, "Time-resolved chlorophyll fluorescence studies on photosynthetic mutants of *Chlamydomonas reinhardtii*: origin of the kinetic decay components", (1987) *Photosyn. Res.* **13**, 125-141.

115. Lebedev, N.N., R.A. Khatypov, V.G. Ladygin and A.A. Krasnovskii, "Fluorescence excitation spectra and decay kinetics of light-harvesting complexes in Chlamydomonas reinhardtii mutants", (1988) *Photosynthetica* **22**, 364-370.
116. Mets, L., Private communications.
117. Spreitzer, R.L. and L. Mets, "Photosynthesis-deficient mutants of Chlamydomonas reinhardtii with associated light-sensitive phenotypes", (1981) *Plant Physiol.* **67**, 565-569.
118. Arntzenl, C.J. and H.B. Pakrasi, "Photosystem II reaction center: polypeptide subunits and functional cofactors", (1986) in [3] section 9.4, 457-467.
119. Holzwarth, A.R., "The functional organization of the photosystems in higher plants and green algae as studied by ultrafast kinetic method", (1989) Lecture 26 in [104].
120. Owens, T.G., S.P. Webb, L. Mets, R.S. Alberte and G.R. Fleming, "Antenna structure and excitation dynamics in photosystem I", (1989) *Biophys. J.* **56**, 95-106.
121. Zankel, K.L. and R.K. Clayton, " 'Uphill' energy transfer in a photosynthetic bacterium" (1969) *Photochem. Photobiol.* **9**,7-15.

LIST OF ABBREVIATIONS

ADP	Adenosine diphosphate
ATP	Adenosine triphosphate
C###	Absorption band centered at ### nm
Chl, Chl <u>a</u> , <u>b</u>	Chlorophyll, chlorophyll <u>a</u> , <u>b</u>
CP	Complex protein
eV	Electron volt
F###	Fluorescence emission band centered at ### nm
k_{ij}	Pairwise excitation-transfer rate from j to i
K_{ij}	Overall excitation-transfer rate from component j to i
LHC	Light-harvesting chlorophyll <u>a/b</u> -protein, also called LHCI by some authors
LHCI	LHC associated with PSI
N_i	Density of first excited singlet excitations of the i^{th} component
N_{i0}	chromophore density of the i^{th} component
NADP	Nicotinamide adenine dinucleotide phosphate
NADPH	A reduced form of NADP^+
OMA	Optical multichannel analyzer
P680, P700	Primary electron donor of PSII, PSI
PSI	Photosystem I
PSII	Photosystem II
RC	Reaction center
σ	Ground-state absorption cross-section
σ'	First excited singlet-state absorption cross-section

Tris

Tris (hydroxymethyl) amino methane

τ_i

Fluorescence lifetime of the i^{th} component

INDEX

Absorption

chlorophyll **a**, chlorophyll **b** of, 10,11,49

chloroplasts of, 10,11

cross-sections, 15,19,85

excited-state, 44

measurement, 28

Annihilation, 18,55

Antenna, 2

chlorophyll-protein complexes, 8

excitation energy transfer, 10,73-75,101-104

internal, 23

LHC, 8,70-72

LHCI, 73-75

PSI of, 73,101

PSII of, 48,70,73,85

structure of, bacteria, 8,9

system, 8

Bacteriochlorophyll **a**-protein

X-ray structure, 8

Boltzmann factor, 65,66

Carotenoid, 49

Cell

higher plant, 4-6

Charge separation, 12-14

Chlorophyll, 2

a/b-protein, light-harvesting, 8

chemical structure, 8

Chlorophyll a, Chlorophyll b, 10,11

cross-sections, 8,10,11,49

densities, 44,59-61

excited state absorption, 19

molecule, 8,9

proteins, 8-10

spectral forms, 10,11

Chlorophyll-protein complex, 8-10

Chlamydomonas reinhardtii, 26,73

chlorophyll-protein complex, 75,83

molecular organization, 73

mutants of, 78,85
spectral properties of, 78-85
thylakoid membranes, 6

Chloroplasts, spinach, 4
absorption, 10,11
electron micrograph, 4,5
fluorescence spectra, 22,48,49,51,52
membranes, 6
model for excitation transfer in, 60
preparation, 26
structure, 4-6
time-resolved fluorescence of, 49,50,53-55,67

Eigenvalue, 19

Electron transport, 12,13
cyclic, 12

Electron
acceptor, 14
donor, 12

Electronic excited state, 10

Energy conversion, 12

Excitation energy transfer, 10

antenna chlorophylls among, 14-17

back transfer, 65,66,104,109

forward, 63

mechanism, 14

migration, 14,16

pathway, 73,75

rate, 14,15,59,60,65,100,102-104

temperature-dependent, 70

theory of, 14,15

uphill, 110

Etalon, 35,36

Excitation intensity, 31,55,66

Excitation pulse, 28,31

Excited-state

absorption, 44

population, 18

Filters

cutoff, 28,31

interference, 31,53

Fluorescence, 2

biphasic rise, 18

chloroplasts from, 21

decay kinetics analysis, 59-61,65-67,95,96,101

decay lifetime, 19

emission band, 21-23,28,51,52,74-76

integrated, 61

lifetime of dyes, 35,37

rise delay, 95,109,110

time-resolved, detection of, 53-55,91-96

yield, 19,50,70

Förster transfer rate, 14-16

Fourth derivative, 38,52,79

Free energy, 12

Gaussian curve, 63

Isolated

PSI particle, 23

PSII particle, 21

subparticle, 74

Kinetic analysis, 44,46,59-61,63,95-97

Kinetic model, 59,60,101-104

simulation, 17,61

three-population, 44-46

tripatite, 48

two-population, 59-61

Laser system, 30,31

LHC, light-harvesting antenna Chlorophyll-protein, 8

energy transfer to PSI, 108-111

energy transfer to PSII, 70-72,108

structure, 8,9

Least-squares fitting analysis, 43-45,55,57,58

Mutant

photosynthetic, 74,78

PSI-deficient, 78,95,101

PSII-deficient, 95,108

Pheophytin, 14

Photon-counting experiments, 19,49,55-57

Photosynthesis

process of, 1,10,12

primary photochemical events, 12-14

Photosynthetic

apparatus, 4-10

assemblies, 6

functions, 4-10

structures, 4-10

Photosystem, 6

Picosecond time-resolved spectroscopy, 23-25

measurement, 30,31

Pockels cell, 28,31

Polarizer, 31

Protein-complex pigment, 83

Quinone, 14

Reaction centers, 2

open, close, 14

P700, PSI, 8,12,14

P680, PSII, 8,12,14

trapping by, 16,17

Reconstructed spectra, 61,63,64,100

Residual background, 39,41

Sample

cooling, 27

preparation, 26

Series scheme, 12

Spectra

blue shift, 68

emission band, 21,63,64,75

reconstructed, 63,64,68

steady-state, 20-23,48,49,51,52,73-75

time-resolved, 20,23-25,50,53-55,76

Streak camera, 32,33

System linearity, 35,38,40

Thylakoid membrane, 6,7

grana, 6

stroma, 6

Trap, 12,16

Tris-acetate phosphate (TAP), 26